INFORMATION TO USERS

This manuscript has been reproduced from the microfilm master. UMI films the text directly from the original or copy submitted. Thus, some thesis and dissertation copies are in typewriter face, while others may be from any type of computer printer.

The quality of this reproduction is dependent upon the quality of the copy submitted. Broken or indistinct print, colored or poor quality illustrations and photographs, print bleedthrough, substandard margins, and improper alignment can adversely affect reproduction.

In the unlikely event that the author did not send UMI a complete manuscript and there are missing pages, these will be noted. Also, if unauthorized copyright material had to be removed, a note will indicate the deletion.

Oversize materials (e.g., maps, drawings, charts) are reproduced by sectioning the original, beginning at the upper left-hand corner and continuing from left to right in equal sections with small overlaps.

Photographs included in the original manuscript have been reproduced xerographically in this copy. Higher quality 6" x 9" black and white photographic prints are available for any photographs or illustrations appearing in this copy for an additional charge. Contact UMI directly to order.

Bell & Howell Information and Learning
300 North Zeeb Road, Ann Arbor, MI 48106-1346 USA
800-521-0600

4

CHARACTERIZATION AND TIME RESOLVED DYNAMICS OF NANOSTRUCTURES FOR NONLINEAR OPTICAL APPLICATIONS

by

Gul H. Yaglioglu

A dissertation submitted to the Graduate Faculty in Engineering in partial fulfillment of the requirements for the degree of Doctor of Philosophy, The City University of New York

2001

This manuscript has been read and accepted by the Graduate Faculty in Engineering in satisfaction of the dissertation requirement for the degree of Doctor of Philosophy.

November 17, 2000 — Date

Chair of Examining Committee:
Dr. Roger Dorsinville, Professor, Department of Electrical Engineering, The City College of The City University of New York.

November 17, 2000 — Date

Executive Officer
Professor Mumtaz K. Kassir

Dr. Ardie Walser Associate Professor, Department of Electrical Engineering, The City College of the City University of New York.

Dr. Fred Moshary Associate Professor, Department of Electrical Engineering, The City College of the City University of New York.

Dr. Ping Pei Ho Professor, Department of Electrical Engineering, The City College of the City University of New York.

Dr. Andrew Edwards Member of Technical Staff, JDS Uniphase, 625 Industrial Way, Eatontown, NJ 07724

Supervisory Committee

THE CITY UNIVERSITY OF NEW YORK

Abstract

CHARACTERIZATION AND TIME RESOLVED DYNAMICS OF NANOSTRUCTURES FOR NONLINEAR OPTICAL APPLICATIONS

by

Gul H. Yaglioglu

Advisor: Professor Roger Dorsinville

The femtosecond and picosecond nonlinear optical properties of various nanostructures have been studied. The studied nanostructures are Gd_2 doped metallofullerenes, TDBC (1,1'-diethyl-3,3'-bis(4-sulfobutyl)-5,5',6,6'-tetrachloro-benzimidazolo carbocyanine) J-aggregates on nanosized colloidal suspensions, Langmuir-Blodgett films of some aromathic polydiacetylenes, and Si nanocrystals into silica matrix. The observed dynamics are sensitive to the specific excited state dynamics of the sample, as well as to the experimental technique and the characteristics of the excitation, such as the wavelength and pulse duration.

Single-beam Z-scan and transient absorption experiments were carried out between 400 nm and 1000 nm in $Gd_2@C_{80}$ (Gd_2 doped C_{80} metallofullerene) thin films and solutions. The third-order nonlinearity was large, negative, and strongly dependent on the pulse-duration and wavelength. Transient absorption results suggest that the fast

nonlinear response is enhanced by two-photon-induced ground-state absorption and excited-state bleaching effects.

Femtosecond transient absorption experiments with white light continuum were conducted on TDBC J-aggregates on colloidal surfaces. The transient absorption spectra showed stimulated emission, which has not been seen in TDBC J-aggregates in water. The effects of the pump power, the probe power, and the pump wavelength on the transient absorption spectrum were investigated. The experimental results suggest that the transition from the two-exciton state to the one-exciton state stimulates the transition from the one-exciton state to the ground state.

The third order nonlinear optical properties of Langmuir-Blodgett films made from aromatic polydiacetylenes were studied for the first time by using the Z-scan technique. The values of the third order nonlinear optical susceptibilities of four different aromatic polydiacetylenes were substantially larger than the published values of aliphatic polydiacetylenes. The enhancement of the nonlinearity was attributed to the incorporation of the aromatic groups.

The nonlinear optical properties of silicon nanocrystals within a fused silica matrix were investigated systematically by the Z-scan technique. Nonlinear measurements at various wavelengths showed the role of three bands in the visible spectrum. Measurements at various laser pulse durations showed several time constants, which, illustrated the role of quantum confined and surface states.

In memory of my father
İlyas Coşkun
who encouraged me to continue my studies
and
who passed away while I was working on this degree

Acknowledgements

I am grateful to my advisor, Dr. Roger Dorsinville, for giving me a chance to study with him in the field of nonlinear optics. Even when I wanted to give up, speaking with him always gave me the courage and the strength to continue working on this thesis. His trust motivated me to be a better student and researcher. I truly thank him for all his help, guidance, and support during this study.

I would like to thank Dr. Ardie Walser for his helpful discussions on some of the problems in this thesis and for proofreading this thesis. I also thank the members of the committee for their guidance and insight.

It was a great pleasure to work with our collaborators Dr. J. Z. Liu at American High-tech Material Company, Dr. Serdar Ozcelik at Bilkent University in Turkey, Dr. Ogawa and his group in New Mexico, Dr. Haim Grebel and his group at The New Jersey Institute of Technology. I specifically thank Dr. Sankaran Vijayalakshmi for being a great work partner and a friend.

A special thank goes to the members of the CASI office for their support. Especially, I would like to thank Dr. Ronald H. Brown and Sandra Smith. Their guidance was always helpful in my college and social life.

Thanks to my friends Dr. David L. Harris, Dr. Richard Presley and Dr. Andrew Edwards for teaching me how to use the systems in our laboratory. I also thank my friend Robinson Pino for his enjoyable partnership in the laboratory.

I would like to thank Dr. Fuat Bayrakçeken from Turkey and my friend Metin Aydın for encouraging me to apply for this graduate study at The City College of New York and for helping me during the application process.

I could not thank enough my family, my father İlyas Coşkun, my mother Gürsel Coşkun, my sister Gonca Talu, and my brother Osman Coşkun, for their support and understanding.

Most importantly, I thank my husband Mutlu Yağlıoğlu. I could not have completed this degree without him. He was always with me during this journey. His love and support kept me going through hard times.

Table of Contents

List of Tables

Chapter 3

Chapter 5

List of Figures

Chapter 2

Chapter 3

Chapter 4

Chapter 5

Chapter 6

CHAPTER 1

INTRODUCTION

1.1. Thesis Statement

The third order nonlinear optical property of a material makes it possible to control light with light. A material with large third order susceptibility has an index of refraction and absorption that is dependent on the intensity of the light that travels through it.[1] Devices made from such materials have numerous applications, such as protection for the human eyes or optoelectronic sensors from unwanted or stray sources. Other applications of these materials include using them in optical processors and storage devices or high-speed modulators and demodulators, which are very important in communication technology. These nonlinear optical devices will allow parallel processing with greatly enhanced speed. The potential for making suitable materials and optical devices motivates much of the current fundamental research of the third order nonlinear optical response of new materials.

Nanostructures unique properties are attributed to the comparable size of the structure to the critical scale length of physical phenomena. High surface area and confinement effects are characteristic properties of these materials and are quite different than those found in conventional materials. Thus, nanostructures create an opportunity for application of innovative principles of operation to devices and instruments. Due to the importance of nanostructures in nonlinear optical applications, this thesis concentrates

on characterization of nonlinear optical and time resolved dynamics of excited states of the following materials: metallofullerenes thin films, organic multilayered thin films, J-aggregates adsorbed on nanosize colloidal surfaces, and Si nanoclusters implanted in SiO_2 matrices and crystals.

1.2. Organization of thesis

Chapter 2 presents experimental techniques used in this thesis including the experimental apparatus, the third order nonlinear susceptibility measurement method (Z-scan technique), pulse duration measurements (autocorrelation and cross-correlation techniques) and transient absorption measurements (femtosecond pump-probe spectroscopy technique). Chapter 3 contains experiments and results of our first organic nanostructure $Gd_2@C_{80}$ (Gd_2 doped C_{80}). This section gives information about some of the general properties of fullerene-based materials and their applications, the material preparation technique and the results of Z-scan and pump-probe experiments performed on the endohedral metallofullerene. Our second nanostructure TDBC (1,1'-diethyl-3,3'-bis(4-sulfobutyl)-5,5',6,6'-tetrachloro-benzimidazolo carbocyanine) J-aggregate adsorbed onto nanosize colloidal silver surfaces is discussed in chapter 4. Chapter 4 also includes theoretical background on J-aggregates, information about material preparation and the femtosecond time-resolved dynamics of J-aggregates adsorbed on colloidal surfaces. Our last organic nanostructures are Lagmiur-Blodget membranes of aromatic polydiacetylenes. Chapter 5 presents the third order nonlinear susceptibility results in these materials. Chapter 6 contains experiments and results on semiconductor nanoclusters. Nonlinear optical characterization of Si nanoclusters formed by ion implantation in SiO_2 matrices are investigated and presented as the last project.

1.3. Nonlinear Optics and Photonics

Nonlinear optics is the study of phenomena that occurs as a result of the modification of the optical properties of a material by the presence of intense light. Nonlinear optics plays an important role in photonics. Photonics is similar to electronics in that it describes the technology in which photons instead of electrons are used to acquire, store, transmit, and process information. Photonics has many applications in many areas of information and image processing technology.

The field of nonlinear optics has been progressing with the advent of lasers. The strong oscillating electric field of the laser beam creates a nonlinear polarization response. That response can act as a source of new optical field with altered properties. One of the most visually dramatic nonlinear optical processes is frequency doubling which is used in the field of optical information storage to convert near-infrared laser light to blue light. The size of a focused spot of light is inverse proportional to its wavelength. Because of that, second harmonic generation can increase information storage capacity of optical disks. Using related phenomena one can build devices, such as frequency mixers for generating new light sources, light modulators for controlling the phase or amplitude of a light beam, optical switches, optical logic, optical information storage, optical limiters, and different ways of processing the data or image information.

Optical computing and optical information processing are the most attractive applications of photonics. Gain in photonics switching functions is a major advantage. Photonics switching can take place with femtosecond speeds, which are many orders of magnitudes over that of electronic processes. The other advantage of working at optical

frequencies is providing a gain in the bandwidth of information processing. On the other hand, since interaction of optical fields with each other is weak it is a necessity to develop materials where these interactions can be maximized. Thus studying interaction of light with matter has been an appealing research subject.

For many applications the nonlinear optical response time needs to be smaller. A nonresonant electronic optical nonlinearity has the fastest response time, limited by the width of the driving laser pulse. By using femtosecond lasers a few femtosecond response time can be achieved. On the other hand response time of the resonant nonlinearity is limited by the lifetime of the excitation.

1.4. Nonlinear Materials

Basically, all materials exhibit nonlinear optical phenomena to some extent. This includes all forms of matter-glasses, liquids and solids. The required power of the optical field to observe these effects is very large when the effect is small. Nonlinear optical effects of materials depend on the detailed nature of the electronic structure of the atomic and molecular structures, their dynamic behavior, as well as the symmetry and details of their geometrical arrangement in the medium. In this section, the nonlinear optical materials are reviewed and the reasons for selecting organic materials (metallofullerenes, polydiacetylenes, and J-aggregates) for this thesis are discussed.

The most promising nonlinear optical (NLO) materials are found in the following areas[2]: 1) bulk materials (mostly semiconductors, glasses and semiconductor-doped glasses), 2) multiple-quantum wells (MQW), 3) photorefractive materials, 4) liquid crystals, 5) inorganic frequency conversion materials, and 6) organic and polymeric materials.

Bulk materials, particularly solid-state crystals, are classic NLO materials for such application as frequency conversion. Bulk semiconductors are some of the most universal nonlinear optical materials; under proper condition they can demonstrate almost any possible nonlinear optical effect and can be used for applications from 0.3-12 μm wavelengths with a variety of materials. The nonlinear phenomenon in bulk semiconductors that has attracted most of the attention is the nonlinear refractive index and related effects.

Quantum well (QW) and multiple quantum well structures (QWSs) are semiconductor structures (such as GaAS and GdSe) with two-dimensional carrier confinement. Good quality QWSs can be produced using advanced growth techniques[3, 4, 5] developed in the 1980s, such as molecular beam epitaxy and metallo-organic chemical vapor deposition, and advanced processing techniques such as reactive ion beam etching and electron beam lithography[6, 7, 8]. One of the important concerns about these materials is the mechanical stability of the structures grown, especially when there is a considerable lattice mismatch between neighboring layers.

Photorefractive materials are electro-optic crystals such as $LiNbO_3$ in which absorption of photons triggers a charge separation resulting in a modulation of the materials refractive index[9].

Potassium dihydrogen phosphate (KDP) and potassium titanyl phosphate (KTP) are examples of inorganic crystals. These crystals are used as frequency conversion materials.

The history of organic materials is quite new compared to inorganic materials. Organic and polymeric materials are considered as the most promising group of nonlinear optical materials[10]. This thesis will mostly concentrate on the third order nonlinear optical properties of organic materials. Different types of organic materials and their benefits are summarized in the following paragraphs.

When a compound involves a chain or ring of bonded carbon atoms with alternate single and multiple bonds, the π electrons can move over the entire length of the molecule and the structure is called conjugated. This delocalization makes π electron distribution highly deformable in conjugated electronic systems, which gives rise to large

optical nonlinearities[10]. The nonlinear polarization of π electrons is large even for frequencies of radiation far away from electronic resonance (i.e. linear absorption frequencies).

Organic polymers have other additional advantages, including: synthetic and processing options that are not available with the single crystal and multiple quantum wells classes of nonlinear materials. Structurally, polymers can be made into thin or thick films, bulk crystals, or liquid and solid solutions. They can be formed into layered film structures with molecular engineering providing different optical properties from layer to layer. Mechanically, the materials can be strong and resistant to radiation, shock, and heat. There is no diffusion problem in polymers. Additionally, organic and polymeric materials can exhibit high optical damage thresholds, broad transparency ranges, and can be polished to high optical quality surfaces.

Considerable interest has been directed to conjugated polymers. Quasi-one dimensional conjugated polymers such as polydiacetylenes, polyacetylenes, and polythiophenes are characterized by a large nonlinear optical response and fast response time.[11, 12, 13, 14] Conjugated polymers have in general highly anisoptropic optical, dielectric, conducting and mechanical properties. This is because the valence electrons are responsible for these properties. Those electrons respond more easily to perturbations along the direction of conjugation than in other directions. The delocalization of those electrons in the other directions is hindered by saturated bonds. This causes the conjugated system to have an isolator type behavior in the direction across the conjugation direction, but a semiconducting behavior along the conjugation direction.

The polysilanes represent another class of polymers that has been extensively studied for nonlinear optical amplifications[15]. These polymers have a molecular structure $(R_1\text{-Si-}R_2)_n$ that is a long catenated σ-bonded silicon back bone with two side group R_1 and R_2. Side groups are usually carbon based and attached to each Si atom in the backbone chain. In spite of σ-bonded nature of the backbone, the polysilanes show extensive electronic delocalization, resulting in strong transitions for excitations polarized parallel to the backbone[16]. They are transparent through the visible to the infrared spectral regions in contrast to the π electron polymers.

Part of this thesis will present the results of the investigations of a very promising π electron conjugated polymer system, polydiacetylene. A review of earlier works on polydiacetylenes is given in chapter 5.

Conjugated polymers have also some disadvantages. Conjugated polymers possess hydrogen atoms and therefore are characterized by a residual absorption in the near infrared due to the overtones of C-H stretching vibrations. This constitutes an important limitation for their applications in the near infrared, which is used in optical communication. Recently, a new type of organic materials called fullerenes, with C_{60} as a prototype, has attracted researchers attention as a novel class of nonlinear optical materials[17, 18]. Fullerenes are uniquely composed of carbon atoms and therefore do not have residual infrared absorption due to overtones of C-H stretches.

The discovery in 1985 of C_{60} and C_{70} molecules[19] was the starting point of intense research and collaboration between chemist, physicists and material scientists. Fullerenes named after architect Buckminster Fuller, who designed the geodesic domes, represent a class of unique organic materials. They are a new form of pure carbon besides graphite

and diamond. In fullerenes, carbon atoms come together to form a hollow soccer ball shape molecule. The existence of C=C double bonds in the molecule provide the fullerene materials with 3D delocalized π electrons (a sphere of mobile electron) around the cage, which is the reason for their high nonlinearity.

Some of the properties needed before a material can be considered for device applications are large nonlinear optical response, high laser damage thresholds, optical transparency, ease of processability, chemical modification, and thermal and oxidative stability. Prepared high quality optical films show that fullerenes are highly processable. Fullerenes possesses a high thermal oxidative stability compared to any nonlinear optical organic material. Fullerenes are transparent from the mid infrared to the visible spectral range. They also have a high laser damage threshold.

After the discovery of a new method for mass production[20], various types fullerenes have been produced: Higher cage fullerenes (C_{76}, C_{78}, C_{82}, C_{84} etc.), nanotubes, carbon onions, endohedral metallofullerenes[21] ($La@C_{80}$, $Er_2@C_{82}$, $Er_2@C_{84}$, $Er_2@C_{90}$ etc.), noble gas fullerenes ($He@C_{60}$), and derivatives of C_{60}.

The nonlinear optical properties of different size fullerenes, such as C_{60}[22, 23], C_{70}[24, 25] and higher cage size fullerenes[26] have been studied extensively. On the other hand, the nonlinear optical properties of metallofullerenes have not been explored extensively. This motivated us to study the nonlinearity of one of the metallofullerenes. A detailed review of earlier experiments on fullerenes and metallofullerenes is given in chapter 3.

The nonlinear optical properties of organic molecules[27] and semiconductor nanostructures such as quantum wells[28], quantum dots[29] with quantum confinement effect have been a subject of active study. However new materials based on organic nanostructures are needed for optical computing applications. The J-aggregates are

regarded as promising nonlinear optical materials because of the co-operative response of confined Frenkel excitons to the light field. In molecular J-aggregates, the electron and holes are situated in the same molecule, and they form a Frenkel exciton by dipole-dipole interaction. The transition dipole moment of the Frenkel exciton is predicted to have coherence length-dependent enhancement[30]. With an enhanced transition dipole moment molecular aggregates are expected to have a very large third order optical nonlinearity and a fast response time caused by supperradiant decay[31].

This thesis will present .the excited state dynamics of colloidal J-aggregates. Detailed explanations about colloidal J-aggregates can be found in chapter 4.

Semiconductor nanoclustors are also promising nonlinear optical materials. Semiconductor nanocrystals have been widely studied for nonlinear optical applications and they showed high third order nonlinearity[32, 33]. Thus, we will also present an investigation of the nonlinearity of 3 and 5 nm Si nanoclusters in a silica matrix.

Besides high nonlinearity, materials investigated in this thesis have another common property. All the studied materials are nanostructures. Studying the nonlinear optical properties of nanostructures has been an appealing subject in nanotechnology. This is because, when dimensions of materials are on the order of wavelengths, materials show interesting properties. The next section gives a brief description of nanotechnology and it's applications.

1.5. Nanotechnology and Nanostructured Materials

The word "nanotechnology" has become very popular and it describes many types of research where the characteristic dimensions are less than 100 nanometers. Nanotechnology is defined as fabrication of devices with atomic or molecular scale precision. Nanotechnology is an extension of microtechnology. Microtechnology is the basis of making computer components.

Information storage might be a good example of nanotechnology. The current size of a spot on a CD disk is on the order of 100 μm^2. If this area is reduced to nm^2, a much smaller disk might carry information equivalent to 1,000 CDs.

Development of nanoscale science and engineering has many applications in material science, information and medical technology: In material science, new materials many times stronger or far lighter than anything known today can be made; new materials with enhanced optical properties can be achieved for optical switching and optical computing applications. In information technology, quantum computers and computer chips that store trillions of bits of information on a pinhead device can be manufactured. In medical science improved drug and gene delivery, biocompatible materials for implants and nanoscale sensors for detection of disease can be possible.

In the case of nonlinear optical devices, one of the goals in the use of the quantum confinement is to optimize the optical nonlinearity per valence electron in a given frequency and time range. Its usefulness comes from the possibility of artificially modifying the material characteristics, and selectively enhancing or suppressing certain polarization mechanisms with respect to the unconfined materials. The confinement of

the valence charges within a potential well of dimensions $L<a_c$ (where, a_c is the Bohr radius) enhances the kinetic energy over the potential energy[34]. Thus, the electrons are free to move within an artificial potential well whose eigenstate spacing and dynamics depend on the dimension L. Consequently, the third order nonlinear response of the material to the external field is modified since the charge structure is now maintained by the confinement potential.

Currently photolithography that uses ultraviolet light to etch out patterns on silicon chips is the dominant technology for making microstructures. Lithography technique cannot go below 100 nm, and 3-D structures cannot be built with this technique. New techniques are needed to fabricate micro- and nanostructures. Self-assembly is considered as a new approach to fabricate such small structured materials[35]. Molecular self-assembly is the spontaneous organization of molecules into stable, structurally well-defined aggregates[36]. The appeal of this approach is the design flexibility and being able to construct a structure layer by layer. Films with a few nm thicknesses can be prepared. Since the wave vector of a propagating mode in a waveguide is thickness dependent, films prepared by these techniques might have phase relationship between modes over considerable distances. Since nonlinear interactions are phase dependent these films have potential advantage[37].

There are two different approaches to prepare molecular assemblies: The first of these is Langmuir-Blodgett (LB) technique. In this technique, assemblies of molecules with polar head groups and long aliphatic tails are deposited onto a substrate from the surface of a liquid (usually water). When the molecules spread onto the surface of water, they are compressed laterally to orient the molecules with polar head groups at the water

surface and the tails perpendicular to the surface. These highly organized molecules can be transferred onto substrates.

Multilayered LB films of aromatic polydiacelynes are a good example of nanostructures prepared with this technique. Detailed information about these films can be found in chapter 5.

The second molecular self-assembly technique is called "Self-Assembled Monolayers" (SAMs). SAMs are simple to generate and can be formed from a wide variety of ligands and supports. A molecule, essentially an alkane chain, is given a head group with a strong preferential adsorption to the substrate used. Thiol (S-H) head groups and Au(111) substrates have been shown to work very well. The thiol molecules adsorb readily from solution onto the gold, creating a dense monolayer with the tail group pointing outwards from the surface. By using thiol molecules with different tail groups, the resulting chemical surface functionality can be varied within wide limits. Alternatively, it is also possible to chemically functionalize the tail groups by performing reactions after assembly of the SAM.

Carbon-based fullerene molecules are the examples of molecular self-assembled nanostructures. For example, C_{60} with a diameter 0.7 nm presents one of the most producible nanostructures. Organic dye aggregation on nanometer sized colloidal surfaces might be another example of molecular self-assembled nanostructures. When organic dyes are adsorbed onto colloids, dye molecules stick to the surfaces of the colloids and form nanostructures. SAMs can be prepared by using these materials.

Visible light emission from semiconductor nanostructures, such as Si, Ge, has stimulated extensive research into semiconductor nanoclusters. Among semiconductor

nanoclusters, Si is considered a promising candidate for application in Si-based optoelectronics because of their efficient photoluminescence[38]. Quantum confinement effects are expected to play an important role on the nonlinear response of these materials.

In summary, in this research we have investigated nanostructured and highly nonlinear materials for potential applications in nanotechnology.

References:

[1] H.M. Gibbs, Optical Bistability: Controlling Light with Light, Academic Press, Orlando, Florida (1985)
[2] D. H. Auston, et al., Appl. Opt., 26, 211 (1987).

[3] E. Kopan, M. C. Tamargo, D. M. Huan, Appl. Phys. Lett, 50, 347 (1987).

[4] P. M. Petroff, A. C. Gossard, and W. Wiegman, Appl. Phys. Lett. 45, 620 (1984).

[5] H. M. Cox, P. S. Lin, A. Yi Yan, K. Kash, M. Seto, and P. Bastos, Appl. Phys. Lett., 55, 472 (1989).

[6] Z. L. Zang, and N. C. MacDonald, J. Vac. Sci. Technol. B, 4, 2538 (1993).

[7] J. Yao, S. Arney, and N. C. MacDonald, J. of Microelectromechanical systems 1, 14 (1992).

[8] J. Yao, and N. C. MacDonald, J. Microtech. Microeng.,5, 257 (1995).

[9] J. H. Hong, and D. Psaltis, in "Contemporary Nonlinear Optics", edited by G. P. Agrawal, R. W. Boys, Academic Press, p246 (1992).

[10] P. N. Prasad, D. J. Williams, Introduction to nonlinear optical effects in molecules and polymers, John Willey and Sons, New York (1991).

[11] J. Messier, F. Kajzar, P. N. Prasad, and D. Ulrich, in "Nonlinear Optical Effects in Organic Polymers", Kluwer Academic, Dordrecht (1989).

[12] J. L. Bredas, and R. R. Chance, Conjugated Polymeric Materials: Opprotunities in Electronics, Optoelectronics, and Molecular Electronics, Kluver academic, Dordrecht (1990).

[13] L. Y. Chiang, P. M. Chaikin, and D. O. Cowan, Advanced Organic Solid State Materials, MRS, Pittsburgh (1990).

[14] J. Messier, F. Kajzar, and P. Prasad, Organic Molecules for Nonlinear Optics and Photonics, Kluver Academic, Dordrecht (1991).

[15] L. Yang, Q. Z. Wang, P. P. Hho, R. Dorsinville, R. R. Alfano, W. K. Zou, N. L. Yang, Appl. Phys. Lett., 53, 1245 (1988).

[16] M. J. S. Dewar, J. Am. Chem. Soc., 106, 669 (1984).

[17] Z. H. Kafafi, et al., Chem. Phys. Lett., 188, 492 (1992).

[18] S. R. Flom, et al., Phys. Review B, 46, 15598 (1992).

[19] H.W. Kroto, J. R. Heath, S. C. O'Brien, R. F. Curl, and R. E. Smalley, Nature 318, 162 (1985).

[20] W. Kradschemer, L. D. Lamb, K. Fostiropoulos, and D. R. Huffman, Nature 374, 354 (1990).

[21] Y. Chai, T. Guo, C. Jin, R. E. Haufler, L. P. F. Chibante, J. Fure, L. Wang, J. M. Alford, and R. E. Smalley, J. Phys. Chem., 95, 7564 (1991).

[22] M. J. Rosker, H. O. Marcy, Y. C. Tallis, J. T. Kooury, K. Hansen, R. L. Whetten, Chem. Phys. Lett., 196, 427 (1992).

[23] J. R. Lindle, R. G. S. Pong, F. J. Bartoli, Z. H. Kafafi, Physical Review B, 48, 9447 (1993).

[24] F. Kajzar, C. Taliani, R. Danieli, S. RRRossini, R. Zamboni, Phys. Rev. Lett., 73, 1617 (1994).

[25] L. Yang, E. Royer, A. D. Walser, R. Dorsinvile, Chem. Phys. Lett., 239, 399 (1995).

[26] H. Huang, G. Gu, S. Yang, J. Fu, P. Yu, G. K. L. Wong, Y. Du, J. Phys. Chem. B, 102, 61 (1998).

[27] G. M. Carter, Y. J. Chen, S. K. Tripathy, Appl. Phsy. Lett. 43, 891 (1983).

[28] D.A.D.Miller, D. S. Chemla, D. J. Eilenberger, P. W. Smith, A. C. Gossard, and W. T. Tsang, Appl. Phys. Lett., 41, 679 (1982); 42, 925 (1983).

[29] R. K. Jain, R. C. Lind, J. Opt. Soc. Am. 73, 647 (1983).

[30] J. Drag, G. Hernandez, S. Mukamel, Phys. Rev. A, 37, 3835 (1988).

[31] F. C. Spano, and S. Mukamei, J. Chem. Phys. 91, 683 (1989).

[32] W. L. Wilson, P. F. Swajowski, and L. E. Brus, Science, 262, 1242 (1993).

[33] M. Ehbrecht, H. Ferkel, F. Huisken, L. Holz, Y. N. Polivanov, V. V. Smirnov, O. M. Stelmakh, and R. Schmid, J. Appl. Phys., 78, 5302 (1995).

[34] C. Flytzanis, and J. Hutter, in "Contemporary nonlinear optics", Academic Press Inc., New York, p 299 (1992).

[35] G. Timp, Nanotechnology, Springer Verlag, New York, p 330 (1999).

[36] J. S. Lindsey, NewJ. Chem., 15, 153 (1991).

[37] P. N. Prasad, D. J. Williams, Introduction to nonlinear optical effects in molecules and polymers, John Willey and Sons Inc., p .161 (1991).

[38] L. Canham, Appl. Phys. Lett., 57, 1046 (1990).

CHAPTER 2

THEORETICAL BACKGROUND AND EXPERIMENTAL TECHNIQUES

2.1. Introduction to nonlinear optics

Nonlinear optics is the study of phenomena that occurs as a result of modification of the optical properties of a material system by the presence of sufficiently intense laser light. In order to describe an optical nonlinearity precisely, the relationship between the polarization of a material and the strength of the applied electric field should be considered.

When electromagnetic waves propagate in a material, the atoms and molecules oscillate at the frequencies of the electric field applied and at different combinations of those frequencies as a result of the nonlinear response of the medium. When an electric field is applied, positively charged particles move in the direction of the applied field and negatively charged particles move in the opposite direction of the field. Displacement of the positive and negative charged particles creates a dipole moment. Induced polarization of the medium is described as a dipole moment per unit volume.

In the case of linear optics i.e. when the applied electric field is sufficiently small, the induced polarization is linearly proportional with the applied electric field E

$$P=\chi^{(1)}.E, \tag{2.1}$$

where $\chi^{(1)}$ is known as the linear susceptibility. In nonlinear optics i.e. when the applied electric fields are high enough, the relationship between the induced polarization and the applied field is given by the following nonlinear equation,

$$P=\chi^{(1)}E+\chi^{(2)}EE+\chi^{(3)}EEE+\ldots, \tag{2.2}$$

$$P=P^{(1)}+P^{(2)}+P^{(3)}\ , \tag{2.3}$$

where $\chi^{(2)}$ and $\chi^{(3)}$ are second- and third-order nonlinear susceptibilities respectively. The first term is responsible for linear absorption and refraction. The second-order nonlinear optical interactions can occur only in noncentrosymmetric crystals i.e. crystals that do not have inversion symmetry. Since liquids, gases, amorphous solids (such as glass), and many crystals have inversion symmetry, $\chi^{(2)}$ is zero for such media. Third-order nonlinear optical interactions described by $\chi^{(3)}$, can occur both for centrocymetric and noncentrosymmetric materials. The real and imaginary parts of $\chi^{(3)}$ give nonlinear refraction and two-photon absorption, i.e. nonlinear absorption, respectively.

In general the electric field has several different frequency components. Lets consider the simple case in which the applied field is given by

$$E(t)=\varepsilon\cos\omega t. \tag{2.4}$$

Since, $\cos^3\omega t=(1/4)\cos 3\omega t+(3/4)\cos\omega t$, the third order nonlinear polarization $P^3(t)$ can be written as

$$P^3(t)= =(1/4)\chi^{(3)}\varepsilon^3\cos 3\omega t+(3/4)\chi^{(3)}\varepsilon^3\cos\omega t. \qquad (2.5)$$

The first term is the response of the applied electric field at frequency ω. This term correspond to the third harmonic generation process, which is illustrated in Fig. 2.1. Third harmonic generation is a process in which three photons of frequency ω are destroyed and one photon of frequency 3ω is created.

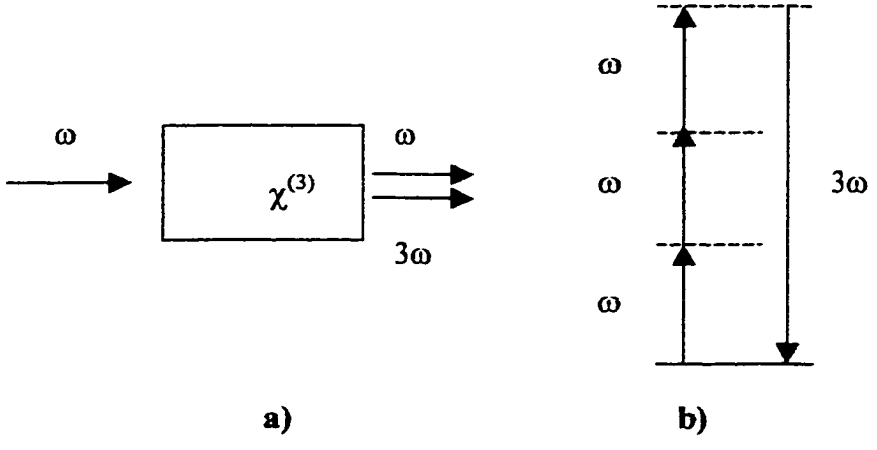

Fig.2.1 Third-harmonic generation a) Geometry of interaction b) Energy-level diagram

The second term of the equation above gives a nonlinear contribution to the polarization at frequency ω. This term leads to a nonlinear contribution to the refractive index experienced by a wave at frequency ω. The intensity dependent refractive index is expressed as follows.

$$n = n_0 + n_2 I \tag{2.6}$$

In equation 2.6 the n_0 represents the linear or low intensity refractive index; n_2 represents the nonlinear refractive index; I represents the intensity of the incident wave.

The development of fiber optic communication and the potential of optical computing have increased the interest in optical switches and optical couplers because of their size, fast response and low loss properties. For example, an all-optical on-off switch can be formed using a Mach-Zender interferometer (see figure 2.2). A Kerr medium (i.e. medium with high χ^3) is placed on one arm of the interferometer. The transmittance of the interferometer can be turn on and off by turning the controlling light on and off. This is because turning the controlling light on will induce a power dependent phase shift (nonlinear phase shift) in the nonlinear media. As a result of the intensity dependent refractive index, the amount of the phase shift can be adjusted to produce constructive or destructive interference at the end of the interferometer.

In order to build such nonlinear optical devices the intensity dependent refractive index of the nonlinear material needs to be measured and optimized. The intensity dependent refractive index is proportional to the third order nonlinear susceptibility of the material. In general, the third order nonlinear susceptibility is considered to be a complex quantity.

$$\chi^{(3)} = \chi^{(3)}_R + i\chi^{(3)}_I \tag{2.7}$$

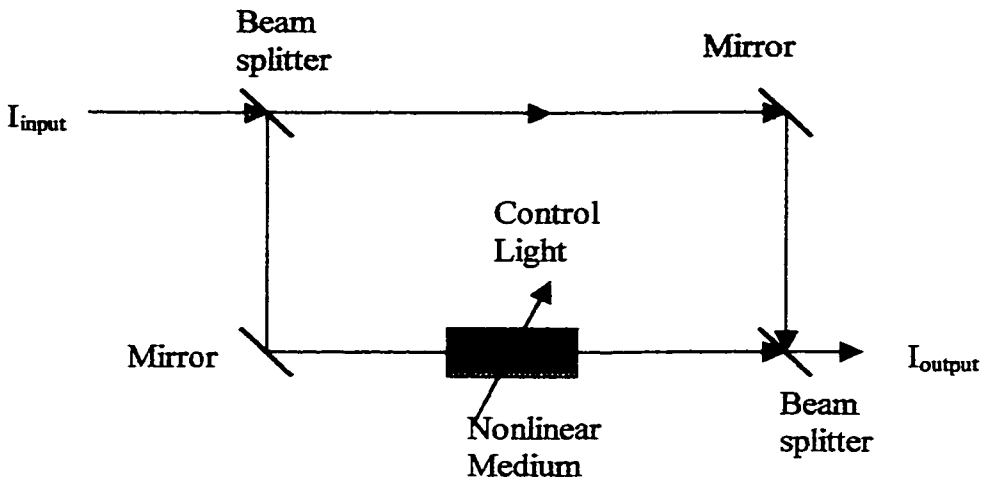

Fig.2.2 The all-optical on-off switch formed by a Mach-Zender interferometer

Where the real part is related to the nonlinear refractive index and the imaginary part is related to two-photon absorption described below.

The two-photon absorption process occurs when the material has an electronic excited level at twice the frequency ω of the input beam. In this process, an atom makes a transition from its ground state to an excited state by simultaneous absorption of two laser photons. The absorption cross section in this process increases linearly with laser intensity. This process is illustrated in Fig. 2.3.

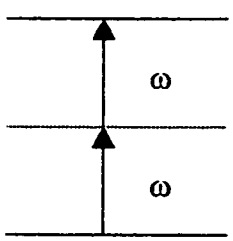

Fig.2.3 Two-photon absorption

Five experimental techniques are currently widely used to characterize the third order nonlinear optical coefficient χ^3 of a material: the degenerate four wave mixing technique (DFWM), which gives the magnitude and response time of χ^3; the optical Kerr effect (OKE), which is normally sensitive to the real part of χ^3 but can be modified to determine the imaginary part; the Z-scan technique which gives the size and the sign of the nolinearity; the third harmonic generation (THG), which probes the purely electronic component of the nonlinearity; and the electric field induced second harmonic generation (EFISH) technique, which is used in liquids to measure the reorientational component of the nonlinear response. Detailed descriptions of these experiments can be found in a recent review paper[1]. In this thesis the single beam Z-scan experimental technique, which is described in section 2.3 is used to measure the real and imaginary part of the nonlinear susceptibility.

The dynamics of the electronic structure of a material plays an important role in its nonlinear optical behavior. In this thesis, the pump and probe spectroscopic technique is used to understand this behavior. A detailed explanation of this technique is given in section 2.4.3 and 2.4.4.

2.2. *Experimental apparatus*

A schematic diagram of the laser system used for the experiments is shown in Fig. 2.4. A diode pumped CW Nd:YVO_4 laser with 5 W power at 532 nm is used to pump a Ti:Sapphire oscillator. The output of the Ti:Sapphire oscillator at 800 nm, 800 mW power, and 80 fs pulse duration is used as a seed beam for a Ti:Sapphire regenerative amplifier. The regenerative amplifier is pumped by a Nd:YLF laser which has 10 W output power, 10 ns pulse duration and 532 nm wavelength. The regenerative amplifier provides an 800 nm wavelength output at 1 KHz repetition rate and allows us to change the pulse duration of the beam from 100 fs to about 2 ps.

The Ti:sapphire amplifier setup can be devided in three part. The first part is the pulse stretcher. During the amplification process, the laser beam needs to be focused to a small spot size. When a short pulse laser is focused, the increased intensity causes optical damage. Thus, before amlifying a short pulse, the pulse needs to be broadened. The pulse stretcher increases the pulse duration of the seed beam coming from the Ti:sapphire oscillator. The broadened seed beam is directed to the second part of the Ti:Sapphire amplifier called the regenerative amplifier. In the regenerative amplifier, the pump beam at 532 nm is focused into a Ti:Sapphire rod and the broadened seed beam at 800 nm is amplified. After amplification, the seed beam goes to the pulse compressor. The pulse compressor compresses the amplified seed beam down to 100 fs by using a grating and a motorized delay. Finally, the compressed beam is sent to the output. The pulse duration of the output beam can be adjusted by changing the delay position. Thus, the output of the amplifier can be used to perform pulse duration dependent experiments.

The optical parametric amplifier, is used to generate an output wavelength tunable from the infrared to the near ultraviolet (2 μm to 400 nm). The optical parametric amplifier uses the output of the Ti:Sapphire amplifier. 1% of the Ti:Sapphire amplifier is used to generate a white light continuum, the rest is used for amplification. The white light continuum and the input beam at 800 nm are frequency mixed in a LBO crystal to generate tunable signal (at about 1000 nm) and idler (at about 2000 nm). The wavelengths of the signal and idler can be tuned by changing the phase matching angle of the crystal and by adjusting the time delay for that particular angle. The signal and idler beams can be used to generate second harmonic wavelengths by using NLO crystals. One can get all the wavelengths between 400 nm and 2000 nm by tuning signal and idler wavelengths and by using second harmonics of these wavelengths. The white light continuum generation and frequency mixing techniques are explained in section 2.4.2.

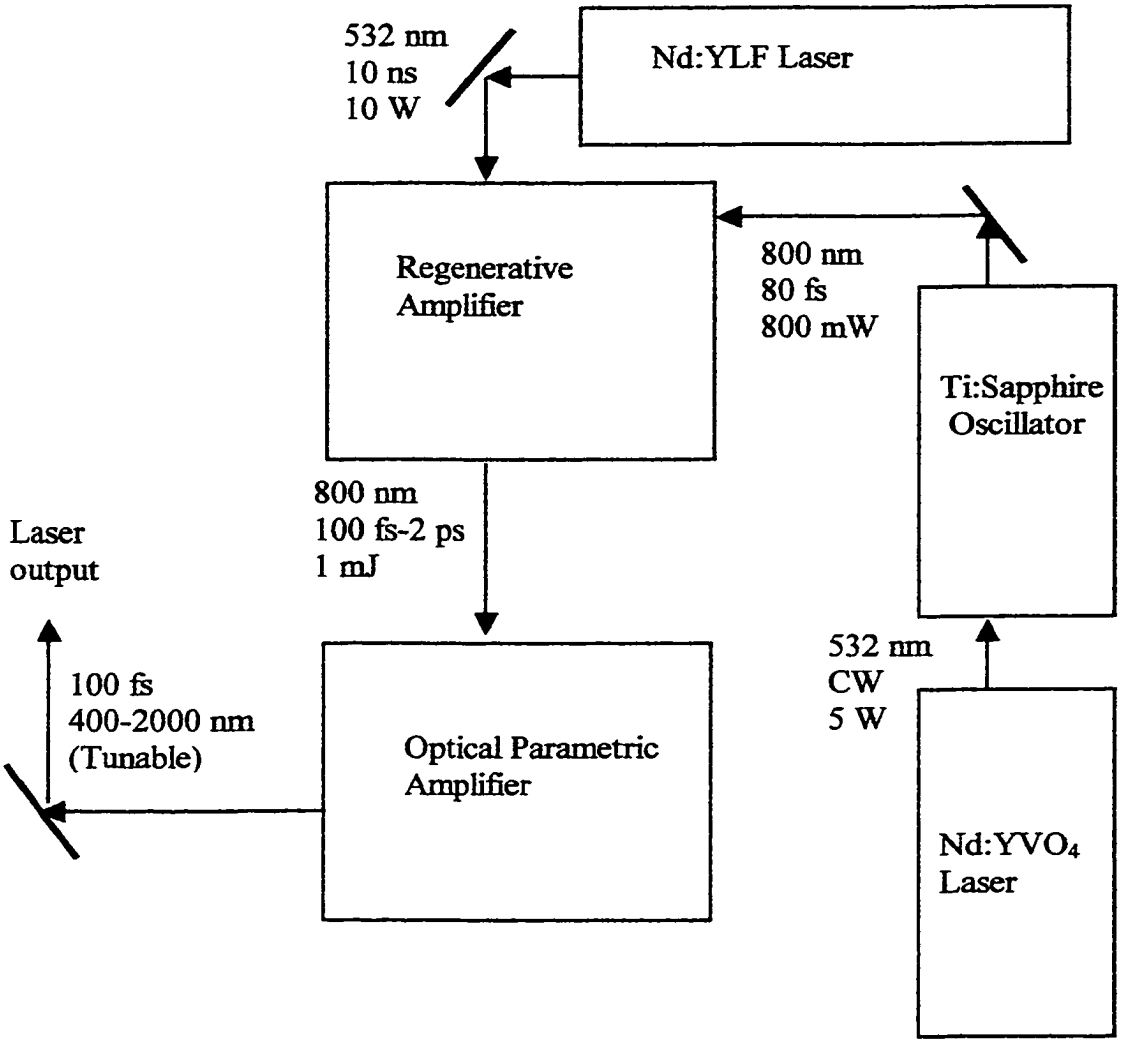

Fig.2.4 Schematic diagram of the laser system

2.2. *Measurement of the third order nonlinearity*

2.2.1. Z-Scan technique

Z-scan[2, 3] is a simple and sensitive single beam technique for measuring the magnitude and sign of χ^3. From this measurement, both the size and the sign of the third order nonlinearity can be determined.

The experimental apparatus used to perform the Z-scan technique is illustrated in Figure 2.5. If the nonlinear material has a negative n_2 as the sample is translated from -z to +z, its behavior will act as a thin lens with a varying focal length. When the sample is far from the focal point, since the intensity is relatively low, little nonlinear refraction occurs and the transmittance remains constant. While the sample approaches the focal point, the intensity increases causing a change in the negative self-lensing effect.

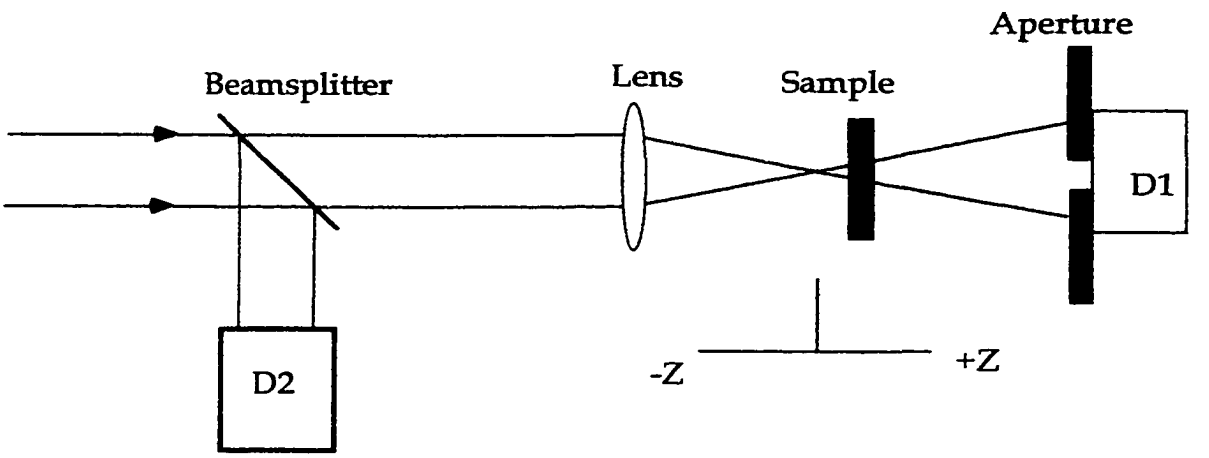

Fig.2.5 The Z-scan experimental apparatus in which the ratio D2/D1 is recorded as a function of the sample position z

A negative self-focusing effect before the focal plane causes a collimation or narrowing of the beam, which in turn increases the transmittance at the aperture. While the sample is scanning to the +z side after passing the focal point, the self-defocusing effect increases the divergence of the beam at the aperture and causes a decrease in the transmittance.

For materials with a negative (positive) n_2, the profile of the Z-scan transmittance curve will consist of a peak (valley) followed by a valley (peak) as the sample is translated from -z to +z. Figure 2.6 shows the valley-peak (v-p) sequence for positive nonlinearity and a peak-valley (p-v) sequence for negative nonlinearity.

The index of refraction n is expressed in terms of the nonlinear indexes n_2 (esu) or n_2 (MKS) through

$$n = \left\{ n_0 + \frac{n_2}{2} |E(\omega)|^2 \right\}_{esu} = \left\{ n_0 + n_2 I \right\}_{MKS} \tag{2.8}$$

n_o is the linear index of refraction, E is the peak electric field (cgs), and I represents the irradiance (W/m^2 in mks units) of the laser in the sample. The relationship between n_2 (esu) and n_2 (mks) is n_2 (esu) = $(cn_o/40\pi)$ n_2 (mks) where c (m/s) is the speed of light in vacuum. Lets assume a TEM_{00} beam with a Gaussian spatial profile (and beam waist radius of w_o) traveling in the +z direction. This beam is expressed[4] as:

$$E(z,r,t) = E_0(t)\frac{w_0}{w(z)}\exp\left(-\frac{r^2}{w^2(z)} + \frac{ikr^2}{2R(z)} + i\phi(z,t)\right) \tag{2 .9}$$

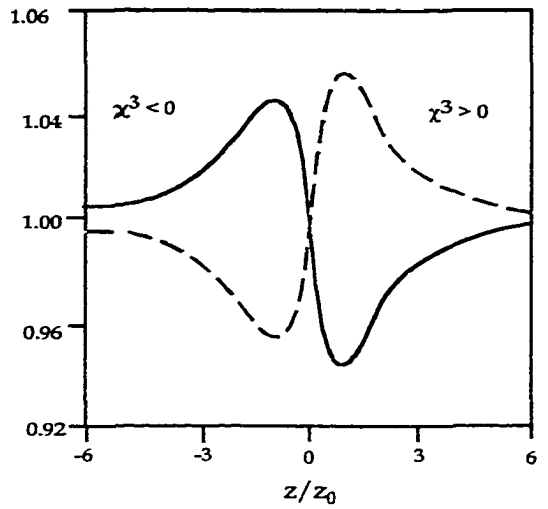

Fig.2.6 Calculated Z-scan profile

where $w^2(z) = w_0^2 (1 + z^2/z_0^2)$ is the beam radius, $R(z) = z (1 + z_0^2/z^2)$ is the radius of curvature of the wave-front at z , $z_0 = kw_o^2/2$ is the diffraction length of the beam, $k = 2\pi/\lambda$ is the wave vector and λ is the laser wavelength in free space.

The spatial shape of the beam plays an important role in the analysis of the Z-scan profile, a point that will be examined in greater detail later on. The sample is assumed to be thin which means that the medium length is short enough that changes in the beam diameter in the sample due to nonlinear refraction or diffraction can be neglected. This assumption is applicable for $L << z_o/\Delta\Phi(0)$, in fact it has been shown that the condition $L < z_0$ is restrictive enough for the thin film approximation. The input beam is traced through the optical apparatus to find the normalized transmittance at the aperture (normalized Z-scan).

The electric field exiting the sample E_e,

$$E_e(r,z,t) = E(r,z,t)e^{-\alpha L/2}e^{i\Delta\Phi(z,r,t)} \qquad (2.10)$$

contains the nonlinear phase term

$$\Delta\Phi(z,r,t)=\Delta\Phi_0(z,t)\exp\left(-\frac{2r^2}{w^2(z)}\right) \tag{2.11}$$

with

$$\Delta\Phi_0(z,t)=\frac{\Delta\Phi_0(t)}{1+z^2/z_0^2} \tag{2.12}$$

$\Delta\Phi_0(t)$ is the on-axis phase shift at the focus defined as

$$\Delta\Phi_0(t)=k\Delta n_0(t)L_{eff} \tag{2.13}$$

where $L_{eff} = (1 - e^{-\alpha L})/\alpha$ is the effective sample length, α is the linear absorption coefficient, $\Delta n_0 = n_2(\text{mks})\, I_0(t)$ with $I_0(t)$ the on-axis intensity at the focus point (i.e. $z = 0$).

Using the "Gaussian decomposition" (GD) method[5], where the complex electric field at the exit plane of the sample is decomposed into a summation of Gaussian beams via a Taylor series expansion of the nonlinear phase term,

$$e^{i\Delta\Phi(z,r,t)}=\sum_{m=0}^{\infty}\frac{[i\Delta\Phi_0(z,t)]^m}{m!}e^{-2mr^2/w^2(z)} \tag{2.14}$$

the resultant electric field pattern at the aperture is reconstructed as

$$E_a(r,t)=E(z,r=0,t)e^{-\alpha L/2}\sum_{m=0}^{\infty}\frac{[i\Delta\Phi_0(z,t)]^m}{m!}\frac{w_{m0}}{w_m}\cdot\exp\left(-\frac{r^2}{w_m^2}-\frac{ikr^2}{2R_m}+i\theta_m\right) \tag{2.15}$$

by propagating each Gaussian beam to the aperture plane. The propagation distance in free space from the sample to the aperture plane is defined by d and all other parameters are expressed as

$$g = 1 + d / R(z) \tag{2.16}$$

$$w_{m0}^2 = \frac{w^2(z)}{2m+1} \tag{2.17}$$

$$d_m = \frac{kw_{m0}^2}{2} \tag{2.18}$$

$$w_m^2 = w_{m0}^2 \left[g^2 + \frac{d^2}{d_m^2} \right] \tag{2.19}$$

$$R_m = d \left[1 - \frac{g}{g^2 + d^2 / d_m^2} \right]^{-1} \tag{2.20}$$

and

$$\theta = \tan^{-1} \left[\frac{d / d_m}{g} \right] \tag{2.21}$$

The GD method is very useful for small phase distortions, which are detected using the Z-scan technique since only a few terms of the sum are needed. In addition, this method can be easily extended to higher order nonlinearities.

Spatially integrating $E_a(r,t)$ to the aperture radius r_a results in the transmitted power through the aperture, giving

$$P_T(\Delta\Phi_0(t)) = c\varepsilon_0 n_0 \pi \int_0^{r_a} |E_a(r,t)|^2 r dr \tag{2.22}$$

where ε_0 is the permittivity in vacuum. The normalized Z-scan transmittance T(z) is calculated using

$$T(z) = \frac{\int_{-\infty}^{\infty} P_t(\Delta\Phi(t))dt}{S\int_{-\infty}^{\infty} P_i(t)dt} \tag{2.23}$$

where

$$P_i(t) = \pi w_0^2 I_0(t)/2 \tag{2.24}$$

is the instantaneous input power in the sample and

$$S = 1 - \exp(-2r_a^2 / w_a^2) \tag{2.25}$$

is the aperture linear transmittance, with w_a as the beam radius at the aperture in the linear regime.

While the Z-scan experimental apparatus is simple, curve fitting the experimental data is not entirely trivial, thus detracting a bit from its appeal as a working experimental tool. However, it has been shown[2, 3] that an easily measurable quantity such as the difference between the normalized peak and valley transmittance ($\Delta T_{p-v} = T_p - T_v$) can be used to estimate the nonlinear index (n_2) with considerable accuracy (i.e. ΔT_{p-v} variations within +/- 2%) by using the following expression

$$\Delta T_{p-v} \approx 0.406(1-S)^{0.25}|\Delta\Phi_0| \tag{2.26}$$

for $|\Delta\Phi_0| \leq \pi$ after a Z-scan is performed.

Nonlinear Absorption Effects: Nonlinear absorption can have a strong effect on the Z-scan profile. When the nonlinear absorption is significant the closed aperture Z-scan transmittance will be distorted (where in some cases the peak will be suppressed and the valley enhanced). If we consider only the effects of two-photon absorption (TPA) the third-order nonlinear susceptibility can be considered complex and represented by a real ($\chi_R^{(3)}$) and imaginary part ($\chi_I^{(3)}$) as it is written in equation 2.7. The imaginary part of the third-order nonlinear susceptibility is related to the TPA coefficient β through

$$\chi_I^{(3)} = \frac{n_0^2 \varepsilon_0 c^2}{\omega}\beta \tag{2.27}$$

and the real part is related to n_2(mks) through

$$\chi_R^{(3)} = 2n_0^2 \varepsilon_0 c n_2(mks). \tag{2.28}$$

When the aperture is removed (S =1), the Z-scan transmittance is only a function of the nonlinear absorption. The open aperture Z-scan profile is symmetrical with respect to the focus plan (z = 0) where the transmittance is a minimum (i.e., multiphoton absorption) or a maximum (i.e., absorption saturation).

Provided that $\beta I_0 L_{eff} < 1$ is satisfied there is a simple method for separating β and n_2(mks). The refractive part of $\chi^{(3)}$ can be determined by dividing the closed aperture (S < 1) normalized Z-scan (with a low irradiance background Z-scan subtraction to reduce sample inhomogeneities) by the open-aperture (S = 1) normalized transmittance. This will result in a new Z-scan where ΔT_{p-v} agrees to within +/- 10 % of that obtained from a purely refractive Z-scan.

One can calculate $\chi^{(3)}$ relative to a reference material under the same excitation and experimental conditions. In this case, the combination of equations (2.13), (2.26) and (2.28) can be used:

$$\frac{\chi^{(3)}_{sample}}{\chi^{(3)}_{reference}} = \left(\frac{n_0^2 \Delta T_{p-v}}{L_{eff}}\right)_{sample} * \left(\frac{L_{eff}}{n_0^2 \Delta T_{p-v}}\right)_{reference} \tag{2.29}$$

In the case of two-photon absorption, normalized close aperture measurement and normalized open aperture measurement should be divided. This divided curve gives the normalized z-scan measurement. ΔT_{p-v} can be calculated from the distance between the peak and the valley of normalized z-scan measurement.

If the sample is a thin film on a clean glass substrate both open aperture and far field small aperture z-scan transmittance measurements should be carried out on the thin film on a substrate and on a clean substrate to take into account the substrate contribution. In order to get ΔT_{p-v} for the film, the normalized z-scan measurement of the clean substrate should be subtracted from that of the thin film on a substrate.

2.4. Ultrafast measurement methods

2.4.1. Pulse duration measurements (autocorrelation and cross-correlation techniques)

Autocorrelation and cross-correlation measurements are standard techniques used to measure ultrashort laser pulse duration. Figure 2.7 shows the experimental setup for the autocorrelation technique.

The autocorrelation technique is based on the following principle[6]. The optical pulse with ΔT pulse duration is split into two pulses, which travel different distances. For a travel difference $\Delta S=S_1-S_2$, the time difference between the two pulses is given by $\tau=\Delta S/C$. Then the two pulses are focused into a nonlinear crystal (in this case KDP: Potasium-dihydrogen-phosphate) which doubles the optical frequency. When the photons

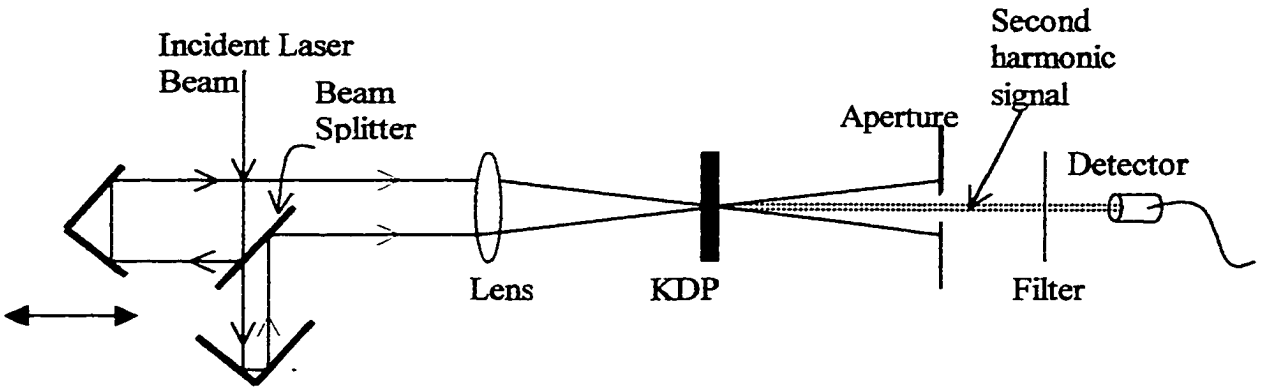

Fig.2.7 Autocorrelation setup

coming from each beam overlap on the crystal temporally and spatially, a second harmonic signal in the phase matched direction can be detected. The detected second harmonic signal intensity versus delay time gives the autocorrelation function. The pulse duration of the laser can be obtained by deconvolution.

In this thesis, two 800 nm pulses split from one pulse are focused by a 20 cm focal lens into a 200 μm KDP nonlinear crystal. The generated second harmonic signal at 400 nm wavelength is detected by a silicon photodetector while varying the delay of one pulse. Since the laser generates nearly gaussian pulses, the detected second harmonic intensity versus delay time curve is fitted to a gaussian distribution. The pulse duration of the laser is determined by calculating the full width half maximum (FWHM) from the curve fitting.

If two pulses have different wavelengths, this technique is called the cross-correlation technique. In the case of cross-correlation two pulses with frequencies ω_1 and ω_2 ($\neq\omega_1$) are focused into a KDP crystal and sum frequency $\omega_3=\omega_1+\omega_2$ is detected in the phase matched direction of the crystal. The pulse duration of the white light continuum and the chirp in the continuum are measured by using the cross correlation technique as described in the next section.

2.4.2. White light continuum generation and analysis

Spectroscopic measurements such as pump and probe spectroscopy techniques require a spectrally broad short pulse (i.e. white light continuum) to measure the transient absorption spectrum. By focusing a short pulse laser into a transparent medium, self

phase modulation (SPM) leads to the generation of white light continuum[7, 8]. White light continuum maintains it's short pulse duration. SPM is the change in the phase of an optical pulse due to the nonlinearity of the refractive index of the material[9] (see equation 2.6). When an intense short pulse described by the electric field

$$\vec{E}(z,t) = \vec{A}(z,t)e^{i(k_0 z - \omega_0 t)} + c.c. \tag{2.30}$$

propagates through a nonlinear medium, the phase of the pulse's electric field can be written as:

$$\phi(z,t) = \omega_0 t - kz = \omega_0 t - \frac{\omega_0 n(t)}{C} z = \omega_0 t - \frac{[n_0 + n_2 I(t)]\omega_0}{C} z \tag{2.31}$$

The temporal variation dϕ/dt of the pulse gives the frequency ω(t):

$$\omega(t) = \frac{d\phi(z,t)}{dt} = \omega_0 - \frac{n_2 z \omega_0}{C} \frac{dI(t)}{dt} \tag{2.32}$$

As it is seen from equation 2.31 and 2.32, the time dependent refractive index modulates the instantaneous phase and consequently generates different frequency components. Therefore, both redder and bluer frequencies relative to the input frequency are generated. If the nonlinear refractive index is positive (n_2>0), the leading edge of the

incident pulse $\left(\frac{dI(t)}{dt} > 0\right)$ generates lower frequencies (redder components) and trailing edge of the pulse generates higher frequencies (bluer components).

In this thesis, white light continuum is generated by focusing the amplified 100 fs pulse with a 6 cm focal lens into a 2 mm thick Sapphire plate. White light continuum is collimated by a 5 cm focal lens into a 4 mm spot size beam. Figure 2.8 shows the spectrum of the continuum detected by Ocean Optics Fiber Optic Spectrometer.

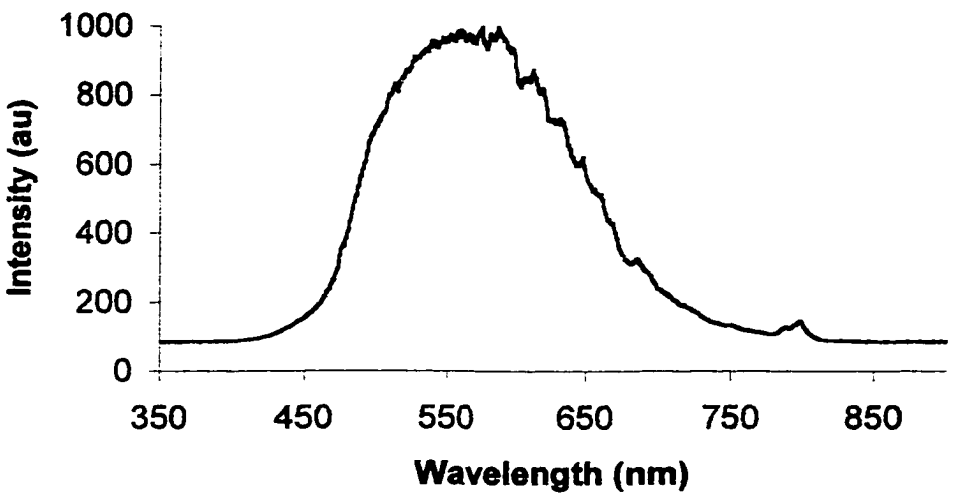

Fig.2.8 White light continuum generated by focusing 800 nm short pulse into a Sapphire plate

The group velocity dispersion (GVD) of the white light continuum is very large due to its broad bandwidth. The group velocity dispersion can be explained as follows:

When an optical pulse with the spectral amplitude distribution E(ω) propagates through a medium with refractive index n(ω), it's group velocity is given by

$$v_g = \frac{d\omega}{dk} = \frac{d}{dk}(v_{ph}k) = v_{ph} + k\frac{dv_{ph}}{dk} \tag{2.33}$$

the group velocity of the pulse shows dispersion:

$$\frac{dv_g}{d\omega} = \frac{dv_g/dk}{d\omega/dk} = \frac{1}{v_g}\frac{d^2\omega}{dk^2} \tag{2.34}$$

For $\left(d^2\omega/dk^2\right) \neq 0$, the velocity changes for different frequency components of the pulse (i.e. shape of the pulse will change during its propagation through the medium).

For a medium with "normal dispersion" (such as glass) the GVD generates a frequency chirp in the white light continuum such that the leading edge is red shifted and the trailing edge is blue shifted from the incident carrier frequency. The chirp of the white light is measured by using the cross-correlation method. Figure 2.9 shows the cross correlation setup. The 800 nm laser beam and the white light continuum are focused into a 200 μm thick KDP crystal by using 40 cm and 15 cm focal length lenses respectively. Different angles of the crystal are phase matched to one particular wavelength of the white light continuum resulting in the generation of a UV wavelength. The UV signal is selected by a spectrometer (SPEX 270 M) and detected by a UV sensitive photomultiplier tube. The continuum frequency ω_c can be obtained by measuring the UV signal frequency:

$$\omega_c = \omega_{800} + \omega_{UV} \tag{2.35}$$

where ω_{800} is the frequency at 800 nm pulse and ω_{UV} is the measured sum frequency UV pulse. The UV signal is detected only when two pulses overlap in time and in space at the correct angle of the crystal. Note that this angle is determined by the wavelengths of the two pulses and the crystal structure. Time overlap is achieved by changing the position of the delay line. Since the white light continuum is chirped, only one wavelength of the continuum will overlap with the 800 nm pulses in time for each position of the delay line. Thus, different UV wavelengths are detected at different times (i.e. delay line positions). So, by detecting the UV wavelengths and the time differences, we can determine the dispersion of the continuum. Figure 2.10 shows the dispersion curve of the white light continuum generated by a 2 mm thick Sapphire plate.

One can always get a rough estimate of the white light's pulse duration at a particular wavelength by detecting the frequency mixed UV light versus delay time and fitting this curve to a gaussian distribution. This technique is used in chapter 4.

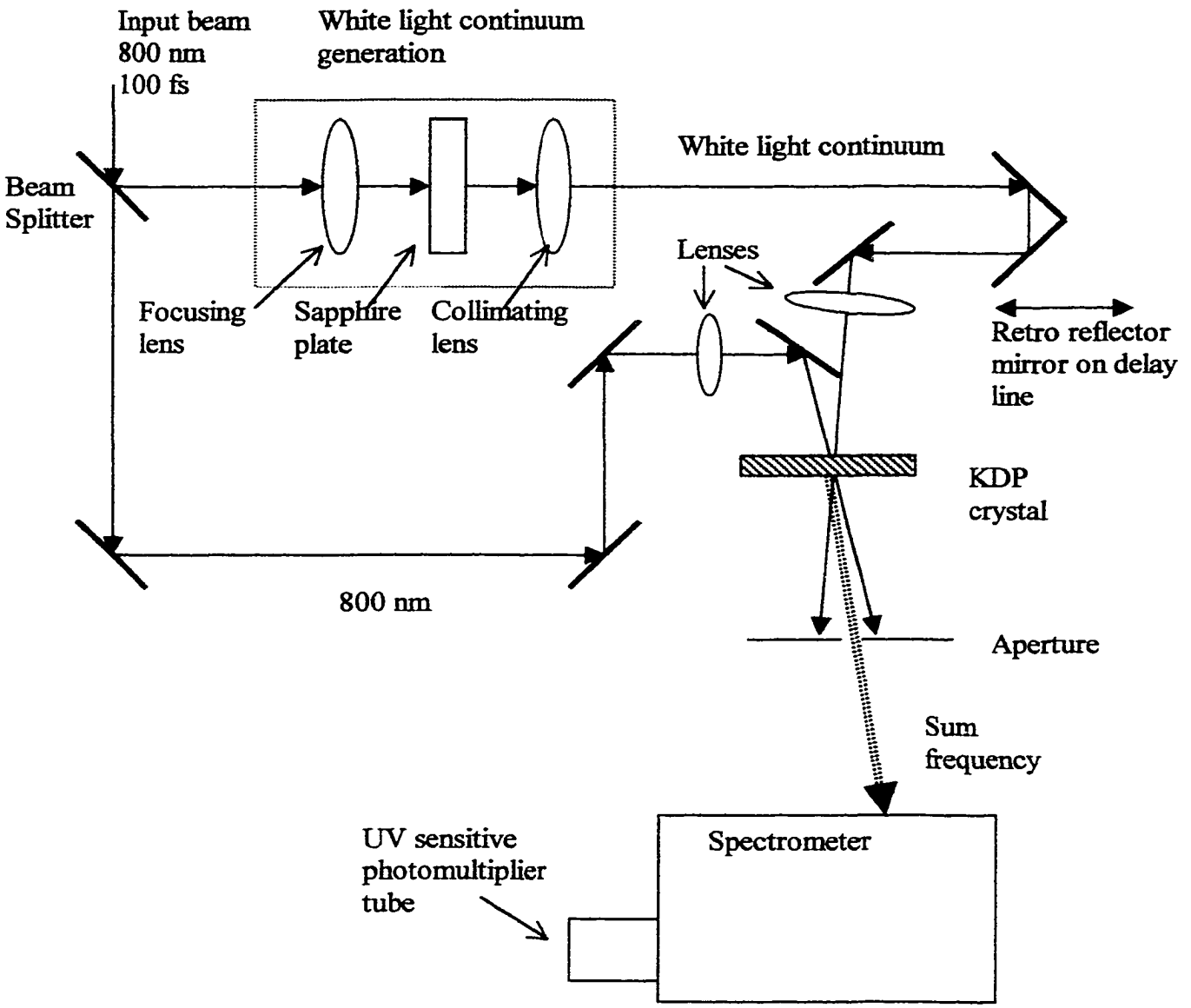

Fig.2.9 Cross-correlation setup to measure the chirp of white light continuum

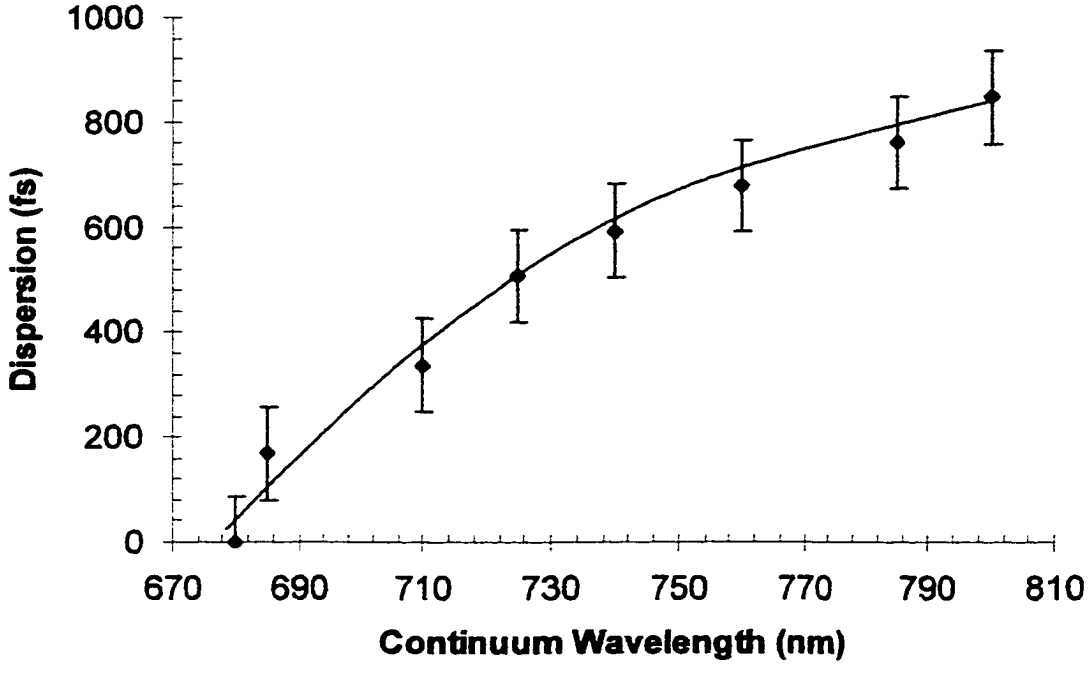

Fig.2.10 Dispersion of white light continuum generated by 2 mm thick sapphire plate relative to 680 nm

2.4.3. Time resolved pump-probe spectroscopy with white light continuum

The pump and probe technique is used for transient absorption spectroscopy. Figure 2.11 shows the setup for pump-probe spectroscopy with white light continuum.

The pump probe technique is based on the following principle. The molecules under investigation are excited by an intense and fast laser pulse. A weak probe pulse with a variable time delay probes the time evolution of the population density of excited states while the material relaxes to its original state or moves through some photochemical reaction.

The output of the OPA (Optical Parametric Amplifier) is used as a pump beam in order to have a tunable pump between 400 nm-2000 nm. The probe beam, the white light continuum is generated by focusing the residual 800 nm from the OPA into a transparent medium. A fiber optics spectrometer (Ocean Optics. Inc.) with two fiber channels is used for this experiment. A small portion of the probe is focussed into channel 1 of the spectrometer as a reference beam $I_R(\lambda)$. Pump and probe pulses are focused and physically overlapped on the sample by using 20 cm focal length lenses. The pump pulse is dumped after the sample while the probe pulse is focused into the other channel of the spectrometer $I_T(\lambda)$. The time delay between the pump pulse and the probe pulse is adjusted by changing the path length of the white light continuum with a retroreflector mirror mounted on a long delay line (approximately 40 cm). The physical overlap of the pump and probe beams in the sample should not be changed during the experiment even while changing the path length of the probe.

The time overlap of the pump and probe pulses is an important parameter in this experiment. To adjust the time overlap, the sample is replaced with a second harmonic nonlinear crystal. A 200 μm thick KDP crystal cut for the 800 nm wavelength is used for this purpose. The pump pulse (587 nm) and the 800 nm beam associated with the white light are mixed in this crystal. After aligning the crystal's phase matching angle, the time delay between the two pulses is adjusted to find the frequency mixed signal generated by the crystal. When the 587 nm and 800 nm pulses overlap in time and in space, the second harmonic signal around 339 nm is detected at the phase matching angle of the crystal. The position of the delay line is marked as the zero time delay and is used as a reference during the experiment.

$I_T(\lambda,t)$ and $I_R(\lambda,t)$ are the transmitted spectra and the reference spectra respectively. The transmitted background spectra $I_{TB}(\lambda)$ and reference background spectra $I_{RB}(\lambda)$ are detected, when both pump and probe pulses are blocked; and are substracted from $I_T(\lambda,t)$ and $I_R(\lambda,t)$ respectively. The normalized transmission $T(\lambda,t)$ is the ratio $\frac{I_T(\lambda,t)-I_{TB}(\lambda)}{I_R(\lambda,t)-I_{RB}(\lambda)}$. The reference transmission $\left[\frac{I_T(\lambda)-I_{TB}(\lambda)}{I_R(\lambda)-I_{RB}(\lambda)}\right]_{ref}$ is calculated when there is no pump. Both the normalized transmission and the reference transmission are averaged in order to reduce the signal to noise ratio. Data acquision is achieved by using a Labview program. The following formula gives the normalized transmission change:

$$\frac{\Delta T}{T}=\frac{\dfrac{I_T(\lambda,t)-I_{TB}(\lambda)}{I_R(\lambda,t)-I_{RB}(\lambda)}}{\left[\dfrac{I_T(\lambda)-I_{TB}(\lambda)}{I_R(\lambda)-I_{RB}(\lambda)}\right]_{ref}}-1 \qquad (2.36)$$

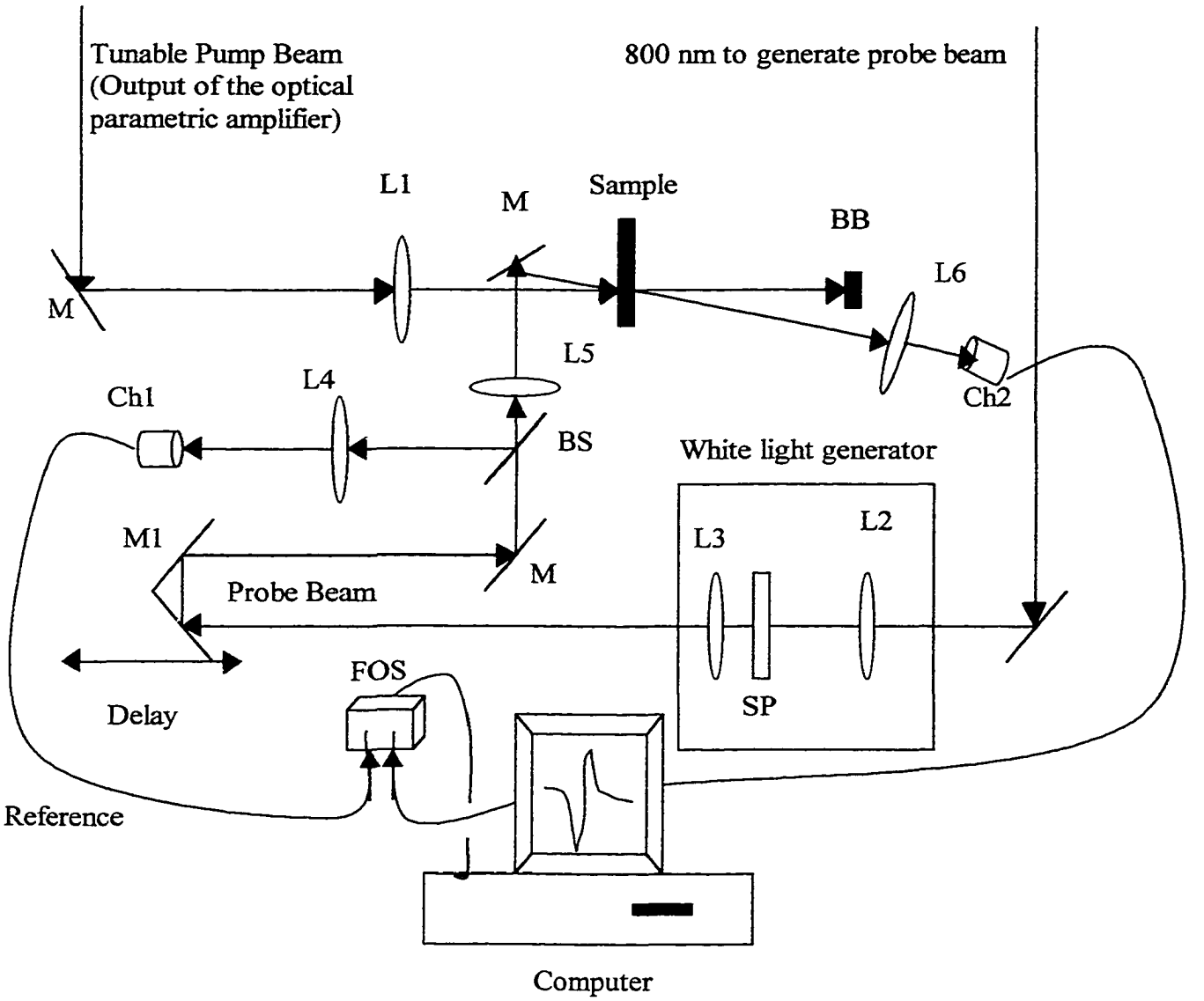

Fig.2.11 Pump-probe transient absorption setup (M:mirror; L1,L2, L4, L5, L6: focusing lenses; L3: columating lens for whight light continuum; SP: Sapphire plate; M1: retroreflector mirror; BS: beam pllitter; FOS: fiber optic spectrometer; Ch1, Ch2: channels of the fiber optic spectrometer)

2.4.4. 800 nm-pump and 800 nm-probe time resolved spectroscopy

Single wavelength time resolved spectroscopy is used to look at the dynamics of excited states at a specific wavelength. The experimental setup used for 800 nm- pump and 800 nm-probe time resolved spectroscopy is shown in figure 2.12.

Less than 10% of the main 800 nm beam is used as a probe beam while the rest is used as a pump.

The pump beam power can be varied with a ½ wave plate-polarizer pair as described below. The ½ wave plate is used to rotate the polarization of the input beam. When the polarization of the input beam is set such that it is perpendicular to the polarization state of the polarizer the input beam is reflected by the polarizer. By varying the polarization of the input beam with respect to the analyzing polarizer we can adjust the value of the input power used in the experiment. We do not use neutral density filters to reduce the power because the 800 nm fs pulses would bleach these filters.

Usually the pump and probe beams are cross-polarized to get rid of the 'coherent artifact'. The coherent artifact is an additional signal around zero delay due to coherent coupling between both optical beams. When the optical pulses overlap in time, more permutations in the field ordering contribute to the observed signal at finite delay. Hence, a rapid initial decrease of the signal is observed for small delays.

Pump and probe beams are focused into the sample by using 20 cm focal length lenses. In order to get better spatial overlap the angle between pump and probe beams should be very small (around 10 degree).

Another polarizer is set to transmit only the polarization of the probe to make sure that the scattered pump beam does not contribute to the detected probe signal. The detected beam is averaged by using a computer controlled Boxcar integrator. The time delay between pump and probe pulses is adjusted by a computer controlled motorized stage. The signal is detected and averaged for every position of the stage. The detected probe beam as a function of delay gives the time-resolved dynamics of the sample at this specific wavelength (800 nm).

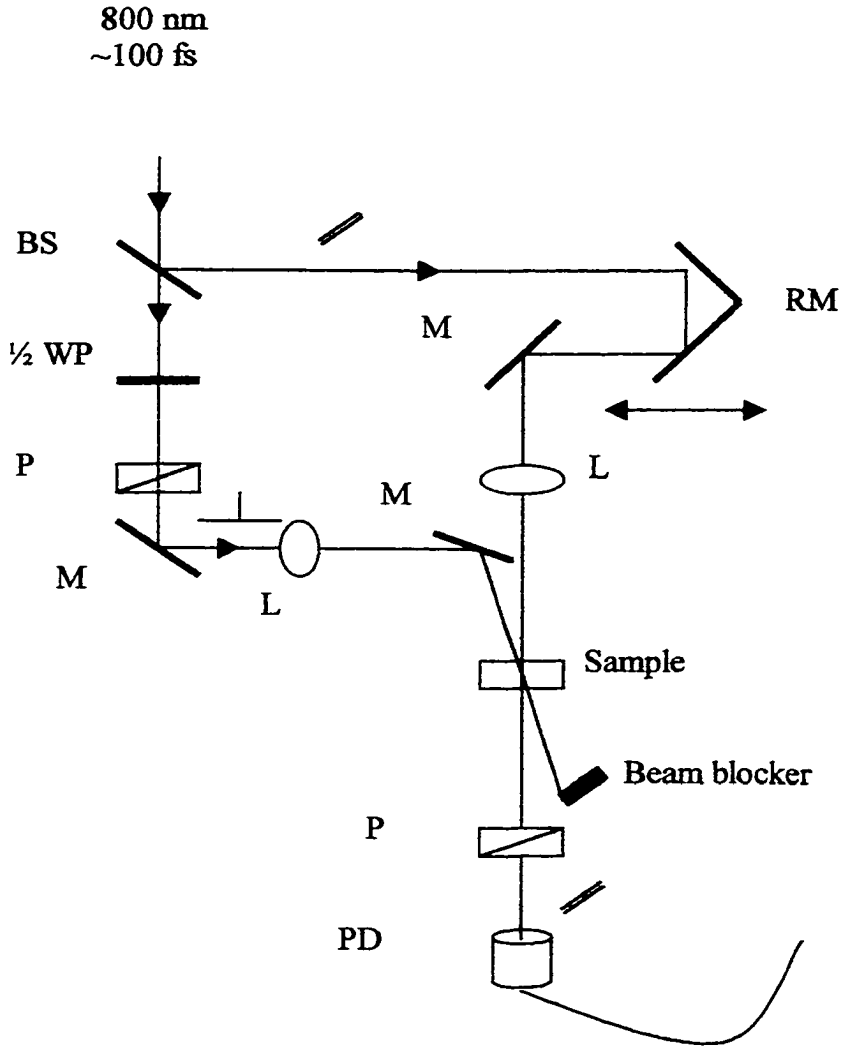

Fig.2.12 Experimental setup for 800 nm-pump 800 nm-probe time resolved spectroscopy (M: mirror; RM: retroreflective mirror; P: polarizer; ½ WP: half wave plate; L: lens; BS: beam splitter; PD: photo diode)

References:

[1] A. D. Walser, G. Coskun, R. Dorsinville, in "Electrical and optical polymer systems fundamentals, methods, and applications" edited by L. W. Donald, E. W. Gary, J. T. Debra, M. C. Thomas, D. G. Joseph, Marcel Dekker, New York, pp 423-452.

[2] M Sheik, A. A. Said and E. W. Van Stryland, Opt. Lett. 14, 955 (1989).

[3] M . Sheik, A. A. Said, T. H. Wei, D. J. Hagan and E. W. Stryland, IEEE J. Quantum Electron. QE-26, 760 (1990)

[4] H. Kogelnik, T. Li, Appl. Opt., 5, 1550 (1966).

[5] D. Weaire, B. S. Wherrett, D. A. B. Miller, and S. D. Smith, "Effect of Low Power Nonlinear Refraction on Laser Beam Propagation in LnSb," Optics Lett., vol. 4, pp. 331-333, (1974)

[6] W. Demtroder, Laser Spectroscopy: basic concepts and instrumentation, Second edition, Springer Verlag, Berlin, Germany (1996).

[7] R. Alfano, S. L. Shapiro, Phys. Rev. Lett., 24, 584 (1970).

[8] M. Yang, PhD thesis submitted to Graduate faculty in Electrical Engineering Department, The City University of New York (1993).

[9] R. W. Boyd, "Nonlinear Optics", Academic Press, London, UK, p275 (1992).

CHAPTER 3

NONLINEAR OPTICAL PROPERTIES OF METALLOFULLERENES

3.1. Review on fullerenes and metallofullerenes

Fullerenes represent the third form of pure carbon after the well-known structures of graphite and diamond. C_{60} was the first fullerene discovered. It has a soccer ball structure consisting of 12-five membered rings separated by 20 hexagonal benzene like rings. The structure of C_{60} is shown in figure 1. Because of the similarity of this structure with geodesic domes of Buckminister Fuller, they are named "Buckministerfullerene".

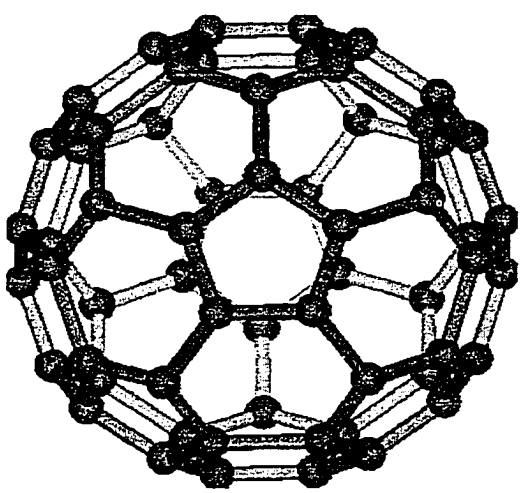

Fig.3.1 Structure of C_{60}

With a diameter of 0.7 nm, C_{60} represents one of the most reproducible nanostructures. The high reproducibility of C_{60} in the self-assembly process might indicate that there is only one way to assemble 60 carbon atoms in a closed cage configuration which obeys the isolated pentagon rule[1].

C_{60} has I_h (icosahedron) symmetry. This symmetry has the identity operation, 6 five-fold axes through the centers off the pentagonal faces, 10 three-fold axes through the centers of the hexagonal faces, 15 two-fold axes through the centers of the edges joining two hexagons. All the symmetry axes combined with the inversion operation results in 120 independent symmetry operations[2] in the icosahedral point group I_h. I_h is the highest possible point group symmetry for any molecule.

The recent discovery of a new mass production method,[3] allow the production of larger weight fullerenes such as C_{70}, C_{76}, C_{78}, C_{82}, C_{84}. Among these, C_{70} is the most studied fullerene. C_{70} has the lower symmetry D_{5h}, which is a subgroup of I_h (there is no inversion symmetry in this group). C_{70} exhibit a rugby-ball shape[4]. Usually fullerenes form isomers i.e. a given number of atoms can correspond to closed cage molecules with different geometrical structures. Each structure is called an isomer. For example, there are seven isomers (D_2, D_{5d}, C_{2v}, $C_{2v'}$, D_3, D_{5h} and I_h) for the C80 fullerene, which satisfy the isolated pentagon rule[5]. The characterization and isomer distribution of C_{80} (the first higher fullerene beyond C_{60} to allow I_h symmetry) have attracted considerable interest since C_{80} was not produced between C_{60} and C_{96}[6] (because of the difficulty in separation). C_{60} (I_h), C_{70} (D_{5h}), and C_{76} (D_2) are the three fullerenes obeying the isolated pentagon rule and having just a single isomer. Figure 3.2 shows the seven isomers of C_{80}[7].

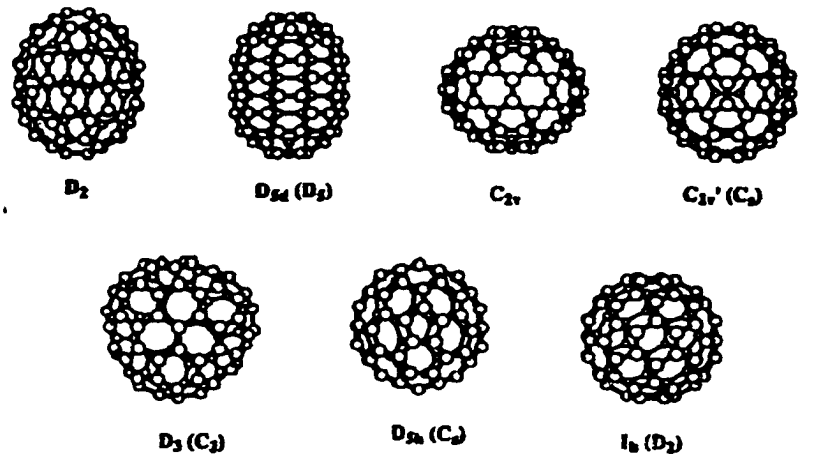

Fig.3.2 Seven isomers of C_{80}, which satisfy the isolated pentagon rule. Relaxed symmetries after geometry optimization are in parentheses.

Since the initial discovery[8] and development of macroscopic preparation technique[3] for fullerene, fullerene-based structures such as higher fullerenes, charge-transfer complexes, fullerene derivatives, super conducting exohedral-doped fullerenes and carbon nanotubes have been produced. Among these, endohedral fullerenes are one of the most interesting classes. To produce endohedral fullerenes dopant atoms are enclosed within the fullerene cage. These fullerene-derived species are also known as metallofullernenes. Many metal atoms have been successfully inserted into the interior hollow core of fullerenes with different number of carbon atoms to form a metallofullerene. More than one atom can be inserted inside a single fullerene cage. The enclosed atoms transfer multiple electrons to the fullerene cage.

In addition to fullerenes, several metallofullerenes, which contain one or several metal atoms inside the fullerene cage, have been produced[9] ($La_2@C_{80}$, $Er_2@C_{82}$,

$Er_2@C_{84}$, $Er_2@C_{90}$ etc.). $La_2@C_{80}$ has interesting property. Recent NMR studies have shown that the two La^{3+} metal atoms inside the C_{80}^{6-} cage are in circular motion[7]. Theoretical calculations show that the I_h isomer of C_{80} is the most unstable configuration of the isomer. However according to the calculations, the encapsulation of La_2 inside the I_h isomer makes it highly stabilized[10].

K. Kobayashi et al. investigated the encapsulation of group 3 and lanthanide metals inside C_{80} isomers by using ab initio molecular orbital and non-local density functional methods[11]. They encapsulated two Gd ($4f^75d^16s^2$) atoms inside the I_h cage of C_{80} without optimization of the cage. According to their work, the two Gd atoms did not completely fill up the fourfold degenerate HOMOs of the I_h cage of C_{80} (one orbital remained singly unopened). On the other hand, metals which can fill up the fourfold degenerate HOMOs are considered the most favorable in stabilizing $M_2@C_{80}$ and encapsulation of such metals is expected to allow isolation and extraction in large quantities. This is not the case for $Gd_2@C_{80}$ metallofullerene, which has not been studied prior to our work. Figure 3.3 shows two metal atoms inside I_h cage of C_{80}.

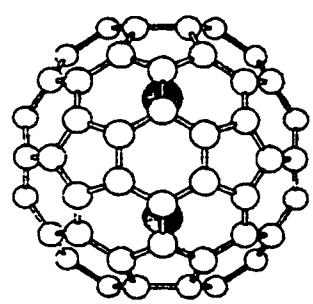

Fig.3.3 Two metal atoms inside the I_h cage of C_{80}[11]

Since their initial discovery[8], fullerenes and fullerenes based materials are considered very interesting materials for applications in nonlinear optics. The advantage of fullerene-based materials are summarized below:

1) Fullerene based materials are expected to have large nonlinearity, because of their large 3-D π-electron conjugation.
2) Fullerene based materials do not have absorption in the near IR region because of the absence C-H and O-H bonds found in conjugated polymers. This property is important in optical communication applications.
3) Resonances in fullerenes are expected to be sharper than conjugated polymers since electronic bands in fullerene-based materials are narrower than in conjugated polymers[12, 13].
4) There is a charge transfer from the entrapped metal atoms to the fullerene cage[14, 15] in metallofullerenes. The nonlinear optical response of the metallofullerenes might be enhanced by this charge transfer mechanism[16].

Nonlinear optical properties of fullerenes have been studied by different groups by using different techniques, different wavelengths and different pulse durations. Some of the values of the third order susceptibilities for different fullerenes are summarized in table 3.1. As it is seen from the table, there are big differences between the third order susceptibilities of fullerenes obtained by different groups. Clearly, experimental technique, wavelength and pulse duration play an important role in determining the nonlinearity. Thus, performing wavelength and pulse duration dependence experiments

might explain these differences. On the other hand, nonlinear optical properties of metallofullerenes have not been explored yet. At this point studying the nonlinear optical properties of one metallofullerene at different wavelengths and pulse duration might make a valuable contribution to fullerene science. This chapter of the thesis investigates the nonlinearity of $Gd_2@C_{80}$ metallofullerene.

Table 3.1 Third order nonlinear optical properties of fullerenes studied by different groups

Molecule	$\chi^3(esu)$	Wavelength (nm)	Pulse duration	Exp. technique	Ref.
C_{70} Film	$\approx 10^{-10}$	633	140 fs	DFWM	17
C_{70} Film C_{60} Film	$\approx 10^{-11}$ $\approx 0.7*10^{-11}$	1064	35ps	DFWM	18
C_{70} Film	$\approx 0.9*10^{-10}$	1420		THG	19
C_{70} in CS_2	$\approx 4*10^{-13}$	532	70 ps	DFWM	20
C_{70} in Toluene	$\approx 1.7*10^{-13}$	532	25 ps	DFWM	21
C_{60} in Toluene	$\approx 3.4*10^{-11}$	520	ns	Z-scan	22
C_{60} in Toluene	$\approx 9*10^{-14}$	1064	10 ns	THG	23

3.2. Introduction

Early electronic structure calculations for C_{60} metallofullerene containing a central metal atom showed that by encapsulating the metal atom inside the cage, the C_{60} energy levels shift down uniformly and metal valence electrons transfer to the cage LUMO (lowest unoccupied molecular orbital)[24]. Several other calculations for metallofullerenes also predicted the metal to cage charge transfer mechanism [25, 26, 27]. On the other hand, electron parametric resonance (EPR) spectroscopy has been used to get detailed information about the electronic structure and chemical nature of metallofullerenes. Several metallofullerene EPR studies for $La@C_{82}$ [28] and $Y@C_{82}$ [29, 30] proved that electrons are transferred from the metal atom to the fullerene cage[15].

Large nonlinear optical responses have been reported in solutions of endohedral metallofullerenes[16, 31, 32]. The enhancement of the nonlinear coefficient was attributed to a metal-to-cage charge-transfer mechanism[16]. In this thesis, we are presenting for the first time investigations of the nonlinear optical properties of a thin film endohedral metallofullerene, $Gd_2@C_{80}$.

3.3. Material Preparation

The synthesis of metallofullerenes is normally carried out either by laser vaporization of a dopant impregnated graphite target or by using a dopant impregnated graphite positive electrode where a carbon arc discharge is used to produce the fullerene. This ensures that the dopant and carbon atoms are simultaneously present in the gas phase during the formation process.

The $Gd_2@C_{80}$ sample was synthesized and purified by Dr. J. Z. Liu at American Hightech Materials Company (AHMCO) using a modified method based on previous reports[15].

Mass spectrometry and molecular beam techniques are powerful tools of fullerene research[33]. This combination of techniques provided the crucial evidence that led to the discovery of fullerenes and metallofullerenes[34]. The mass spectrum of HPLC purified $Gd_2@C_{80}$ is shown in figure 3.4. The peak centered at 1275 m/z is consistent with the predicted isotope distribution for $Gd_2@C_{80}$.

The thin films were spin coated from solutions and were about 0.2 μm thick. The absorption spectrum in a wavelength range of 300-1500 nm is shown in figure 3.5.

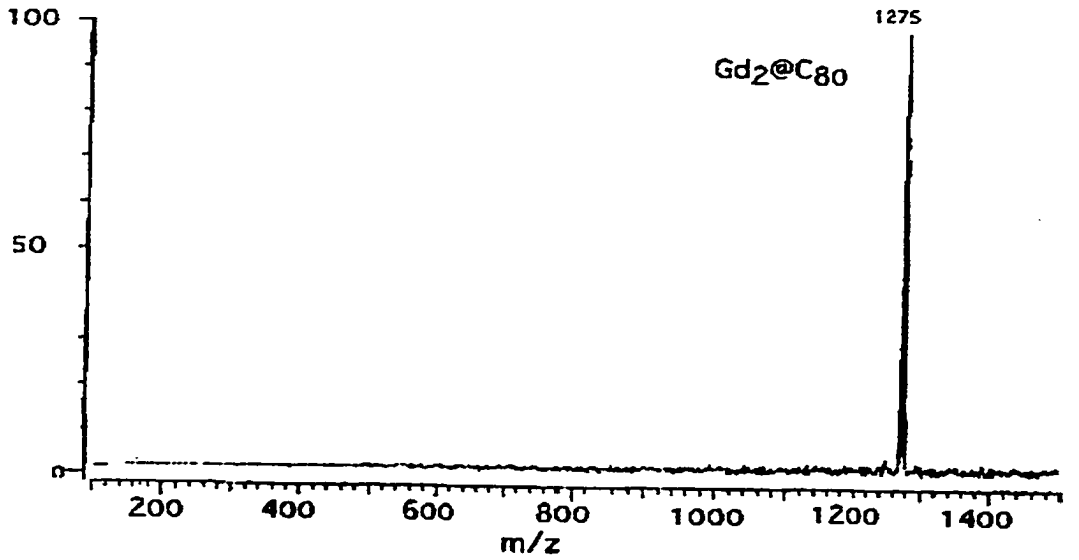

Fig.3.4 The mass spectrum of HPLC purified $Gd_2@C_{80}$

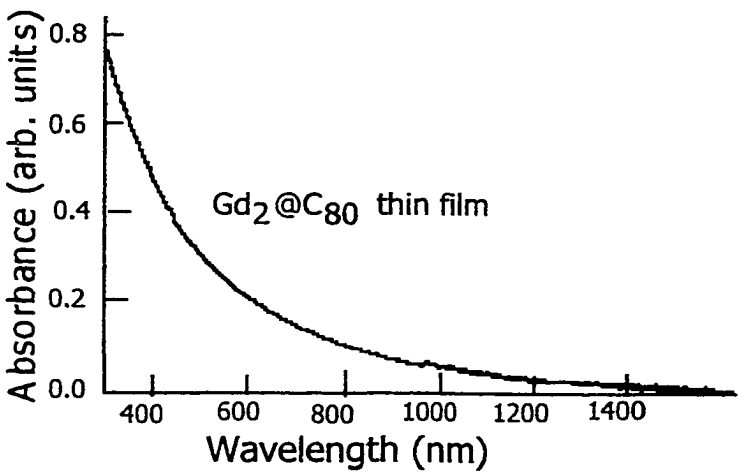

Fig.3.5 Absorption spectrum of $Gd_2@C_{80}$

3.4. Experimental techniques

The single beam z-scan technique (see chapter 2) was used to determine the nonlinear coefficient $\chi^{(3)}$. The energy per pulse varied from about 1.5 μJ to 8 μJ. A single Gaussian beam was tightly focused (f= 25 cm) into a thin nonlinear medium. Both open aperture and far field small aperture z-scan transmittance measurements were carried out on $Gd_2@C_{80}$ thin films on SiO_2 substrates and on clean SiO_2 substrates to take into account the substrate contribution. Contrary to reported results in some other fullerenes,[35] the open aperture measurements showed negligible nonlinear absorption at all the investigated wavelengths. Since the value of $\chi^{(3)}$ for SiO_2 is well known, the SiO_2 was used as a reference to determine the magnitude of $\chi^{(3)}$ for the $Gd_2@C_{80}$ thin films.

3.5. Results and discussion

Figure 3.6 shows the z-scan signal observed for a clean SiO_2 substrate and for a thin $Gd_2@C_{80}$ film on silica glass substrate at 800 nm.

Figure 3.7 gives the $Gd_2@C_{80}$ film nonlinear optical response. The appearance of a peak before a valley indicates a negative nonlinearity for the $Gd_2@C_{80}$ film. The relative value of $\chi^{(3)}$ for $Gd_2@C_{80}$ at 800 nm was calculated to be about 3000 times larger than the value for SiO_2 .

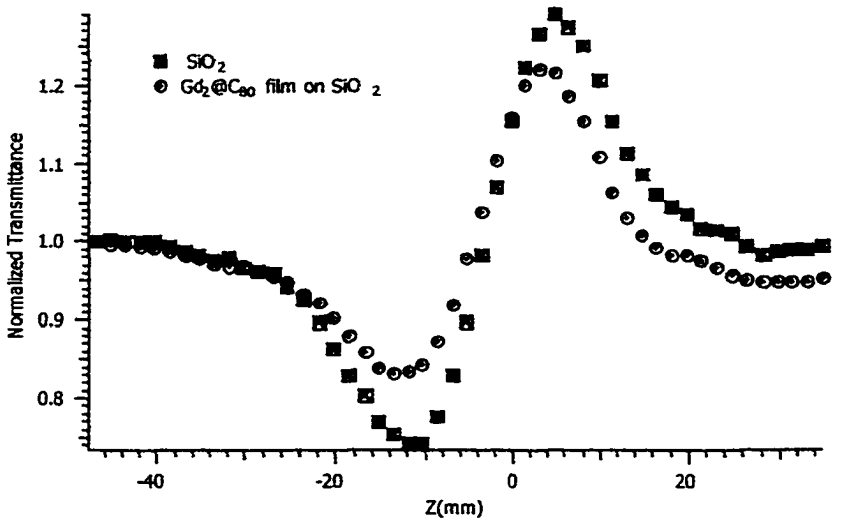

Fig.3.6 The z-scan signal observed for a clean SiO_2 substrate and for a thin $Gd_2@C_{80}$ film on silica glass substrate at 800nm

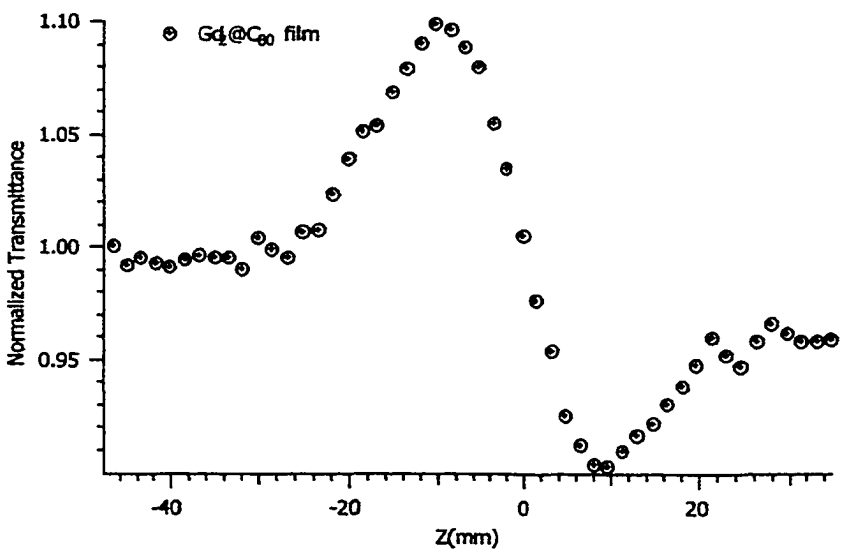

Fig.3.7 The z-scan curve obtained by substracting the substrate z-scan response from the film/substrate response

In figure 3.8 the variation of the relative value of $\chi^{(3)}$ as a function of wavelength at 130fs is depicted for the $Gd_2@C_{80}$ thin film. The value of the nonlinear coefficient is more than one order of magnitude larger at 400 nm ($|\chi^{(3)}(Gd_2@C_{80})/|\chi^{(3)}(SiO_2)|$ =25000) than at 1000 nm ($|\chi^{(3)}(Gd_2@C_{80})/|\chi^{(3)}(SiO_2)|$ =1500). Since the absorption coefficient at 400 nm is also about an order of magnitude larger than at 1000 nm, the increase in the magnitude of the nonlinear optical response can be attributed to single photon resonance enhancement.

Absolute values of the magnitude of $\chi^{(3)}$ were obtained by multiplying the relative values by the value of $\chi^{(3)}$ for silica glass, which is (2.0 ± 0.5 10^{-14} esu). This value was very close to published values [36]. $\chi^{(3)}$ values for our sample for different wavelengths are between 5 10^{-10} esu at 400nm to 1.5 10^{-11} esu at 1000 nm.

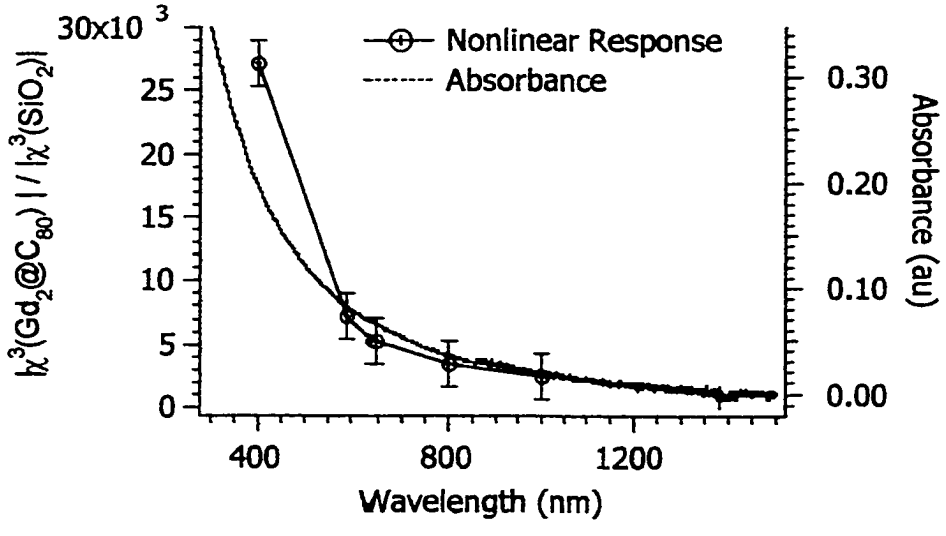

Fig.3.8 The variation of the relative value of $\chi^{(3)}$ as a function of wavelength

The absolute value of $|\chi^{(3)}|$ was reported as 1.1 10^{-9} esu for $Er_2@C_{82}$ [3], and 9.2 10^{-13} esu for $Dy@C_{82}$ [32] in the literature. The $|\chi^{(3)}|$ value for $Er_2@C_{82}$ is about two order of magnitude larger than the value reported here for $Gd_2@C_{80}$ and about four order of magnitude larger than the value for $Dy@C_{82}$. The $Er_2@C_{82}$ and $Dy@C_{82}$ measurements were made in CS_2 solutions using DFWM techniques. $Er_2@C_{82}$ $|\chi^{(3)}|$ values were based on measurements made with nanosecond pulses, while picosecond pulses were used for $Dy@C_{82}$. Minoshina et al[37] and S. Couris et al[38] have observed large differences in the values of the nonlinear response in CS_2 related to differences in pulse-duration. Specifically, short pulses yielded smaller values of $|\chi^{(3)}|$. In order to investigate the role of pulse-duration on the measured value of the nonlinear coefficient we carried out a series of z-scan experiments at 800 nm using different pulse-duration.

Figure 3.9 depicts the ratio $|\chi^{(3)}(Gd_2@C_{80})|/|\chi^{(3)}(SiO_2)|$ as a function of pulse-duration from 100 fs to 1 ps. The ratio increases from about 3000 at 120 fs (this corresponds to $|\chi^{(3)}| = 6\ 10^{-11}$ esu for the $Gd_2@C_{80}$) to more than 16000 at 1 ps ($|\chi^{(3)}| = 3.2\ 10^{-10}$ esu). This shows that the nonlinear response is strongly pulse-duration dependent. Even though some of the very large non-resonant values reported were obtained with long nanosecond pulses,[39] it is difficult to compare these results with other nonlinear optical measurements in fullerenes in the literature since experimental conditions are different.

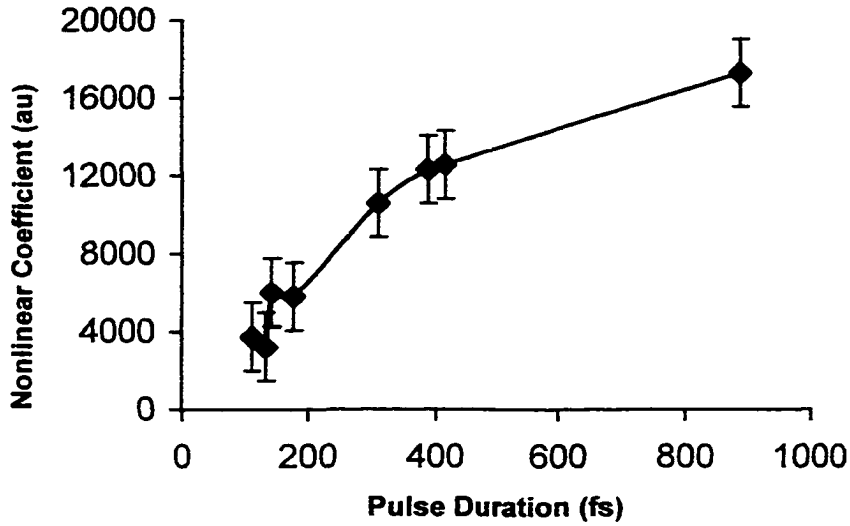

Fig.3.9 Pulse-duration dependence of the nonlinear optical coefficient of $Gd_2@C_{80}$ film relative to silica $\left(\chi^3(Gd_2@C_{80})/\chi^3(SiO_2)\right)$

The pulse-duration dependence of the nonlinearity of $Gd_2@C_{80}$ films could be related to both intermolecular and intramolecular excited-state dynamics. In an attempt to isolate the intramolecular contributions, additional pulse-duration dependence experiments were carried out in $Gd_2@C_{80}$ DMF solutions.

Figure 3.10 shows the ratio $|\chi^{(3)}(Gd_2@C_{80})|/|\chi^{(3)}(SiO_2)|$ as a function of pulse-duration for a $Gd_2@C_{80}$ solution in DMF. Concentration of the solution was less than 10^{-3} M. The ratio $|\chi^{(3)}(Gd_2@C_{80})|/|\chi^{(3)}(SiO_2)|$ increases about 5 times between 120 fs and about 1 ps. These results are very similar to the results for the $Gd_2@C_{80}$ films shown in figure 3.9. By comparing Fig.3.9 with Fig.3.10 we can conclude that the pulse-duration dependent nonlinear response is probably mainly related be to the specific excited-state dynamics of the $Gd_2@C_{80}$ molecule.

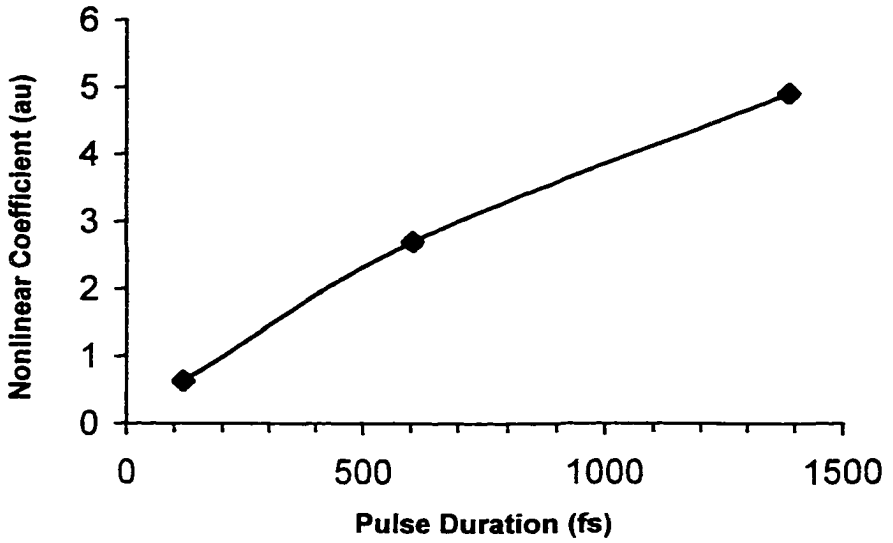

Fig.3.10 Pulse-duration dependence of the nonlinear optical coefficient of $Gd_2@C_{80}$ - DMF solution relative to silica $\left(\chi^3(Gd_2@C_{80})/\chi^3(SiO_2)\right)$

In order to clarify the possible role of photo-induced states we have carried out transient absorption measurements at 800 nm with short pulses (150 fs, figure 3.11) and long pulses (1.9 ps, figure 3.12). Both curves exhibit relatively long decay components (2-3 ps). In addition, strong bleaching is observed for long pulses. These results strongly suggest that the size and pulse duration dependence of the nonlinear response at 800 nm is the result of at least two resonance effects: two-photon resonance and subsequent resonance absorption and bleaching of photo-induced optical transitions.

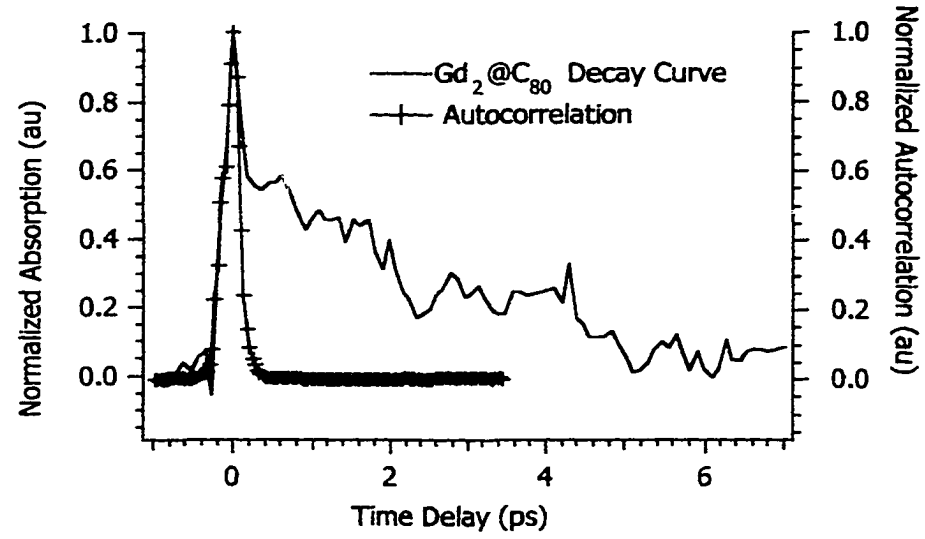

Fig.3.11 Transient absorption dynamics with short (150 fs) pulses at 800 nm

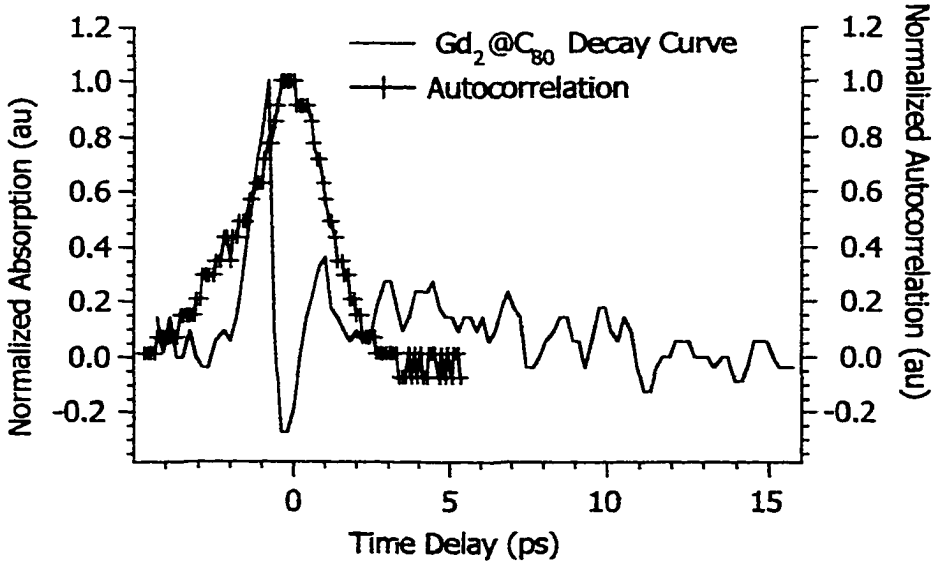

Fig.3.12 Transient absorption dynamics with long (1.9 ps) pulses at 800 nm

We propose a model to explain the bleaching effect seen on pump-probe experiment with long pulse-duration. Our model includes two-photon absorption and excited-state absorption. A simplified energy diagram of our model is shown in Fig. 3.13. In this model, the lowest excited-state S_1 is populated through two-photon absorption. Then, strong single photon absorption and bleaching effects occur between S_1 and S_2 states, when the S_1->S_2 transition is probed at the same frequency.

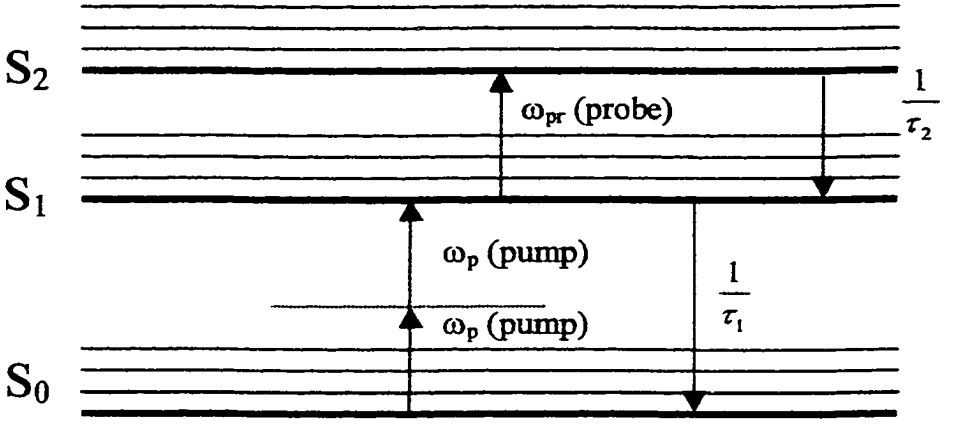

Fig.3.13 Simplified schematic energy level diagram

According to this model, the rate equations governing the dynamics of the excitation populations N_0 in S_0, N_1 in $S_1$and N_2 in S_2 can be written as

$$\frac{dN_0(t)}{dt} = -\frac{\sigma_{2Ph} I_p(t)^2}{(h\nu_p)^2} N_0(t) + \frac{1}{\tau_1} N_1(t) \qquad (3.1)$$

$$\frac{dN_1(t)}{dt} = \frac{\sigma_{2Ph} I_p(t)^2}{(h\nu_p)^2} N_0(t) - \frac{\sigma_{12} I_{pr}(t)}{h\nu_{pr}} N_1(t) - \frac{1}{\tau_1} N_1(t) + \frac{1}{\tau_2} N_2(t) \tag{3.2}$$

$$\frac{dN_2(t)}{dt} = \frac{\sigma_{12} I_{pr}(t)}{h\nu_{pr}} N_1(t) - \frac{1}{\tau_2} N_2(t) \tag{3.3}$$

where σ_{2ph} is the S_0->S_1 two-photon absorption cross section, I_p and I_{pr} are the pump and probe intensities respectively, ν_p and ν_{pr} are the pump and probe frequencies, τ_1 and τ_2 are the lifetime of S_1 and S_2, σ_{12} is the S_1->S_2 absorption cross section.

Our main goal here was to attempt to reproduce the time dependence of the PA experiments, not to obtain precise values for the various parameters in these equations. The rate equations were solved numerically by using fourth-order Runge-Kutta methods[40]. The best fit to the experimental data were obtained for a single photon excited-state absorption cross section $\sigma_{12} \approx 3\ 10^{-17}$ cm^2 and a ground-state two-photon absorption cross section $\sigma_{2ph} \approx 20$ GM (1 GM=10^{-50} cm^{4}sec molecule^{-1} photon^{-1}). The value of σ_{12} is close to published value for excited-state absorption cross-section for C_{70} and other fullerenes [41]. A Gaussian-shaped temporal profile was used for the optical pulses. The pulse energy of the pump pulse was kept constant (about 30 μJ to 40 μJ) for all pulse-durations. The lifetimes τ_1 and τ_2 of the excited-states were calculated from the best fit to the experimental data as about 2.5 to 3 ps. The best theoretical fits to the data are shown in figure 3.14 and 3.15.

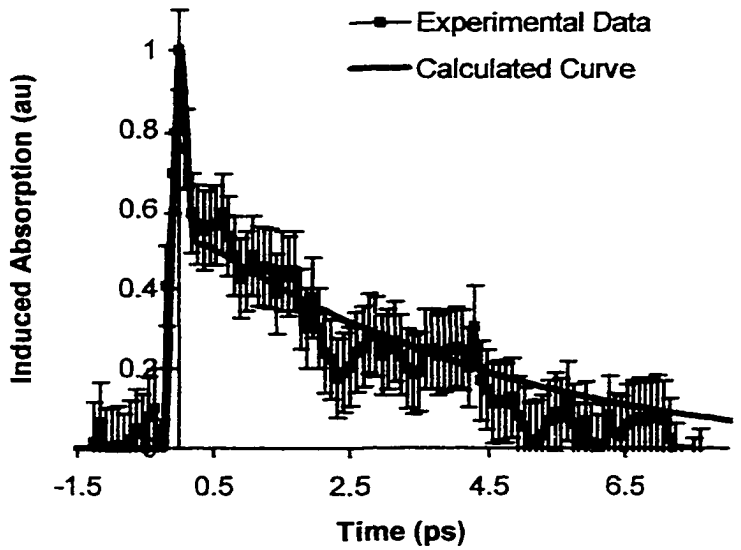

Fig.3.14 Transient absorption dynamics with short (120 fs) pulses at 800 nm.

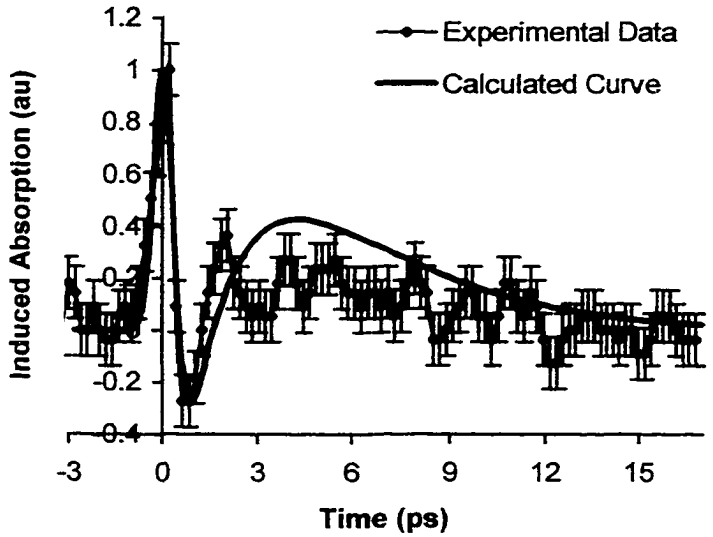

Fig.3.15 Transient absorption dynamics with long (1 ps) pulses at 800 nm

The pump-probe experiment was carried out at lower intensity (same energy) for long pulse (1 ps) than for short pulses (120 fs). However, the longer pulse experiment (1 ps) exhibits strong bleaching effects (figure 3.15), which are absent from the short pulse measurements (figure 3.14). In order to clarify this result we need to compare the excited state populations for short and long pulse durations. The populations of S_0, S_1 and S_2 states for two different pulse durations at the same pump intensities were plotted in figure 3.16 and 3.17. The ratio of pump and probe intensities were kept constant at about 28:1 in both case. Even though both pulses have the same pump intensities, increasing pulse duration gives rise to the S_1-S_2 transition. As a result of that transition, population of S_2 becomes larger than that of S_1 and bleaching effects are observed in the transient absorption spectrum.

The model accurately predicts the onset of bleaching effects in the S_1->S_2 channel when the pulse-duration is increased while the energy is kept constant. Our model may also indirectly explain the pulse-duration dependence of the nonlinear response of $Gd_2@C_{80}$. It is well known that single and multiple photon resonance transitions can substantially increase the nonlinear optical response of a material.[42] This effect can be further enhanced by nonlinear distortions created by absorption bleaching effects[43, 44, 45, 46, 47]. Since bleaching effects in $Gd_2@C_{80}$ increase with increasing the pulse-duration of the laser, the pulse-duration dependence of the nonlinear response can be attributed to nonlinear bleaching effects related to the S_1 -> S_2 transition in $Gd_2@C_{80}$.

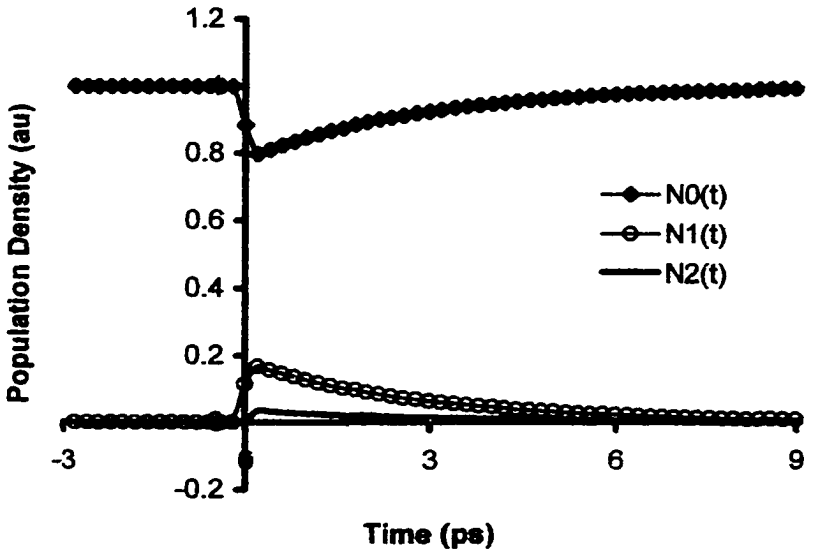

Fig.3.16 Populations of the states for short (120 fs) pulse

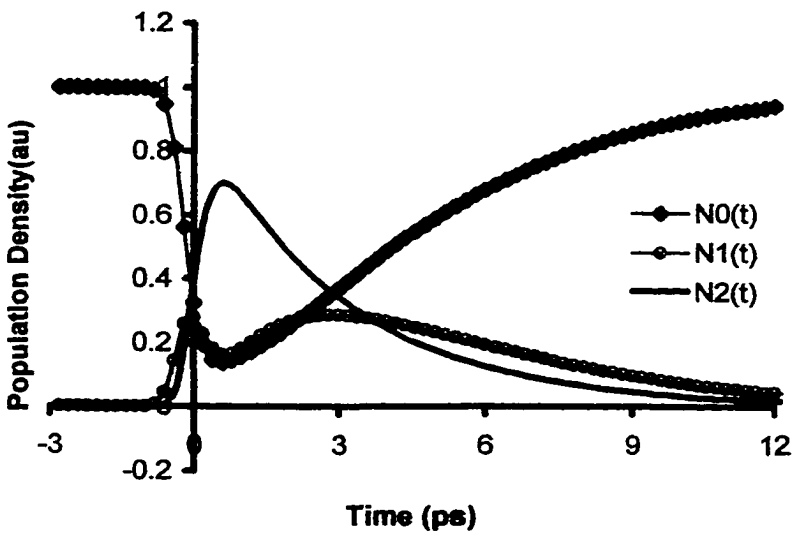

Fig.3.17. Populations of the states for long (1 ps) pulse

3.6. Conclusions

In summary, we have measured the nonlinear optical coefficient in $Gd_2@C_{80}$ films in the visible and near IR. The magnitude of the nonlinarity was strongly pulse-duration dependent. At 800 nm $\chi^{(3)}$ =3.2 10^{-10} esu for a 1 ps pulse. This is substantially larger than reported $\chi^{(3)}$ values in C_{60}[19, 48] and C_{70}. [19, 20, 49]. We have also investigated the excited-state properties of $Gd_2@C_{80}$. We measured the transient absorption spectrum of $Gd_2@C_{80}$ at 800 nm for different pulse-durations. These experiments showed a relatively long excited-state lifetime (2-3 ps). In addition, transient absorption spectra for long pulses (>1 ps) showed strong bleaching effects. The difference between the transient absorption spectra for long and short pulses was explained with a theoretical model, which combines two-photon absorption and excited-state absorption. This model may also explain the pulse-duration dependence of the nonlinearity of $Gd_2@C_{80}$.

References:

[1]M. S. Dresselhaus, G. Dresselhaus, R. Saito, in 'Nanotechnology' edited by G. Timp, Springeer Verlag, New York (1999).

[2] G. Dresselhaus, M.S. Dresselhaus, P. C. Eklund, Phys. Rev. B, 45, 6923 (1992).

[3] W. Kradschemer, L. D. Lamb, K. Fostiropoulos, and D. R. Huffman, Nature (London) 347, 354 (1990).

[4] J.E. Fischer, P. A. Heiney, A. B. Smith III, Accounts Chem. Res. 25, 112 (1992).

[5] D. E. Manolopoulos, P. W. Fowler, Chem. Phys. Lett., 187, 1 (1991).

[6] Y. Achiba, K. Kikuchi, Y. Aihara, T. Wakabayashi, Y. Miyake, andM. Kainosho, Mat. Res. Soc. Symp. Proc., 359, 3 (1995).

[7] S. Nagase, K. Kobayashi, T. Akasaka, in "Fullerenes", The Electrochemical Society Inc., Pennington New Jersey, 3, 558 (1996).

[8] H.W. Kroto, J.R. Heath, S. C. O'Brein, R. F. Curl, and R. E. Smalley, Nature (London) 318, 162 (1985).

[9] Y. Chai, T. Guo, C. Jin, R. E. Haufler, L. P. F. Chibante, J. Fure, L. Wang, J. M. Alford, and R. E. Smalley, J. Phys. Chem., 95, 7564 (1991).

[10] K. Kobayashi, S. Nagase, and T. Akasaka, Chem. Phys. Lett., 245, 230 (1995).

[11] K. Kobayashi, S. Nagase, Chem. Phys. Lett., 262, 227 (1996).

[12] E. Sohmen, J. Fink, W. Kratschmer, Z. Phys. B, 86, 86 (1992).

[13] F. Kajzar, Y. Okada-Shudo, C. Meritt, Z. Kafafi, Synthetic Metals, 94, 91 (1998).

[14] R. D. Johnson, M. S. de Vries, J. R. Salem, D.S. Bethune, and C. S. Yannoni, Nature, 355, 239 (1992).

[15] D.S. Bethune, R. D. Johnson, J. R. Salem, M. S. de Vries, and C. S. Yannoni, Nature, 366, 123 (1993).

[16] J.R. Heflin, D. Marciu, C. Figura, S. Wang. P. Burbank, S. Stevenson, and H.C. Dorn, Applied Physics Letters, 72, 2788 (1998).

[17] M. J. Rosker, et al., Chem. Phys. Lett., 196, 427 (1992).

[18] J. R. Lindle, R. G. S. Pong, F. J. Bartoli, Z. H. Kafafi, Phys. Review B, 48, 9447 (1993).

[19] F. Kajzar, C. Taliani, R. Danieli, S. Rossini, R. Zamboni, Physical Review Lett, 73, 1617 (1994).

[20] H. Huang, G. Gu, S. Yang, J. Fu, P. Yu, G. K. L. Wong, Y. Du, J. Phys. Chem. B. 102, 61 (1998).

[21] F. J. Aranda, D. V. G. L. N. Rao, J. F. Roach, P. Tayebati, J. Appl. Phys, 73, 7949 (1993).

[22] S. Jouris, E. Koudoumas, A. A. Ruth, S. Leach, J. Phys. B:At. Mol. Opt. Phys. Printed in UK, 28, 4537 (1995)

[23] D. Neher, G. I. Stegeman, F. A. Tinker, N. Peyghambarian, Optics Letter, 17, 1491 (1992).

[24] A. Rosen, and B. Wastberg, J. Am. Chem. Soc., 110, 8701 (1988).

[25] A. Chang, W. C. Ermler, and R. M. Pitser, J. Chem. Phys, 94, 5004 (1991).

[26] J. Feng, M. C. Li, M. C. Li, and M. C. Zerner, Int. J. Quant. Chem., 39, 331 (1991).

[27] S. Saito, and A. Oshiyama, Sollid. St. Commun., 83, 107 (1992).

[28] S. Bandow, et al., J. Phys. Chem., 96, 9609 (1992).

[29] J. Weaver, et al., Chem. Phys. Lett., 190, 460 (1992).

[30] M. Hoinkis, et al., Chem. Phys. Lett, 198, 461 (1992).

[31] H. Huang, G. Gu, S. Yang, J. Fu, P Yu, G. K. L. Wong, Y. Du, Electrochemistry Society Proceedings, 94-14, 401 (1997).

[32] G. Gu, H. Huang, S. Yang, P. Yu, J. Fu, G. K. Wong,, X. Wan, J. Dong, Y. Du, Chem. Phys. Lett. 289, 167 (1998).

[33] S. W. McElvany and M. M. Ross, J. Am. Soc. Mass Spectrum, 3, 268 (1992).

[34] J. R. Heath et al, J. Am. Chem. Soc., 107, 77 (1985).

[35] S. Couris, E. Koudoumas, F. Dong, and S. Leach, J. Phys. B: At. Mol. Opt. Phys., 29 5033 (1996)

[36] R. H. Stolen and C. Lin, Phys. Rev. A17, 1448 (1978)

[37] Minoshina K, Taiji M, and Kobayashi, Opt. Lett., 16, 1683 (1991)

[38] S.Couris, E. Coudoumas, F.Dong, and S. Leach, J. Phys. B.: At. Mol. Opt. Phys., 29, 5033 (1996).

[39] Qihuang Gong, Yuing Sun, Zongju Xia, Y. H. Zou, Zhennan Gu, Xihuang Zhou, and Di Qiang, J. Appl. Phys., 71, 3025 (1992)

[40] S. C. Chapra, R. P. Canale, "Numerical methods for engineers", 3rd ed., McGraw-Hill: Boston, p 701 (1998)).

[41] L.Yang, E. Royer, A.D. Walser, R. Dorsinville, Chem. Phys. Lett. 239, 399 (1995).

[42] M. Zhao, Y. Cui, M. Samoc, P. N. Prasad, M. R. Unroe, B. A. Reinhardt, J. Chem. Phys. 96, 3991 (1991).

[43] E. F. Hilinski, P. A. Lucas, Y. Wang, J. Chem. Phys. 89, 3435 (1988).

[44] H. Kalt, K. Bohnert, D. P. Norwood, T. F. Boggess, A. L. Smirl, I. J. D'Haennes, J. Appl. Phys. **62**, 4187 (1987).

[45] Y. Zhao, C. Wu, P. Shah, M. K. Kim, L. R. Dawson, Appl. Phys. Lett. **63**, 281 (1993).

[46] J. S. Weiner, D. B. Pearson, D. A. B. Miller, D. S. Chemla, D. Sivco, A. Y. Cho, Appl. Phys. Lett. **49**, 531 (1986).

[47] D. S. McCallum, X. R. Huang, M. D. Dawson, T. F. Boggess, A. L. Smirl, T. C. Hasenberg, A. Kost, J. Appl. Phys. **70**, 6891 (1991).

[48] Z. H. Kafafi, J. R. Lindle, R. G. S. Pong, F. J. Bartoli, L. J. Lingg, and J. Milliken, Chem. Phys. Lett. 188, 492 (1992).

[49] J. R. Lindle, R. G. S. Pong, F. J. Bartoli, and Z. H. Kafafi, Phys. Review B **48**, 9447 (1993).

CHAPTER 4

TIME RESOLVED DYNAMICS OF COLLOIDAL J-AGGREGATES

4.1. Introduction

In dilute liquid solutions, absorption spectra of dye molecules are relatively broad and do not usually show any sharp structures. Jelly[1] and Scheibe[2] discovered that upon increasing the concentration of dyes in water, an unusually sharp absorption band arises, that is red shifted relative to the broad absorption band observed in dilute solutions. These aggregates are usually referred to as J-aggregates or Schiebe aggregates.

The excited state dynamics of J-aggregated dyes are of interest for many reasons. Due to their strong absorption, cyanine dyes adsorbed on surface of the silver halide crystals are widely used to extend the spectral sensitivity of photographic materials[3]. For this application, these aggregates function as antenna systems that collect light for the photographical process. In biology, aggregates are of general interest since most photo-biological processes, including photosynthesis, rely on molecular aggregates for energy or charge transfer processes[4]. In addition, nonlinear optical properties of the organic molecular systems with quantum confinement effects have become a subject of active study. The understanding of confinement effects in solid inorganic systems resulted in wide technological use of semiconductor nanostructures for fast signal processing. New nonlinear optical materials for all optical computing applications may be based on organic nanostructures. J-aggregates are regarded as promising nonlinear optical

materials because of the effect of the co-operative response of confined Frenkel excitons to the light field.[5]

Recently, an extremely low threshold for lasing from J-aggregated molecules adsorbed onto colloidal silver was reported[6]. Aggregation on colloidal silver suspension shows superradiant lasing. Aggregation in water does not show this characteristic. This can be explained with the difference on the absorption and emission bands of both systems. Excitonic absorption and emission bands of the J-aggregates in homogeneous solutions strongly overlap. When aggregation is formed on the surface of charged colloidal silica specific interactions of the charged substrate with charged dye molecules results in excitonic emission and absorption bands that are shifted from their overlapping positions. This shift decreases the self re-absorption and increases the superradiant nature of the emission with extremely low excitation threshold[6].

The time resolved dynamics of TDBC (1,1'-diethyl-3, 3'-bis(4-sulfobutyl)-5,5',6,6'-tetrachloro-benzimidazolo carbocyanine) J-aggregates in water have been studied by other groups[7]. To our knowledge, the time resolved dynamics of TDBC aggregates on silver colloids has not been investigated by using the femtosecond pump-probe technique. The difference in the emission characteristics of TDBC aggregates in water and in colloidal suspension can be explained by comparing their fs pump-probe transient absorption spectra. These measurements give also valuable information about the coherence length and resonance nonlinear response of dye aggregates.

4.2. Theoretical Background

Strong interactions between the molecules within the aggregate, which lead to *collective* effects in the optical response, make the physical properties of aggregates distinctly different from those of single molecules. These cooperative effects result directly from the intermolecular interactions that cause delocalization of the electronic eigenstates over many molecules on the chain: exciton bands are formed. The delocalization of excitations causes an averaging over the inhomogeneities in the transition frequencies of the individual molecules, resulting in a narrow absorption band. This mechanism is called motional narrowing or exchange narrowing. In aggregates the delocalized excitations are called *Frenkel excitons*. In a Frenkel exciton the electrons are kept tightly bound to their molecular centers, so only energy is transported. In the case of Wannier excitons, a reduced Coulombic interaction between the electron and positive "hole" increases their separation. Although electron and hole are still weakly bound, the excitation is no longer confined within or near one molecule.

The purpose of this section is to describe the level structure and optical parameters of aggregates in order to evaluate the nonlinear optical response. The linear response involves only the ground state of the aggregate and states in which the molecules share one excitation: the conventional Frenkel excitons or one-exciton states. The nonlinear response involves also states in which two or more excitations are shared by the molecules on one aggregate. Such two-exciton states have been observed in pump-probe absorption measurements by Fidder et al.[8] and by Minoshima et al.[9] on aggregates at low temperatures, by Johnson et al.[10] and van Burgel et al.[7] on aggregates in solution.

Aggregates in solutions are usually described as linear, quasi-*one-dimensional* exciton systems[11, 12]. Experimentally, this follows from the fact that the absorption spectra of most aggregates are taken in flowing jet streams. The flow orientation causes the aggregates to align parallel to the flowing direction[13].

One dimensional conventional exciton band theory can explain the essential features of the absorption spectrum of the aggregates. Possible disorder in the energies of these molecules or in their coupling is ignored in this theory. For homogeneous aggregates, without disorder, the excitations extend over the entire physical size of the aggregate. In reality, localization of the excitation occurs because of the static and dynamic disorder of the molecular energies.

In conventional band theory, the aggregates are modeled as linear chains of N two-levels molecules. Each of the molecules has a dipole allowed optical transition from the ground state to an electronic excited state and the coupling of the transition dipoles of various molecules result in excitonic transfer between them. All transitions dipoles are assumed parallel, having magnitude μ and making an angle θ with the aggregate axis. Distances between the molecules are equal to the lattice constant a (figure 4.1). Since each of the N molecules can be in two states, the chain has 2^N eigenstates.

The electronic states of the aggregates can be described by the Frenkel-exciton-Hamiltonian[14].

$$H = \hbar\sum_{n-1}^{N}\omega_n\hat{b}_n^{\dagger}\hat{b}_n + \frac{1}{2}\hbar\sum_{\substack{n,m-1\\ n\neq m}}^{N}V_{nm}(\hat{b}_n^{\dagger}\hat{b}_m + \hat{b}_m^{\dagger}\hat{b}_n) \equiv \sum_{n,m-1}^{N}H_{nm}\hat{b}_n^{\dagger}\hat{b}_m \qquad (4.1)$$

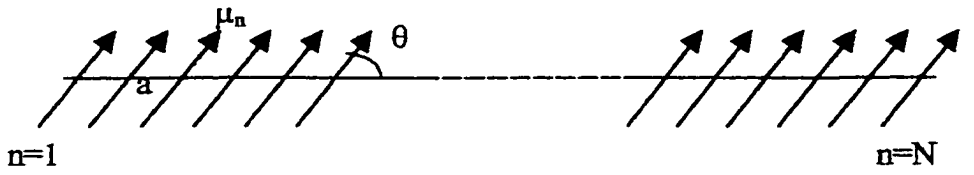

Fig.4.1 Linear aggregate of N two-level molecules with parallel transition dipoles, indicated by the arrows

Here, ω_n is the transition frequency of molecule n, $\hat{b}_n^{\dagger}$ and $\hat{b}_n$ are the conventional Pauli creation and annihilation operators for an excitation on molecule n, and V_{nm} is the interaction between molecules n and m.

When only nearest-neighbor coupling ($V_{nm} = V_{n,n\pm1}$) is considered, the Jordan-Wigner transformation converts the paulions of equation (4.1) into non-interacting fermions, which has the important advantage that all eigenstates of the aggregate can be obtained from the diagonalization of the NxN matrix H_F. The Hamiltonian, H_F is identical to equation (4.1), but $\hat{b}_n^{\dagger}$ and $\hat{b}_n$ are now fermion creation and annihilation operators. This property holds irrespective of the presence of (diagonal) energetic or (off-diagonal) interaction disorder.

Since the number of excitations is conserved in the operation H_F, the aggregate eigenstates separate into N different sets of linear combinations of single-molecule states, each with a fixed number of single-molecule excitations present[7]. These are the one-, two-, three-, ...,N-exciton bands, of which the lowest two are displayed in figure 4.2. The

I-th band contains $\binom{N}{i}$ states, which are labeled with quantum numbers $k_1 > k_2 > \ldots > k_i$ with k=1,...,N. A general eigenstate in the i-th band can be written as:

$$|k_1, k_2, \ldots, k_i\rangle = \sum_{\substack{n_1, n_2, \ldots, n_i = 1 \\ n_1 < n_2 < \ldots < n_i}}^{N} \det(\phi_{k1,n1}, \phi_{k2,n2}, \ldots, \phi_{ki,ni} \,|\, n_1, n_2, \ldots, n_i\rangle \tag{4.2}$$

with eigenfrequency:

$$\Omega_{k_1, k_2, \ldots, k_i} = \Omega_{k_1}, \Omega_{k_2}, \ldots, \Omega_{k_i} \tag{4.3}$$

Here $|n_1, n_2, \ldots, n_i\rangle$ represents a state where molecules $n_1, n_2, \ldots, n_i$ are excited and the others are in the ground state, det(...) is the determinant of the components ϕ_{kn} of the normalized eigenvectors of H and Ω_k is the eigen-frequency of the state with quantum number k. The operator for dipole transitions between these eigenstates is given by:

$$\hat{P} = \sum_{n=1}^{N} \mu_n (\hat{b}_n^{\dagger} + \hat{b}_n) \tag{4.4}$$

where μ_n is the dipole matrix element of the single molecules. This equation shows that optical transitions are only allowed between two consecutive exciton states.

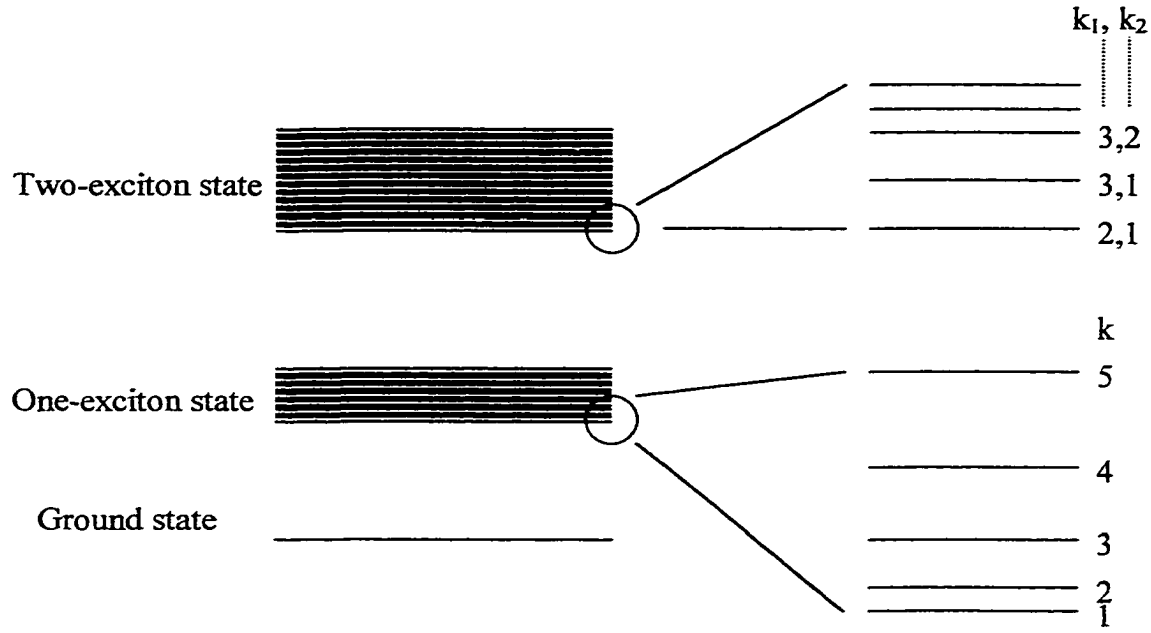

Fig.4.2 Energy diagram of linear aggregates (One- and two-exciton bands are shown out of N exciton band.)[7]

For *homogeneous* aggregates, in which all sites have the same energy ($\omega_n \equiv \omega_{mon}$) and all intermolecular couplings are equal ($V_{n,n\pm1}$ =V), the delocalized eigenstates equation (4.2), the eigenfrequencies equation (4.3), and the transition probabilities equation (4.4) can be found analytically [15, 16, 17]. When static energetic disorder is included in the model the Hamiltonian can only be solved numerically. For small disorder (compared to the intermolecular coupling), the homogeneous eigenstates form a good starting point for perturbative treatments[18].

Since disorder leads to localization, the number of molecules N, which appears in equations (4.1), (4.2) and (4.4), does not refer to the physical size of the aggregates

anymore. The excitation only extends over a smaller subsection of the aggregate chain. This means that N now corresponds to the delocalization length of the excitons, instead of the physical length. The size dependence of the optical properties thus only consists for aggregates that are small compared to this delocalization length.

For homogeneous aggregates (no molecular disorder), the components ϕ_{kn} of the eigenvectors [15, 16, 17]

$$\phi_{kn} = \sqrt{\frac{2}{N+1}} \sin\left(\frac{\pi k n}{N+1}\right) \tag{4.5}$$

and the eigenfrequencies are given by

$$\Omega_k = \omega_{mon} + 2V \cos\left(\frac{\pi k}{N+1}\right). \tag{4.6}$$

By using these results in equations (4.2)-(4.4), the delocalized eigenstates, the eigenfrequencies, and the transition probabilities can be found for all 2^N eigenstates[7].

The one-exciton band is centered at the single-molecule transition frequency ω_{mon}, and has a width of four times the interaction energy V between the molecules in the chain. In the *one-exciton band*, N molecules on the aggregate chain share one single-molecule excitation. The delocalized states are the well-known Frenkel excitons, which are characterized by a single quantum number k. The N eigenstates of this band are:

$$|k\rangle = \sum_{n=1}^{N} \phi_{kn} |n\rangle = \sqrt{\frac{2}{N+1}} \sum_{n=1}^{N} \sin\left(\frac{\pi k n}{N+1}\right) |n\rangle \tag{4.7}$$

while the eigenfrequencies are given by equation (4.6). The states at the bottom of this band are shown enlarged on the lower right side of figure 4.2. The transition moments from the ground state |g> to the various k-states of the one-exciton band are given by:

$$\mu_{kg} = \mu_{mon}\sqrt{\frac{2}{N+1}}\frac{1-(-1)^k}{2}\cot\left(\frac{\pi k}{2(N+1)}\right) \tag{4.8}$$

As it is seen from equation 4.8, only states with an odd quantum number k have oscillator strength (dipole moment squared), and hence only these states are visible in a (linear) absorption spectrum. The state with k=1 contains the biggest oscillator strength: up to $0.81(N+1)\mu_{mon}^2$ for N»1, which is about 81% of the total oscillator strength of the ground state to one-exciton transition. Since the interaction energy V is negative, in J-aggregates the k=1 state is at the bottom of the one-exciton band (see equation (4.6)). Hence, J-aggregates have red-shifted linear absorption compared to the monomer, with an asymmetric tail to the high-energy side where absorption occurs to the higher k states (k=3,5,...). This explains the typical aggregate absorption spectrum. In the case of H-aggregates, named after the discoverer Herz [19], interaction energy between neighboring molecules is positive and only transitions to the upper (high energy) end of the exciton band are allowed. Hence, H-aggregates linear absorption spectrums are blue-shifted relative to monomer absorption spectrum. The large oscillator strength of the k=1 state is responsible for exciton superradiance at low temperatures[20].

Two-exciton band is centered at twice the single-molecule transition frequency ω_{mon}, and has a width of eight times the interaction energy V between the molecules in the chain. In the *two-exciton band*, N molecules on the aggregate chain share two single-molecule excitations. Since optical transitions can only occur between two adjacent exciton bands, two- and higher-exciton states can only be probed by nonlinear optical experiments. The states of the two-exciton band are characterized by two quantum numbers k_1 and k_2 , which can take values from 1 to N ($k_1 > k_2$). The eigenfrequencies are, according to equation (4.3), the sum of the two independent one-exciton eigenfrequencies associated with both k numbers. However, the wave functions of the two-exciton band are *not* the product of two independent one-exciton wave functions. This is a consequence of the Pauli exclusion principle: a molecule cannot be doubly excited. The N(N-1)/2 wave functions of the two-exciton band can be found by inserting equation (4.5) in equation (4.2):

$$|k_1 k_2\rangle = \sum_{\substack{n_1,n_2=1 \\ n_2>n_1}}^{N} (\phi_{k_1 n_1}\phi_{k_2 n_2} - \phi_{k_1 n_2}\phi_{k_2 n_1})\,|n_1, n_2\rangle$$

$$= \frac{2}{N+1}\sum_{\substack{n_1,n_2=1 \\ n_2>n_1}}^{N}\left\{\sin\left(\frac{\pi k_1 n_1}{N+1}\right)\sin\left(\frac{\pi k_2 n_2}{N+1}\right) - \sin\left(\frac{\pi k_1 n_2}{N+1}\right)\sin\left(\frac{\pi k_2 n_1}{N+1}\right)\right\}|n_1, n_2\rangle \qquad (4.9)$$

As it is seen from equation 4.9, because of the pauli exclusion principle there is no state with the two quantum numbers k_1 and k_2 equal. Thus, the lowest energy state of the two-exciton band is $k_1 = 2$, $k_2 = 1$ instead of $k_1 = 1$, $k_2 = 1$. This result leads us to an important feature: larger than the energy difference between the ground state and the bottom of the

one-exciton band. The delocalization length of the exciton can be determined by using this property of J-aggregates. The states at the bottom of the two-exciton band are shown enlarged on the upper right side of figure 4.2.

The general expression for the transition moments between the k-states of the one-exciton band and the k_1 ,k_2 -states of the two-exciton band, is given by [17]:

$$\mu_{k_1k_2,k} = \mu_{mon}\sqrt{\frac{2}{N+1}}\left[\delta_{k_2,k}\frac{1+(-1)^{k_1}}{2}\cot\left(\frac{\pi k_1}{2(N+1)}\right)-\delta_{k_2,k}\frac{1+(-1)^{k_2}}{2}\cot\left(\frac{\pi k_2}{2(N+1)}\right)\right.$$

$$+1/2\left(\delta_{k_1-k_2-k,0}-\delta_{k_1-k_2+k,0}\right)\left\{\cot\left(\frac{\pi k_1}{2(N+1)}\right)+\cot\left(\frac{\pi k_2}{2(N+1)}\right)\right\}$$

$$\left.+1/2\left(\delta_{k_1+k_2+k,2(N+1)}-\delta_{k_1-k_2-k,0}\right)\left\{\cot\left(\frac{\pi k_1}{2(N+1)}\right)-\cot\left(\frac{\pi k_2}{2(N+1)}\right)\right\}\right] \quad (4.10)$$

The dominant transition is from the one-exciton k=1 state to k_1 =2, k_2 =1 state of the two-exciton band, which is located at the bottom of that band. The oscillator strength of this transition is $1.27(N+1)\mu_{mon}^2$ for N»1, which is about 70% of the total oscillator strength of the k=1 one-exciton state to the two-exciton band. Expressions for states in the higher exciton bands can be obtained in the same way, using equations (4.2) to (4.6).

Before finishing this section, it should be noted that one-dimensional conventional exciton band theory has some assumptions, which may not be appropriate to interpret some J-aggregated systems. The purpose of this section is to give a basic model for molecular J-aggregates. The assumptions for this model can be summarized as follows:

Exciton-exciton interactions are neglected in the calculations of the multi-exciton bands. The Frenkel exciton model considered here includes only exciton repulsion through the Pauli exclusion principle. Attractive exciton-exciton interactions may lead to new bound states of two excitons, named as bi-excitons. Bi-excitons usually show up as strong two-photon resonances that are red shifted with respect to the transition to the two-exciton band. The red shift reflects the bi-exciton binding energy[21,22].

The theory explained here is for one-dimensional aggregates with only nearest-neighbor coupling. If interactions between all molecules are taken into account, instead of only nearest-neighbor couplings, exciton energy levels shift downwards[20]. Additional shifts may also occur due to a difference in solvation energy of the aggregates compared to the monomer[23]. These effects mainly lead to a modification in the experimentally determined value of the nearest-neighbor coupling constant V [24], and delocalization length N.

4.3. Adsorption of Dyes onto Surfaces

Two-dimensional J-aggregates of well defined size can be formed by the adsorption of dyes onto crystallites[25, 26] or colloids[27, 28]. In the spectral sensitization of photographic films by J-aggregates, J-aggregates are adsorbed onto silver halide crystallites embedded in gelatin. These crystallites, however, readily undergo electron transfer with the adsorbed dyes. This is the main mechanism for spectral sensitization in these photographic materials. To avoid electron transfer, inert substrates such as silica gel[29] or colloidal silica[30, 31] can be used to study the photophysics of these J-aggregates.

J-Aggregates on colloidal silver suspension shows different characteristics than J-aggregates in water[6]. The coherent emission has been observed only when aggregates form on the colloidal surface[32]. This difference might be explained by studying the excited state dynamics of the same dye in both forms i.e in water and in colloidal suspension. Since excited state dynamics of J-aggregates of TDBC cyanine dye in water has been studied earlier[7], TDBC cyanine dye was chosen to form aggregation on colloidal silver. Pump-probe experiments were performed to compare the results with the earlier works.

4.4. Material preparation

TDBC is the sodium salt of 1,1'-diethyl-3,3'-bis(4-sulfobutyl)-5,5',6,6'-tetrachloro-benzimidazolo carbocyanine. This material was purchased from Moleculer Probe and used without further purification. Aqueous colloidal silver suspension was prepared by reduction of 5mM of $AgNO_3$ with 10mM of $NaBH_4$. 0.3ml $AgNO_3$ was drop-wise added into 49.7ml of $NaBH_4$, with vigorous stirring. This mixture was stirred for 1 hour in an ice bath. The resulting silver solution had an absorption peak at ~384nm, was yellow in color, and stable for several days. Mixing 6ml of 1mM TDBC in methanol solution with 25ml of aqueous silver colloid formed J-aggregates.

4.5. Experimental setup

The optical setup for pump and probe experiments is shown in figure 2.11. The output of the OPA at 587nm wavelength was used as a pump beam. A white light continuum was used as a probe beam. Pump and probe beams were focused onto a flowing sample in a 0.2mm thick flow cell. Time resolved difference absorption spectra were measured while changing the temporal delay between the excitation and the probe. The data collection procedure for transient absorption spectra was explained in chapter 2.

There were two problems with using a J-aggregate as a material. The first was that the emission of the material contributed to the signal. The second was the strong linear absorption of the white light continuum by the J-aggregate. These two effects do not depend on the time overlap of the pump and the probe pulses. To minimize these effects, a reference spectrum was taken when both the pump and the probe pulses were present and the probe pulse was approximately 2 ns before the pump pulse. No signal was seen at the time delays when the probe pulses travel before the pump pulses. A transient absorption signal appeared when both pulses overlapped in time and the signal got smaller when the probe pulses were delayed relative to the pump pulses. This procedure ensures that the regular absorption and emission caused by the pump and the probe pulses, which do not depend on the time overlap of the pulses, do not affect the pump-probe spectrum. With this procedure, we detect only the time dependent absorption or emission caused by the sample.

4.6. Results and discussion

4.6.1. Linear absorption spectrum

Figure 4.3 shows the absorption spectra of the TDBC aggregate and monomer. The monomer spectrum centered at 520 nm, can be observed at very low concentrations ($<<10^{-6}$ M). The monomer absorption band is very broad. At higher concentrations a new much narrower (with a width (FWHM) of 200 cm^{-1} or 6.8 nm) and red shifted (at 587 nm) absorption band appeared as evidence of a J-aggregate formation. This new feature is due to delocalized excited states[33] of assemblies of dye molecules bound by electrostatic forces. The asymmetric tail of the J-aggregate absorption spectrum is evidence of absorption to the upper k levels in the one-exciton band.

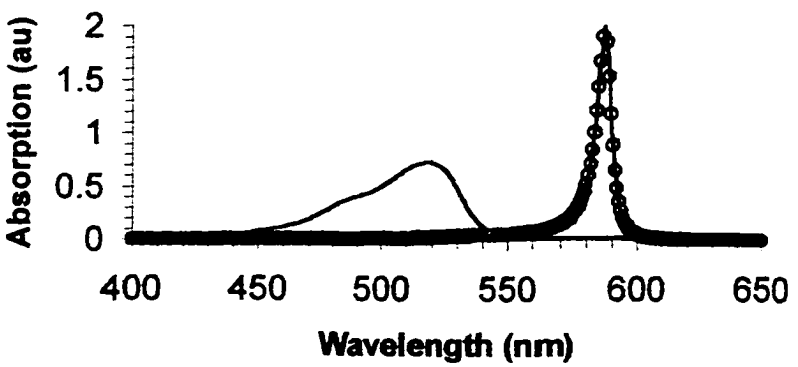

Fig.4.3 Absorption spectra (TDBC_Ag aggregate (o), TDBC monomer (-))

TBDC absorbs and emits light in the J-aggregate band (587nm). It shows a resonance fluorescence feature, a characteristic property of J-aggregates due to the formation of exciton energy levels. The formation of exciton bands dramatically changes the linear and nonlinear optical spectra and dynamics of TDBC molecules.

4.6.2. Cross-correlation function

The 587 nm pump wavelength and the 800 nm wavelength within the white light continuum were mixed by using a 200 μm thick KDP crystal placed at the sample site in the pump probe setup. The cross-correlation technique was described in chapter 2. The mixed frequency around 340 nm was detected with a silicon detector. The detected signal intensity versus delay time was recorded to calculate the pulse duration. Figure 4.4 shows the cross-correlation function of 587 nm and 800 nm wavelengths. The full width half maximum of this function is calculated as 224 fs by using a gaussian curve fit.

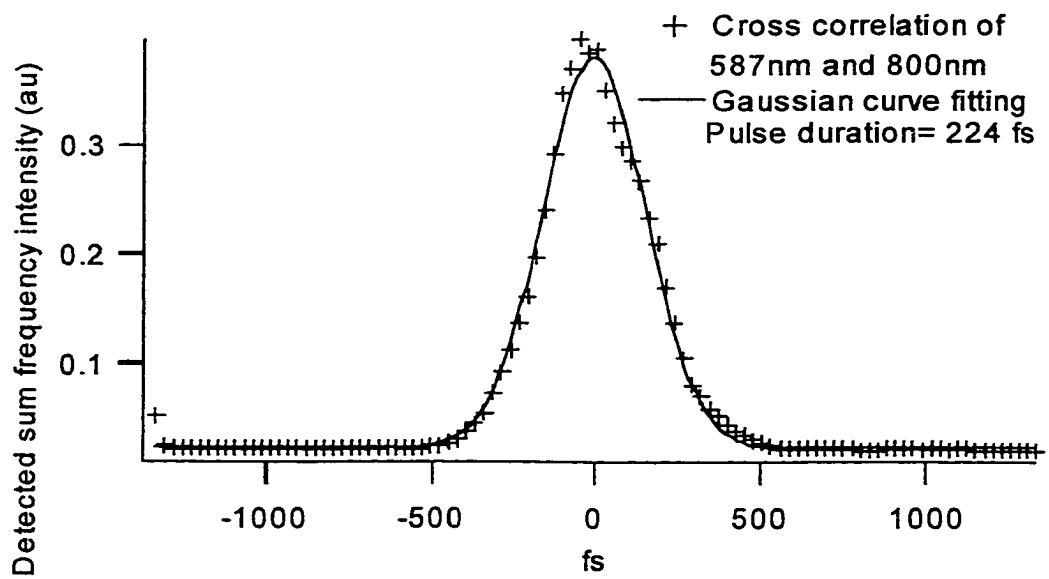

Fig.4.4 Cross-correlation function of 587nm and 800 nm wavelengths

4.6.3. Transient absorption spectrum

Pump-probe experiments in TDBC-Ag colloidal J-aggregates were performed to obtain information about the dynamics of the system. Figure 4.5 shows representative results of the femtosecond pump probe experiments with 130 fs pulses. The differential-spectrum is the difference in the probe absorption spectrum with and without the pump-pulse. Several features stand out in this spectrum:

1) Induced Absorption: An induced absorption band is observed on the high-energy side (blue-shifted signal) for J-aggregates formed in various host matrices and at different temperatures. This blue-shifted signal is assigned to a transition from one-exciton state to two-exciton state [7, 8, 9, 10, 34, 35]. This transition is theoretically explained as an exciton exciton interaction originating from an induced change in the permanent dipole moment[13, 36, 37]. This induced change was attributed to a change in the position of the counter ion of the dye chromophore following optical excitation of the sample [32]. In our pump-probe spectrum this induced absorption appears at 573 nm. In addition to the one-exciton to two-exciton transition, our data shows another induced absorption band centered at 490 nm. This absorption band diminishes within 100 fs. This absorption could possibly arise from a transition between the two-exciton and higher exciton states. Induced absorption to the higher exciton states has been observed in the two dimensional monomolecular layer of squarylium dye J-aggregate with fs pump-probe experiments[38].

2) Bleached absorption: A very strong negative signal at 587 nm is also observed. This signal is the sum of ground state bleaching and stimulated emission.

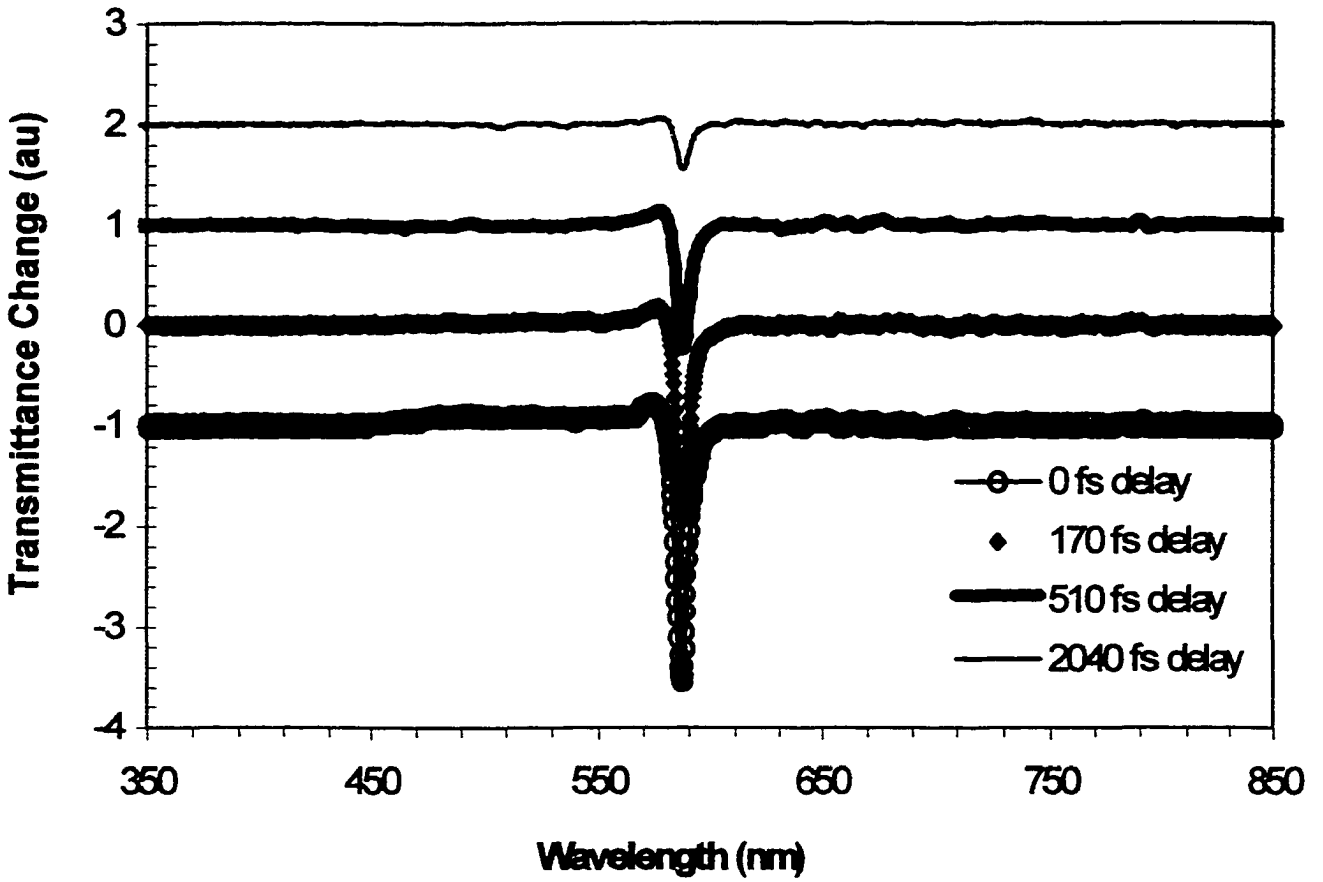

Fig.4.5 Differential transient absorption spectrum of TDBC-Ag J-aggregate at room temperature at different time delays (Note that spectra are shifted on transmittance scale.)

Differential absorption spectrum shown in figure 4.5 also gives information about the coherent size of our J-aggregate system. There are two different sizes of aggregates: One is the physical size (micrometer scale) the second is the coherent size. The coherent size is also called the delocalization length. The delocalization length has been defined as the number of molecules coherently responding to the external (optical or electrical) field. The linear and nonlinear optical properties of aggregates depend on the delocalization length of the electronically excited states. The coherent size of aggregates can be estimated by using the pump probe spectrum[12]. It has been shown that the difference between the bleach/stimulated emission signal and the absorption frequencies is

$$\omega_{bleach/stimulated} - \omega_{absorption} \approx \frac{3\pi^2 V}{(N+1)^2} \tag{4.11}$$

where V is the interaction energy between two molecules at the average nearest-neighbor distance and N is the delocalization length. The frequency of the strongest transition from the ground state to the k=1 state of the one exciton band can be found from equation 4.6.

$$\omega_{aggregate} = \omega_{monomer} + 2V\cos\left(\frac{\pi}{N+1}\right) \tag{4.12}$$

In this equation $\omega_{monomer}$ denotes the monomer absorption peak wavelength (520 nm) and $\omega_{aggregate}$ denotes the J-aggregate linear absorption peak wavelength (587 nm). The

nearest neighbor coupling energy can be estimated as $(\omega_{aggregate} - \omega_{monomer})/2$ in the N>>1 limit.

We estimated the nearest neighbor coupling energy to be 1097 cm^{-1}. By using equation 4.11 we also estimated that N (exciton delocalization length) is equal to 9. Recently the femtosecond dynamics of J-aggregates of TDBC molecules in water at room temperature was studied[7] and the exciton delocalization length was calculated to be 15 in one-dimensional aggregates. If the difference in the environment (in solution and on the colloidal surface) of the J-aggregates are considered, one can find agreement between the numbers.

4.6.4. Decay curves

Figure 4.6 shows the femtosecond optical response of the bleached and induced absorption features as a function of time delay between the pump and probe pulses. Both the induced and bleached absorption signals are normalized. Both signals exhibit multi exponential decays. Decay times are calculated by performing multi exponential curve fitting on induced and bleached absorption decay curves. Time constants are found to be 400 fs and 2.5 ps for the bleached signal, and 670 fs and 4.75 ps for the induced absorption signal. The two time constants are explained mainly by the relaxation process from the one-exciton states to the ground state. The fast and slow decay times can be attributed to the stimulated and spontaneous emissions from the one-exciton band respectively. M. Furuki et al. observed 300 fs for the stimulated emission decay and 12 ps for the spontaneous emission decay[38] for two-dimensional squarliyum J-aggregate film.

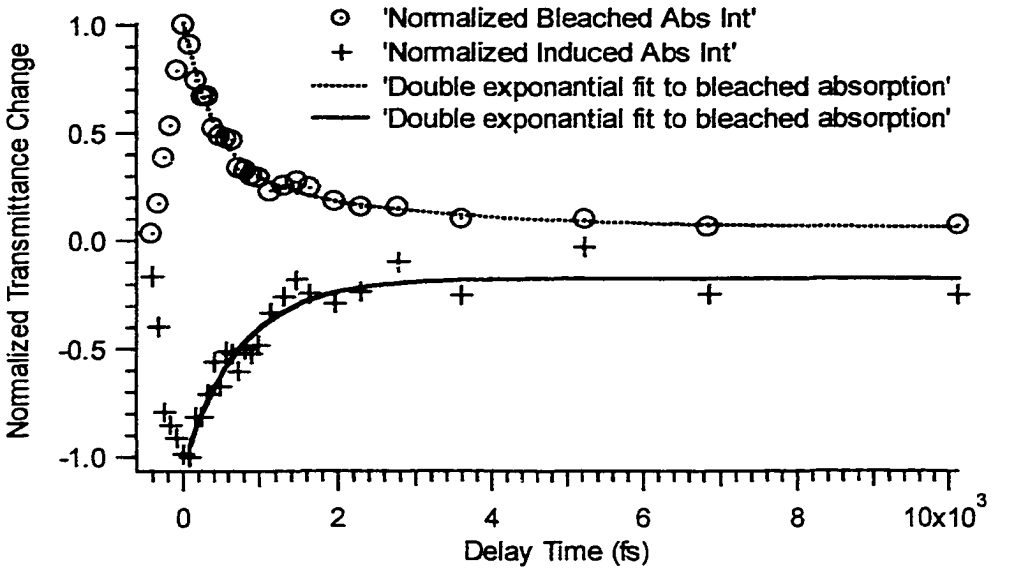

Fig.4.6 Optical intensity decay of the bleached and induced absorption signals as a function of delay time

Experiments with one-dimentional TDBC J-aggregate do not show this fast component[7], i.e. stimulated emission from the one-exciton state. The stimulated emission process was observed and explained for a cyanine dye adsorbed onto colloidal silica by S. Ozcelik et al[6]. Their findings can be summarized as follows: A photon resulting from a transition between the two-exciton band and the one-exciton band stimulates a one-exciton band photon emission at the two exciton band wavelength, thus amplifying the photon flux of the two-exciton state to one-exciton state transition.

For a better understanding, the energy level structure and population dynamic scheme is shown in figure 4.7. The pump pulse at 587 nm populates the one-exciton state. Fig. 4.5 shows the excited state absorption band at 573 nm. This induced absorption

shows that the 573 nm, part of the white light continuum, causes a transition from the one-exciton state to the two-exciton state. If the two- to one-exciton transition stimulates the one-exciton state emission, the increase of the two-exciton state population should result in more stimulated emission. The two-exciton state population can be increased by increasing the probe pulse energy. As a result, an increment in stimulated emission should appear as an increment in the bleached signal.

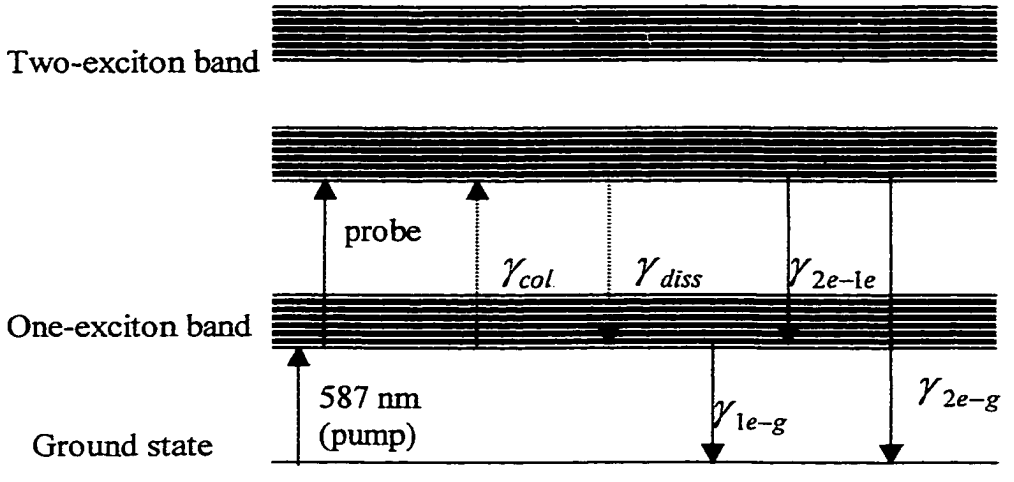

Fig.4.7 Energy level diagram for TDBC J-aggregate onto colloidal silver (γ_{coll}, γ_{diss}: collision and dissociation rare constants respectively; γ_{1e-g}, γ_{2e-g}: rate constants for one-and two-exciton to ground state transitions respectively.)

4.6.5. Pump and probe energy dependence

In order to make sure that the bleached signal contains a contribution from stimulated emission we performed pump-probe experiments at different probe energies while keeping the pump energy constant. Figure 4.8 shows the differential transient absorption spectrum of TDBC-Ag J-aggregate for different probe (white light) energies at zero time delay at room temperature. As expected, the bleached signal increased about 5 times without saturation when the probe energy is increased from about 1 μJ/pulse to 7 μJ/pulse.

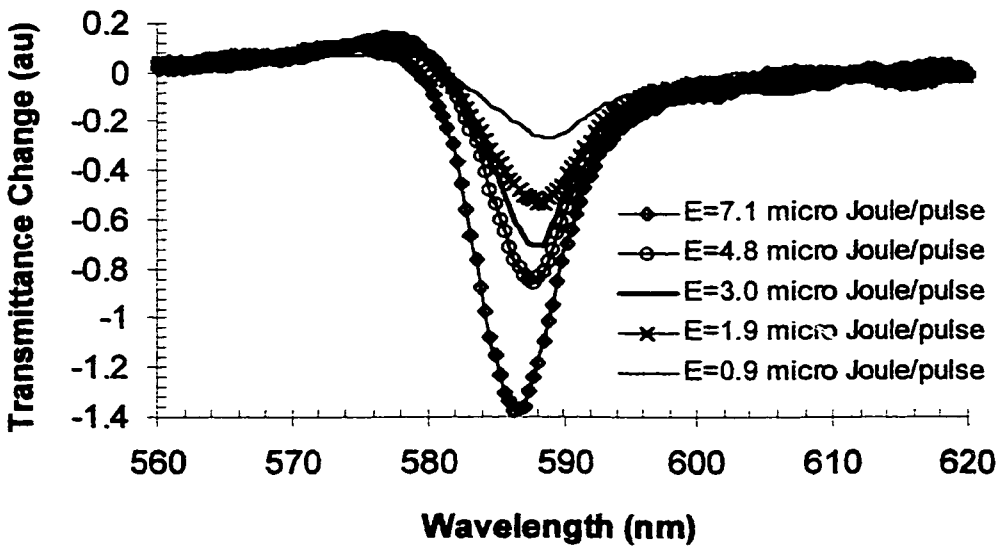

Fig.4.8 Differential transient absorption spectrum of TDBC-Ag J-aggregate for different probe (white light) energies at zero time delay at room temperature room temperature

The bleached signal intensity versus the probe pulse energy is plotted in figure 4.9 to illustrate the relationship between them. Figure 4.10 shows the normalized bleached signal spectra for different probe energies and illustrates the shift (3 nm) in wavelength. As a result, changing the probe pulse energy from 1 μJ to about 7 μJ changed the bleached signal wavelength from 589 nm to 586 nm and the bleached signal bandwidth (FWHM) from 5.1 nm to about 3.9 nm.

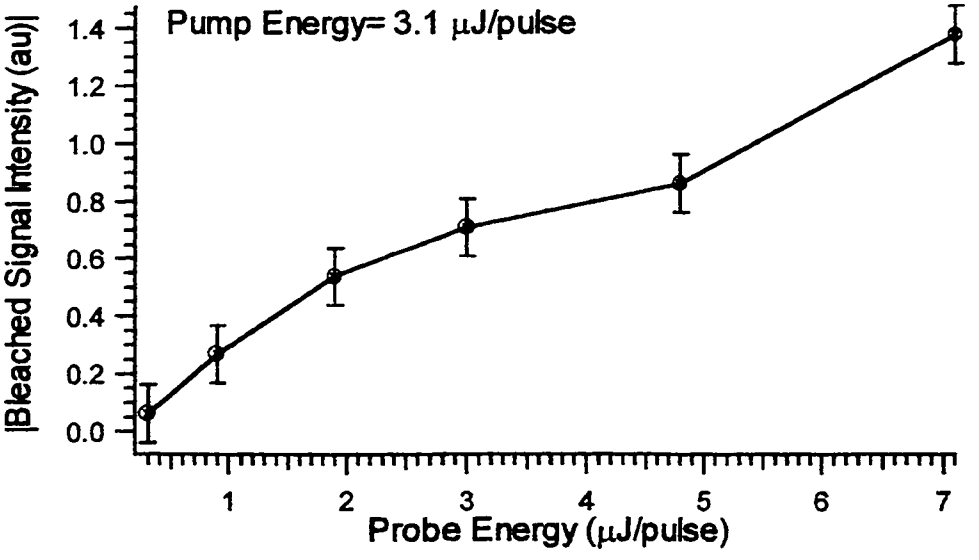

Fig.4.9 Bleached signal intensity versus probe energy per pulse

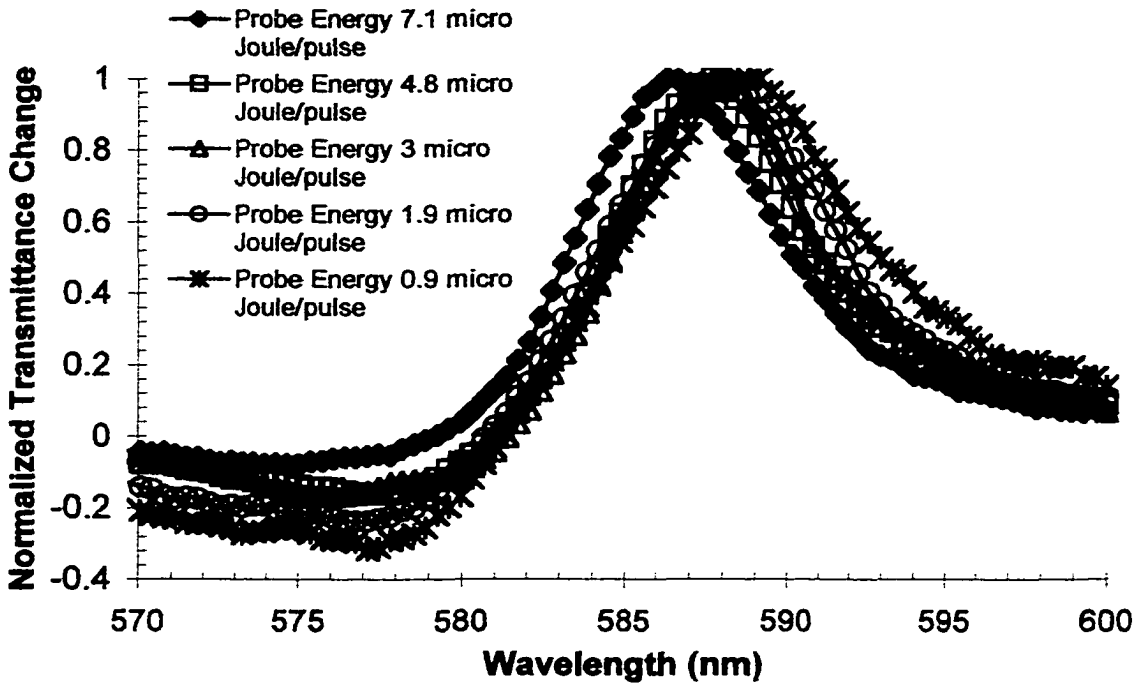

Fig.4.10 Normalized bleached signal spectrums for different probe energies to visualize the shift in wavelength

Before interpreting these results, the data collection procedure explained in the experimental section has to be considered. After changing the probe intensity, a new reference was stored. In other words, increasing the probe pulse intensity does not increase the bleached signal if there is no time dependent emission. These effects strongly suggest that we have detected a strong stimulated emission (superradiant lasing) from TDBC J-aggregates adsorbed onto colloidal silica at room temperature by performing a pump-probe experiment. Stimulated emission has not been seen with pump-probe experiments performed on TDBC-water J-aggregate sample[7, 24].

In order to see the effect of the pump pulse we performed similar experiments while changing the pump energy from about 1 μJ/pulse to 9 μJ/pulse. Figure 4.11 shows the bleached signal intensity versus the pump pulse energy. The bleached signal increased about 1.4 times and saturated when the pump energy was increased from about 1 μJ/pulse to 7 μJ/pulse.

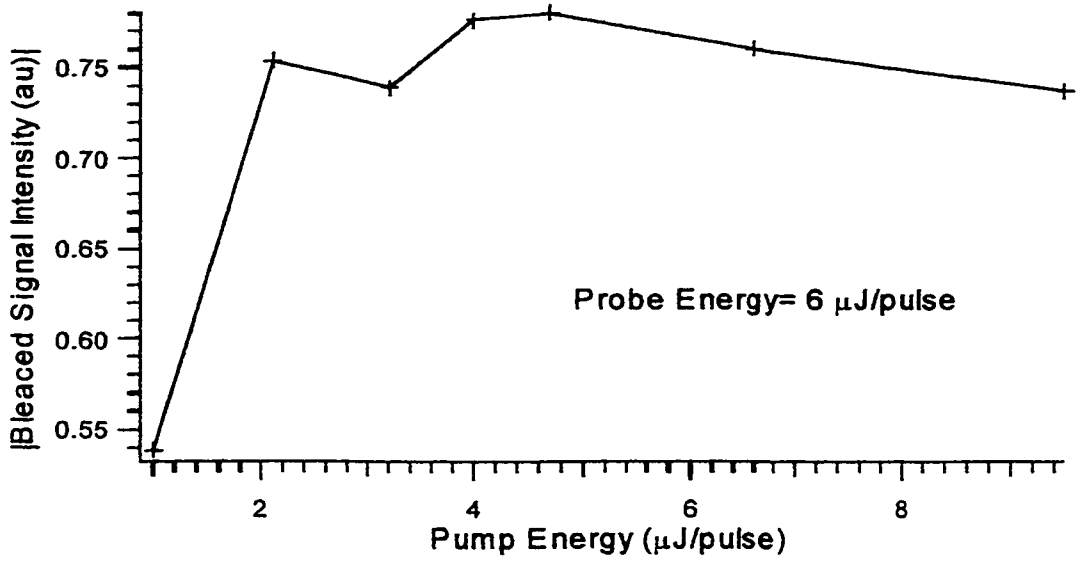

Fig.4.11 Bleached signal intensity versus pump energy per pulse

The saturation effect can be explained as follows: Increasing the pump energy up to 2 μJ/pulse increases the bleaching of the one exciton state. At this energy, the one-exciton band is fully populated because of the long lifetime of the one-exciton band. After that point, increasing the pump pulse energy further cannot excite more ground states to one-exciton transitions. Thus, the bleached signal cannot further increase (i.e. bleached signal saturates). On the other hand, increasing the probe energy does not

saturate the two-exciton state. This is because the two-exciton state has a very short lifetime compare to the one-exciton band.

What happens to the induced absorption signal when the pump and the probe intensities are increased? Since the two-exciton band lifetime is very short, the one-exciton state is almost instantly populated. As a result, the one-exciton state population is always large resulting in a relatively stable value for the absorption. In addition, increasing pump intensity once bleaching is achieved should not increase the induced absorption. Therefore, one should not expect an enhancement of the induced absorption signal when the pump or the probe is increased. Figures 4.12 and 4.13 show the induced absorption signal versus the probe and pump intensity respectively.

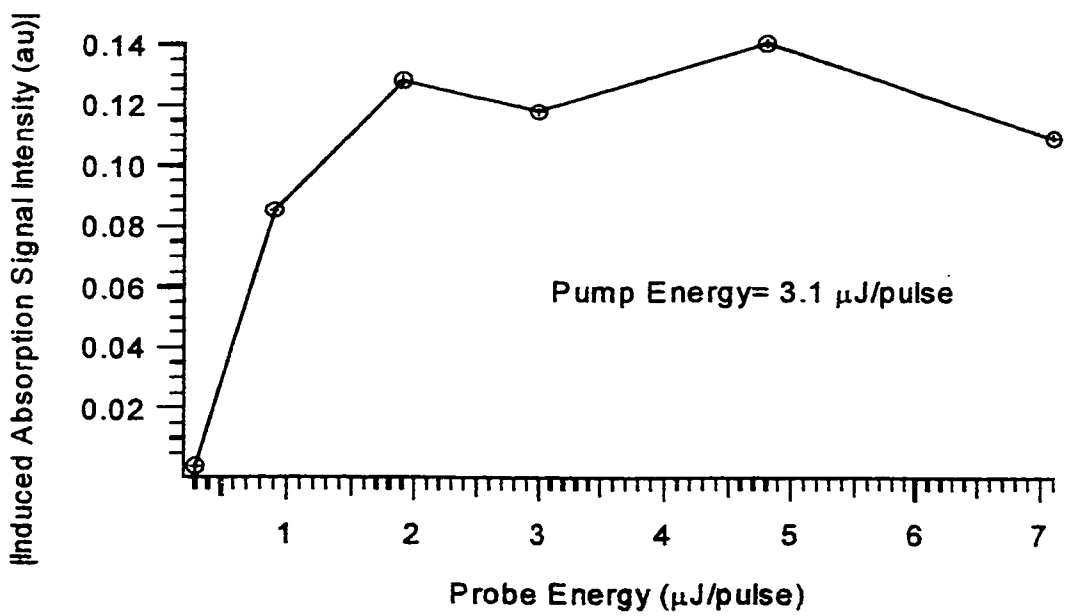

Fig.4.12 Induced absorption signal intensity versus probe energy per pulse

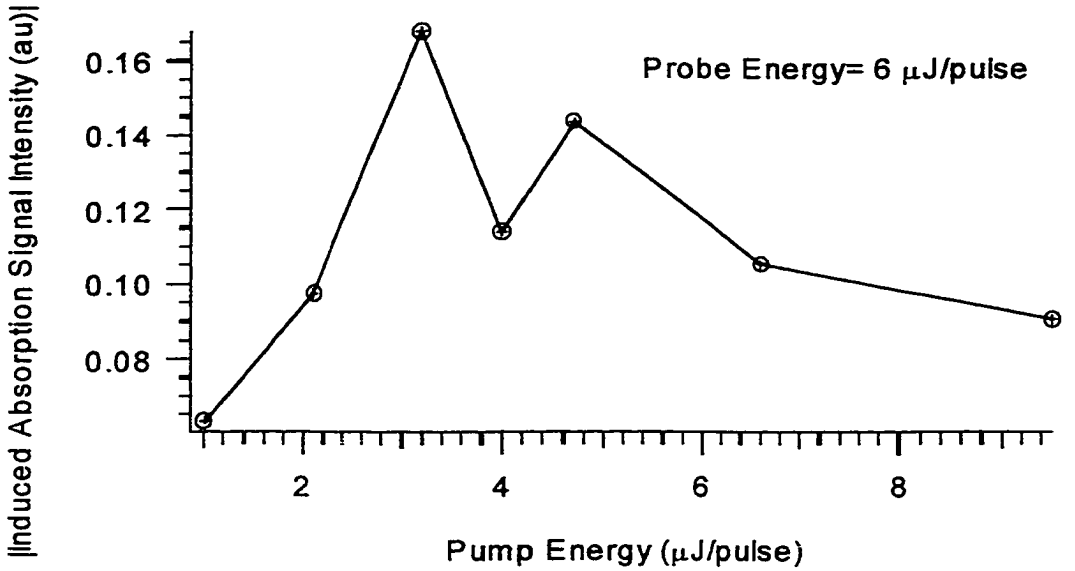

Fig.4.13 Induced absorption signal intensity versus pump energy per pulse

4.6.6. Pump wavelength dependence

In addition to these experiments, pump wavelength dependence experiments were performed. The pump beam at different wavelengths were obtained from the OPA without changing the experimental setup and alignments. The pump and probe energies were kept at 2 μJ/pulse and 3 μJ/pulse respectively for every pump wavelength. Note that, while the total probe energy seems higher than the pump energy, one should consider that the whole probe spectrum shares this energy. Transient absorption spectra were detected at the delay positions were the bleached absorption reached maximum value for each pump wavelength. The bleached and induced absorption signal intensities

versus the pump wavelength are plotted in figure 4.14. Figure 4.14 also shows the linear absorption spectrum of TDBC colloidal aggregates.

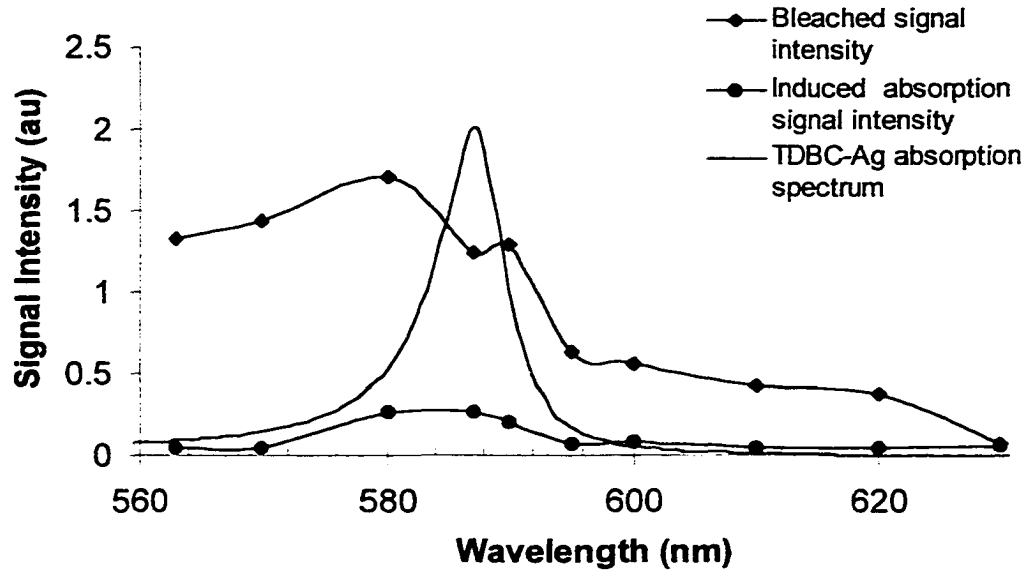

Fig.4.14 Induced absorption and bleached signal intensity versus pump wavelength

Interestingly, the bleached signal maximum appears at 580 nm pump wavelength instead of at the maximum linear absorption wavelength, which is at 587 nm. When we pump with slightly shorter wavelength, the pump beam not only populates the one-exciton state from the ground state, but also populates the two-exciton state from the one-exciton state. This is because in J-aggregates the energy difference between the two- and the one-exciton states is slightly higher than that of the one-exciton state and the ground state. Increasing the population of the two-exciton state contributes to the bleached signal by stimulating the one-exciton to ground state transition. Thus, the 580 nm pump wavelength provides more bleached signal. This finding strongly supports the bleached

signal explanation that we gave earlier i.e. bleached signal is actually a stimulated emission.

4.7. Conclusions

In summary, we have performed for the first time femtosecond pump-probe spectroscopy experiments on TDBC J-aggregate adsorbed onto colloidal silica at room temperature. The measured bleached and induced absorption wavelengths (587 nm and 573 nm respectively) were identical to the result of the experiments performed on TDBC J-aggregates in water. However, our bleached signal had contribution from stimulated emission, which has not been seen in J-aggregates in water. This contribution was proven with pump, probe energy, and pump wavelength dependent experiments. The bleached signal showed two components. The fast and the slow components were assigned to the stimulated emission and the spontaneous emission from the one-exciton state to the ground state, respectively. The lifetimes of the stimulated and the spontaneous emissions were measured as 400 fs and 2.5 ps respectively.

References

[1] E. E. Jelley, Nature, 138, 1009(1936).

[2] G. Scheibe, Angeew. Chem. 49, 563(1936).

[3] W. West, P. B. Gilman, Jr. in "The theory of the photographic process", 4th ed., Macmillan: New York,pg 251(1977).

[4] V. Sundstrom and R. van Grondelle, J. Opt. Soc. Am. B7, 1595 (1990).

[5] F. C. Spano, S. Mukamel, Phys. Rev. A, 40, 5783(1989).

[6] S. Ozcelik, D. L. Akins, Appl. Phys. Lett.. 71, 3057 (1997).

[7] M. Van Burgel, D. A. Wiersma, K. Duppen, J. Chem. Phys. 102, 20 (1995).

[8] H. Fidder, et. al., J. Chem. Phys., 98, 6564(1993).

[9] K. Minoshima, et. al., Chem. Phys. Lett, 218, 67(1994).

[10] A. Johnson, et. al., Chem. Phys. Lett., 211, 511(1993).

[11] S. Makio, N. Kanamaru and J. Tanaka, Bull. Chem. Soc. Jpn. 53, 3120 (1980).

[12] M. Lindrum, A. Glismann, J. Moll and S. Daehne, Chem. Phys. 178, 423 (1993).

[13] K. Misawa, K. Minoshima, H. Ono and T. Kobayashi, Chem. Phys. Lett. 220, 251 (1994).

[14] A.S. Davydov, "Theory of Molecular Excitons", Plenum, New York (1971).

[15] D.B. Chesnut and A. Suna, J. Chem. Phys. 39, 146 (1963).

[16] F.C. Spano, Phys. Rev. Lett. 67, 3424 (1991); 68, 2976 (1992).

[17] J. Knoester, Phys. Rev. A 47, 2083 (1993).

[18] F.C. Spano and S. Mukamel, J. Chem. Phys. 91, 683 (1989).

[19] A.H. Herz, Adv. Colloid Interface Sci. 8, 237 (1977).

[20] H. Fidder, J. Knoester and D.A. Wiersma, J. Chem. Phys. 95, 7880 (1991).

[21] F.C. Spano, V. Agranovich and S. Mukamel, J. Chem. Phys. 95, 1400 (1991).

[22] S. Mukamel, "The Principles of Nonlinear Optical Spectroscopy", Oxford University Press, New York, (1995).

[23] M. Kasha, H.R. Rawls and M. Ashraf El-Bayoumi, Pure Appl. Chem. 11, 371 (1965).

[24] J. Moll, S. Daehne, J.R. Durrant and D.A. Wiersma, J. Chem. Phys. 102, 6362 (1995).

[25] A. Herz, "Theory of photographic process, 4th ed.", Macmillan, New York, pp235-250 (1007).

[26] A. H. Herz, R. P. Danner, G. A. Janusonic, "Adsorption from Aqueous Solution", ACS Monograph 79, Rheinhold, New York, pp 173-197 (1968).

[27] D. L. Akins, J. Colloid Interface Sci., 90, 373 (1982).

[28] X. Li, B. Gu, D. L. Akins, Chem. Phys. Lett., 105, 263 (1984).

[29] K. Kemnitz, K. Yoshihara, T. Tani, J. Phys. Chem., 94, 3099 (1990).

[30] E. L. Quitevis, M. N. Horng., Y. S. Chen, J. Phys. Chem., 92, 256 (1988).

[31] M. L. Horng, E. L. Quitevis, J. Phys. Chem., 93, 6198 (1989).

[32] S. Ozcelik et al, J. Phys.Chem.B, 101, 3021(1997).

[33] J. Franck, et al, J. Chem. Phys. 6, 861 (1938).

[34] J. Durrant, et. al., Chem. Phys. Lett., 222, 450(1994).

[35] A. Chakrabarti, Phys. Rev. B, 57, R4206(1998).

[36] F. Spano, Chem. Phys. Lett., 220, 365(1994).

[37] F. Spano, Chem. Phys. Lett., 234, 29(1995).

[38] M. Furuki, L. S. Pu, F. Sasaki, S. Kobayashi, T. Tani, Appl. Phys. Lett. 72, 2648 (1998).

CHAPTER 5

NONLINEAR OPTICAL PROPERTIES OF LANGMUIR-BLODGETT MEMBRANES OF SOME AROMATIC POLYDIACETYLENES

5.1. Background

5.1.1. Review on Polydiacetylenes

Conjugated polymers with alternate single and multiple bonds in their backbone structure provide a molecular plane for extensive π electron delocalization. Thus, conjugated polymers are the most widely studied group of χ^3 organic materials. Polydiacetylenes (PDAs) are a class of π - electron conjugated polymers. This class of polymers became of interest as a viable group of nonlinear materials after the discovery that they posses a very large nonresonant χ^3. The general structure of polydiacetylenes is:

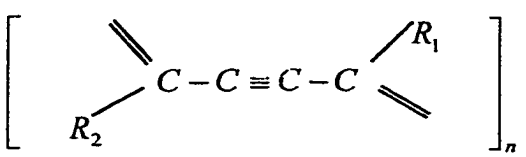

Polydiacetylenes are prepared by solid-state polymerization of the corresponding monomer[1]:

$$R_2\text{-}C{\equiv}C\text{-}C{\equiv}C\text{-}R_1$$

Polymerization can be induced thermally by UV light or by gamma irradiation. If the appropriate substituents are chosen, Langmuir-Blodgett films of polymers can be formed. Depending on the side groups, these polymers can be crystalline, liquid crystalline, monolayer, multilayer, or in solution form.

The third order nonlinear optical properties of the different forms of polydiacetylenes including Langmuir-Blodgett films have been investigated[2]. The large nonlinear coefficient has been attributed to the delocalization of the π electrons along the carbon backbone on polymerization. Each carbon chain can be viewed as a quasi-one-dimensional unit, and these chains are linked by the side groups, R_1 and R_2, which are large molecular groups that determine the structural properties of the polymer. Table 5.1 gives some of the results of χ^3 measurements on various diacetylenes.

The nonlinear optical properties of conjugated polymers can be enhanced by optimizing conjugation length, packing and orientation. The fabrication of compact, oriented monomolecular films can be achieved through the Langmuir-Blodgett technique. The effects of packing and orientation on the nonlinearity of Langmuir-Blodgett films are discussed in the following section. Section 5.1.3 discuses the effect of the conjugation length on the third order nonlinearity.

Table 5.1 χ^3 measurements on various polydiacetylenes

Side groups R_1 and R_2	Measurement Technique	λ (μm)	Material Forms	χ^3(esu)	Ref
$R_1=R_2=(CH_2)_4OCONHC_6H_5$ (TCDU)	THG	2.62	Crystal	$(3.7\pm12.4)*10^{-11}$	3
$R_1=R_2=C_6H_4NHCOC_{17}H_{35}$	THG	1.9	Cast Film	$1.4*10^{-11}$	4
$R_1=R_2=(CH_2)_4OCONHC_3H_7$	THG	1.9	Oriented by unidirectional rubbing	$3.8*10^{-10}$	5
$R_1=R_2=-CH_2-N-C_{12}H_8$ (p-DCH)	THG EFISH	1.35-1.45 1.35-1.45	Monomer vacuum deposited on alkali halide and polymerized	$(1\pm0.1)*10^{-10}$ $(6.4\pm0.4)*10^{-11}$	6
$R_1=CH_3-(CH_2)_{15}$ $R_2=-(CH_2)_8-COOH$	Waveguide coupling	0.650 0.75	LB films (500 A°)	$4*10^{-11}$ $4*10^{-10}$	7
$R_1=R_2=(CH_2)_3OCON(CH_3)_2$ $R_1=R_2=CH_2OCONHC_4H_9$	THG THG	1.9 1.9	Cast Film Vacuum-deposited monomer polymerized by UV light	$5.2*10^{-12}$ $1.4*10^{-11}$	8
$-(CH_2)_4-OC-N-CH_2-C-OC_4H_9$ O H O (Poly-4-BCMU)	DFWM	0.602	Solution cast film in red form	$4*10^{-10}$	9
			Film in yellow form	$2.5*10^{-11}$	10
	DFWM	1.17eV	Solution gel	$1.1*10^{-11}$	11
	Kerr	$\hbar\omega_1$= broad band $\hbar\omega_2$= 1.99 eV	PMMA doped with poly-4-BCMU solution cast film	$\leq3*10^{-10}$ (resonance) $3*10^{-11}$ (non resonance)	12 13
	THG	1.06	LB film	$3*10^{-11}$	14

5.1.2.The effects of packing and confinement on the nonlinearity in Langmuir – Blodgett films

The Langmuir-Blodgett (LB) films are formed by the transfer of a monolayer film of an amphiphilic molecular structure from an air-water interface to a solid substrate. An amphiphilic molecule has a structure that contains a polar head and a nonpolar tail. If this kind of molecule is spread over water, the polar group interacts with water while the nonpolar tail stick out of the water. This creates a non-centrosymmetric ordering of monolayers. Thus, Langmuir-Blodgett films produce net χ^2. Figure 5.1 illustrates the LB film technique.

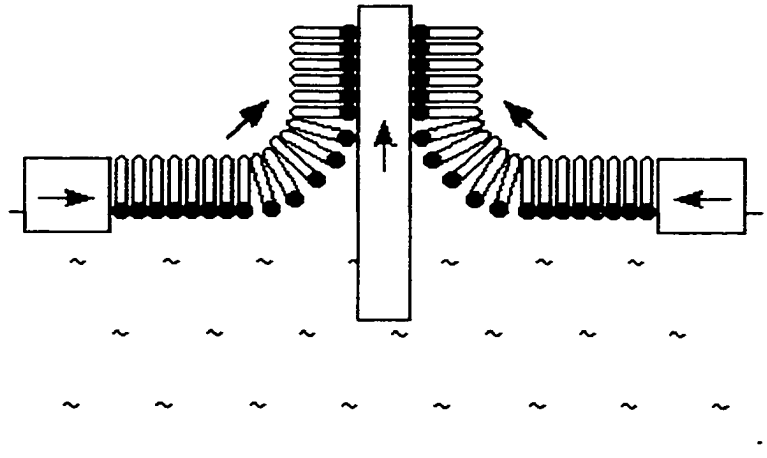

Fig.5.1 Illustration of the LB film technique

By using LB technique, films with thicknesses on the order of several wavelengths can be prepared layer by layer. The wave vector of a propagating mode in a waveguide is thickness dependent. Thus, films prepared by this technique might be able to preserve the phase relationships between modes over considerable distances. Wave

confinement can be achieved by confining the interacting optical beams in multilayer thick LB films.

L. Wang et al.[15] have shown that the third order nonlinear optical susceptibility of Poly(p-phenylene benzobisthiazole) LB film is enhanced by control of the packing density, and χ^3 values increase dramatically with increasing fabrication surface pressure. The effect of the packing on the third order nonlinearity is explained below.

Macroscopically, the polarization (P) of a medium can be related with the applied electric field (E) by the nth order optical susceptibility tensor $\chi^{(n)}_{ijk...}(-\omega;\omega_1,\omega_2,,....,\omega_n)$ [16]

$$P_i^{\omega} = P_i + \chi_{ij}^{(1)}(-\omega;\omega)E_j^{\omega} + \chi_{ijk}^{(2)}(-\omega;\omega_1,\omega_2)E_j^{\omega_1}E_k^{\omega_2} + \chi_{ijkl}^{(3)}(-\omega;\omega_1,\omega_2,\omega_3)E_j^{\omega_1}E_k^{\omega_2}E_l^{\omega_3} + ... \tag{5.1}$$

Similarly, the induced dipole moment of the molecule (p) can be related with the local electric field (E_{loc}) by the microscopic susceptibilities.

$$\begin{aligned} p_i^{\omega} &= \mu_i + \alpha_{ij}(-\omega;\omega)(E_j^{\omega})_{loc} + \beta_{ijk}(-\omega;\omega_1,\omega_2)(E_j^{\omega_1})_{loc}(E_k^{\omega_2})_{loc} \\ &+ \gamma_{ijk}(-\omega;\omega_1,\omega_2,\omega_3)(E_j^{\omega_1})_{loc}(E_k^{\omega_2})_{loc}(E_l^{\omega_3})_{loc} + ... \end{aligned} \tag{5.2}$$

In this equation, μ_i is the molecular dipole moment, α_{ij} is the linear polarizability, and β_{ijk} and γ_{ijkl} are the second and the third order nonlinear electronic microscopic susceptibilities, respectively. The local electric field is related to the macroscopic electric field through the local field factor (f_s^{ω}).

$$(E^{\omega}_{s,loc})_{i'} = (f^{\omega}_{s})_{i'j'} E^{\omega}_{j'} \tag{5.3}$$

The optical response of a macroscopic assembly such as LB film is calculated by simply summing these individual responses, averaged over their orientations. The macroscopic third order susceptibility can be related to the corresponding microscopic susceptibility with the following formula:

$$\chi^{(3)}_{ijkl} = N < a^{s}_{ii'} a^{s}_{jm'} a^{s}_{ko'} a^{s}_{lp'} \gamma_{j'k'l'm'} (f^{\omega}_{s})_{i'j'} (f^{\omega_1}_{s})_{r'n'} (f^{\omega_2}_{s})_{l'o'} (f^{\omega_3}_{s})_{m'p'} > \tag{5.4}$$

where N is the number of the density of the molecules, <...> represents an average over orientational distribution of molecules, $a^{s}_{ii'}$ is the orthogonal transformation matrix that transforms the molecules fixed frames (primed frame) to the laboratory frame (unprimed frame). The packing density (N) can be increased in LB technique by increasing the surface pressure during the fabrication; consequently, enhancement on the third order nonlinear susceptibility can be achieved.

The second order hyperpolarizability of individual molecules and the packing geometry causes the third order nonlinear optical susceptibility to be anisotropic. Based on the assumption that the orientational distribution of the polymer chains follows a Gaussian function, the nonzero $\chi^{(3)}$ tensor components can be calculated by using equation 5.4[16]:

$$\chi^{(3)}_{xxxx} = \frac{N}{C} \gamma^{*}_{yyyy} \int_{0}^{\pi} d\theta \sin\theta \cos^{4}\theta \exp\left[-\left(\frac{\theta}{\theta_0} \right)^{2} \right] \tag{5.5}$$

$$\chi^{(3)}_{yyyy} = \frac{3N}{8C}\gamma^{*}_{yyyy}\int_0^{\pi} d\theta \sin^5\theta \exp\left[-\left(\frac{\theta}{\theta_0}\right)^2\right] \tag{5.6}$$

$$\chi^{(3)}_{off} = \frac{N}{2C}\gamma^{*}_{yyyy}\int_0^{\pi} d\theta \sin^3\theta \cos 2\theta \exp\left[-\left(\frac{\theta}{\theta_0}\right)^2\right] \tag{5.7}$$

where $\gamma^{*}_{i'j'k'l'} = f^{3\omega}_{i'i'}\gamma_{i'j'k'l'}f^{\omega}_{jj'}f^{\omega}_{kk'}f^{\omega}_{ll'}$ is called the "dressed" second order hyperpolarizability, θ is the angle of the individual polymer chain with respect to the dipping direction, θ_0 indicates statistically the orientational degree of the polymer chains and is related to the standard deviation as $\sigma = \theta_0/\sqrt{2}$, and the parameter C is a normalization constant. The parameter $N\gamma^{*}_{yyyy}$ indicates the packing density of the molecules if γ^{*}_{yyyy} is regarded as a constant value.

If the polymer chains are perfectly aligned ($\theta_0 \to 0$) :

$$\chi^{(3)}_{eff} = N\gamma^{*}_{yyyy}\cos^4\phi \tag{5.8}$$

If the polymer chains are randomly oriented ($\theta_0 \to \infty$) :

$$\chi^{(3)}_{eff} = \frac{1}{5}N\gamma^{*}_{yyyy} \tag{5.9}$$

Equations 5.8 and 5.9 clearly show that larger $\chi^{(3)}$ values can be achieved if the molecular chains are perfectly aligned and the polarization of the field is parallel to the chain alignment ($\phi = 0$). The molecular chains can be aligned by using the LB technique. Thus, LB films of organic polymers are expected to have larger $\chi^{(3)}$ values relative to randomly oriented organic polymer films.

5.1.3.The effect of the conjugation length on the third order nonlinearity

The dependence of the third order nonlinearity on the conjugation length can be explained by using a simple free electron model[17]. In this model, π electrons are confined in a one-dimensional box (-L<r<L) of length 2L by an infinite barrier. L is the number of repeat units i.e. the conjugation length. The Hamiltonian for the π electrons in a one-dimensional box, in the presence of an electric field along the chain direction z, can be written

$$H = H^{(0)} + H^{(1)} = -\frac{\hbar^2}{2m}\left(\frac{\partial^2}{\partial z^2}\right) - eEz \qquad (5.10)$$

where the first term is the kinetic energy of the electron in the box of length 2L and the second term is the electric dipole interaction with the electric field polarized along the chain direction z. The Rayleigh-Schrodinger perturbation theory is used[18] to calculate γ. In the Rayleigh-Schrodinger perturbation theory, the infinite sum over the intermediate

states is calculated to obtain higher orders perturbation energies. The expression for γ calculated by this method is given by

$$\gamma = -2\sum_{n=1}^{N}\frac{1}{6}\frac{d^4E^{(4)}}{dE^4} = \frac{128L^{10}}{a_0^3e^2}\sum_{n=1}^{N}\left(\frac{-2}{9\pi^6n^6}+\frac{140}{3\pi^8n^8}-\frac{440}{\pi^{10}n^{10}}\right) \tag{5.11}$$

where $a_0 = \hbar^2/me^2$ is the atomic Bohr radius and the sum is over all occupied levels N. N is also the number of repeater units and 2N is the total number of π electrons in the conjugated structure (i.e. alternately single- and double-bonded structure). For the structure with a large conjugation length L only the first term of the equation 5.11 gives the higher contribution and γ is calculated as

$$\gamma = \frac{256L^{10}}{45a_0^3e^2\pi^6N^5} \tag{5.12}$$

If N∝L is assumed, this equation shows that for a free electron like systems the third order nonlinear microscopic susceptibility is proportional to the fifth order of the conjugation length ($\gamma \propto L^5$).

5.2. Introduction

Diacetylenes[19] and polydiacetylenes (PDAs) were found to have large third order nonlinear optical (NLO) susceptibility[4] by Wegner, and since then a great number of studies have been carried out in this group of polymers. The Langmuir-Blodgett (LB) technique is extensively used to prepare thin films from PDAs[20, 21, 22, 23]. LB films allow controlling the chain conformation, molecular orientation and packaging density of π-conjugated polymer structures. Therefore, LB films have enhanced third order NLO susceptibilities[16]. Recently, a comparison of the NLO properties of electrochemically prepared polythiophene (PT) and LB film of poly(3-alkylthiophene) (PTHT) has shown that the third order NLO susceptibility of LB film is at least one order of magnitude larger than that of electrochemically prepared film [24].

The third order NLO susceptibilities of aliphatic PDA LB membranes have been previously reported[25]. However, no aromatic PDA membranes have been studied. It is thought that the incorporation of aromatic groups into DA groups will increase the conjugation and the substituent groups on the aromatics will contribute to the polarization, thus the NLO susceptibility of PDA LB membranes will increase. M. P. Carreon at al. have recently reported for the first time LB membranes of a few aromatic PDAs[32,26], and found that the DA groups of the LB membranes readily polymerized, but PDA chains degraded on prolonged irradiation of UV light in air. This type of photodegradation of PDA LB membranes was not mentioned in previous studies on the aliphatic PDA LB membranes. Recently an in-situ study of monolayer of DA was reported[27], and a large deformation in the unit cell was seen when polymerized by

irradiation in the presence of oxygen. With respect to the third order nonlinear optical susceptibility, $\chi^{(3)}$, of Langmuir-Blodgett membranes of aliphatic PDAs, Kajzar and Messier have reported $\chi^{(3)}$ values of $(8.0 + 1.0) \times 10^{-12}$ and $(5.6 + 0.6) \times 10^{-11}$ esu determined by THG method (third harmonic generation) for the red[28] and blue[29] films, respectively. Four different aromatic DA LB membranes were prepared and irradiated under argon atmosphere by the group of Dr. Takeshi Ogawa in Mexico, and their third order NLO susceptibilities were determined by Z-scan technique by our group at City College of New York.

5.3. Material preparation

Figure 5.2 shows the molecular structures of studied DA amphiphiles. The synthesis and LB membrane preparation were reported previously[26, 27]. The LB films of these amphiphilic DAs were prepared on quartz substrates using a Miyata-Type moving wall LB film deposition apparatus, Model NL-LB240-MWA, manufactured by Nippon Laser & Electronic Laboratory, as described in previous papers[26, 27]. 30 Layer films were prepared for the Z-scan measurement.

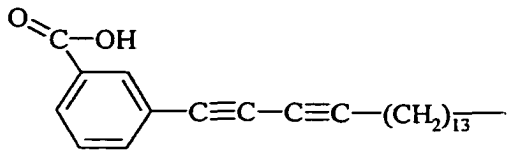

I

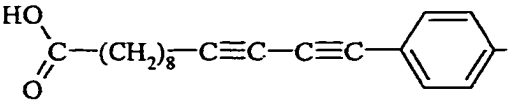

II

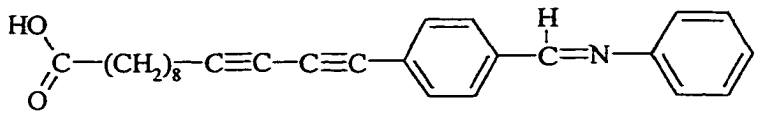

III

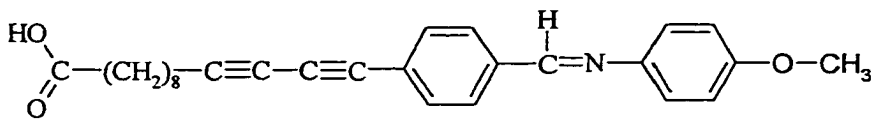

IV

I : 3'-hexadeca-1,3-diynilbenzoic acid.

II : 13-(3'-formylphenyl)-10,12-diynoic acid.

III : 13-[4'-(N-phenylimino)phenyl]-1,3-diynoic acid.

IV : 13-{4'-[N-(4''-methoxy)phenylimino]phenyl}-1,3-diynoic acid.

Fig.5.2 Molecular structures of DA of amphiphiles

5.4. Experimental setup

The single beam Z-Scan technique was used to determine the third order nonlinear optical susceptibility. The Z-Scan technique and experimental apparatus are described in chapter 2. The output of the amplifier, with a 800 nm wavelength, and 130 fs pulse duration is used to measure the nonlinearity. In addition, Z-Scan experiments were performed by using the output of the optical parametric amplifier, which was tuned to 615 nm.

5.5. Results and discussion

Open aperture Z-scan transmittance curves at 800 nm are flat, which means that there is no nonlinear absorption for all samples. Figure 5.3 shows typical curves for LB membrane IV, on quartz substrate at 800nm wavelength with about 3-4 μJ pulse energy. The difference between normalized peak and the valley transmittance is smaller for the film on the substrate than for the substrate alone. That means the sign for the nonlinear optical coefficient $\chi^{(3)}$ is different for the LB film than substrate. Since the Z-Scan transmittance for the substrate shows a minimum followed by a maximum i.e. $\chi^{(3)}$ has a positive sign. Therefore, the LB films have a negative $\chi^{(3)}$. The value of the third order susceptibility is calculated by using equation 2.29. The $\chi^{(3)}$ value of the quartz substrate, which is $2*10^{-14}$ esu, is used to determine the magnitude of $\chi^{(3)}$ for the LB membranes. The magnitude of $\chi^{(3)}$ for the LB membranes I, II, III, IV were determined as $(6\pm2)*10^{-11}$ esu, $(7\pm2)*10^{-11}$ esu, $(8\pm2)*10^{-11}$ esu and $(7\pm2)*10^{-11}$ esu, respectively. As it is seen there

is no change in $\chi^{(3)}$ values with the chemical structures. This could be due to possible deformation of these LB films destroying their ordered structures. Z-Scan measurement at 615 nm wavelength gave the expected resonance enhancement. The resonance values of $\chi^{(3)}$ at 615 nm wavelength for all LB films are about $(2.2\pm0.2)*10^{-10}$ esu which is one order of magnitude larger than at 800 nm.

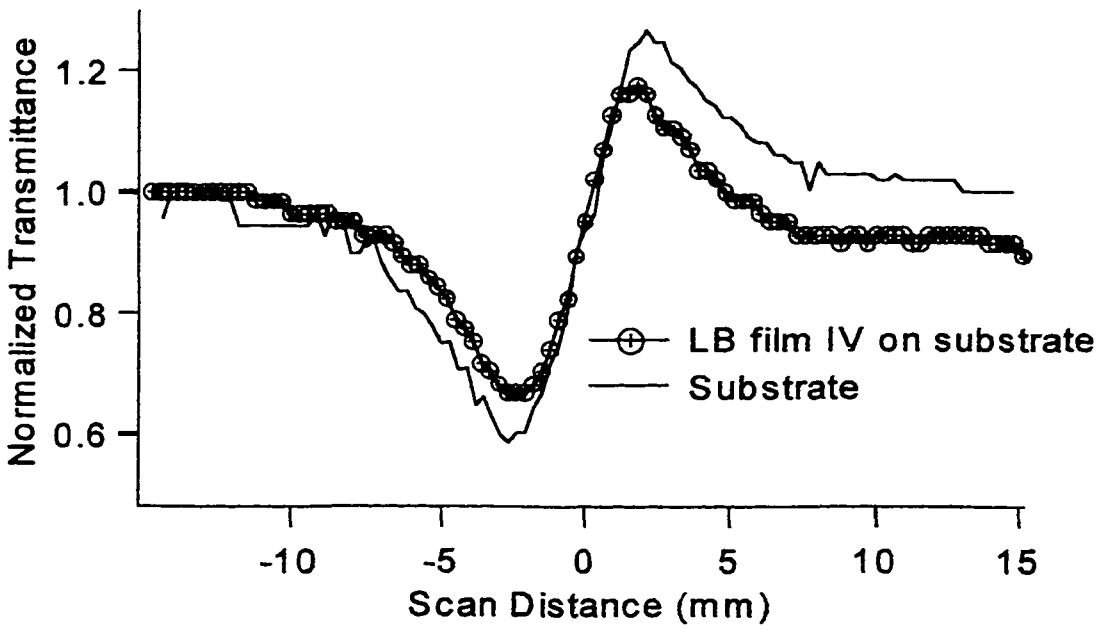

Fig.5.3 Typical curves for LB membrane IV, on quartz substrate at 800nm wavelength with about 3-4μJ pulse energy

5.6. Conclusions

In summary, we have investigated the third order nonlinear optical properties of Langmuir-Blodgett membranes of some aromatic polydiacetylenes for the first time. The measured third order NLO susceptibilities of four different aromatic DA LB membranes were around 10^{-10} esu. This value is substantially larger than that of LB membranes of aliphatic PDAs measured by Kajzar and Messier[10]. Based on these results we can conclude that the incorporation of aromatic groups into DA groups enhanced the third order nonlinear optical susceptibility.

References:

[1] M. Schot, and G. Wegner, in "Nonlinear Optical Properties of Organic Molecules and Crystals", edited by D. S. Chemla and J. Zyss, vol2, Academic Press, New ork.

[2] P. N. Prasad and D. J. Wiliams, "Introduction to nonlinear optical effects in molecules and polymers", John Willey & Sons, New York, (1991).

[3] C. Sauteret, J. P. Hermann, R. Frey, F. Pradere, J. Ducuing, R. H. Baughman, and R. R. Chance, Phsy. Rev. Lett., 36, 956(1976).

[4] T. Kurihara, K. Kubodera, S. Matsumoto, and T. Kaino, Polymer preprints, The Society of Polymer Science, Japan, 36, 1175(1987).

[5] T. Koda, K. Ishikava, T. kanetake, T. nishikawa, Y. yotukara, S. Koshihara, K. Takeda, and K. Kubodera, Third Asia Pacific Physics Confernce, Hong Kong, June (1988).

[6] J. LeMoigne, A. Thierry, P. A. Chollet, F. Kajzar, J. Messier, J. Chem. Phys., 88, 6647(1988).

[7] G. M. Carter, Y. J. Chen, M. F. Rubner, D. J. Sandman, M. K. Thakur, and S. K. Tripathi, in D. S. Chemla and J. Zyss (Eds.), Nonlinear Optical Properties of Organic Molecules and Crystals, Vol. 2, Academic, New York, p. 85 (1987).

[8] S. Tomaru, K. Kubodera, S. Zembutsu, K. Takeda, and M. Hasgawa, Elect. Lett. 23, 585(1982).

[9] D. N. Rao, P. Chopra, S. K. Ghoshal, J. Swiatkiewicz, and P. N. Prasad, J. Chem. Phys. Lett. 84, 7049(1986).

[10] D. N. Rao, J. Swiatkiewicz, P. Chopra, S. K. Ghoshal, and P. N. Prasad, Appl. Phys. Lett. 48, 1187(1986).

[11] J. M. Nunzi, J. L. Ferrier, and R. Chevalier, in J. Messier, F. Kajzar, P. Prasad, and D. Ulrich (Eds.), Nonlinear Optical Effects in Organic Polymers, NATO ASI Series, Vol. 12, Kluwer Academic, Dordrecht, p. 365(1989).

[12] P. P. Ho, R. Dorsinville, N. L. Yang, G. Odian, G. Eichmann, T. Jimbo, Q. Z. Wang, G. C. Tang, N. D. Chen, W. K. Zou, Y. Li, R. R. Alfano, SPIE Proc. 682, 36(1986).

[13] P. P. Ho, N. L. Yang, T. Jimbo, Q. Z. Wang, and R. R. Alfano, J. Opt. Soc. Am. B, 4, 1025(1987).

[14] G. Berkovic, Y. R. Shen, and P. N. Prasad, J. Chem. Phys. 87, 1897(1987).

[15] L. Wang, T. Wada, T. Yuba, M. Kakimoto, Y. Imai, H. Sasabe, J. Appl. Phys. 79, 12 (1996).

[16] R. F. Shi, A. F. Garito, in "Characterization technique and tabulations for organic nonlinear optical materials", edited by M. G. Kuzyk, C. W. Dirk, Marcel Dekker Inc., New York (1998).

[17] P. N. Parasad, D. J. Williams, Introduction to nonlinear optical effects in molecules and polymers, John Willey and Sons Inc., New York, p 54 (1991).

[18] K. C. Rustagi, and J. Ducuing, Opt. Commun., 10, 258 (1974).

[19] G. Wegner, Z. Naturforsch, 2B, 8248(1969).

[20] B. Tieke, G. Lieser, and G. Wegner, J. Polym.Sci., Poly. Chem. Ed., 17, 1631(1979).

[21] B. Tieke and G.Lieser, J. Colloid Interface Sci., 88, 471(1982).

[22] G. Lieser, B. Tieke, and G. Wegner, Thin Solid Films, 68, 77(1980).

[23] B. Tieke and G. Lieser, Macromolecules, 18, 327(1985).

[24] D. Harris et al., Synthetic Metals, 101, 204 (1999).

[25] M.P. Carreon, G. Burillo, V.Agabekov, and T.Ogawa, Polym.J., 29, 103(1997).

[26] M.P. Carreon, G. Burillo, L.Fomina, and T.Ogawa, Poly. J., 30, 95(1998).

[27] S. Yamada, Y. Shimoyama, Jpn. J. Appl. Phys. 36, 5242 (1997).

[28] F. Kajzar and J.Messier, Polym. J., 19, 275(1987).

[29] F. Kajzar and J. Messier, Thin Solid Films, 132, 11(1985).

CHAPTER 6

NONLINEAR OPTICAL PROPERTIES OF SILICON NANOSTRUCTURES IN SILICA MATRIX

6.1. Background

6.1.1.Review of Si nanoclusters

Recently, the physical properties of fine semiconductor particles have attracted the interest of both fundamental and applied researchers. Semiconductor nanostructures show quantum-size effects, consequently, exhibit novel physical properties not seen in bulk materials[1, 2]. Carrier confinement into dimensions on the order de Broglie wavelengths induces some nonlinear optical phenomena. Because of the need for better nonlinear optical materials for optical switching and signal processing application, this topic has been studied by many research groups[3, 4, 5, 6, 7]. Most of the research on nonlinear optics in nanoclusters has been focused on semiconductor-doped glasses (SDGs) where ultrafine semiconductor particles are uniformly dispersed in an insulating matrix[8].

It has been considered that indirect semiconductors are not suitable for photonic devices such as light emitting devices since they weakly interact with photons. Substantial studies have been concentrated only on the direct-band-gap III-V or II-VI compounds. Si is an indirect-gap material in the bulk form. However, confinement

induced mixing of states can lead to an indirect to direct gap transformation in Si nanoclusters[9]. Recent observations of visible photoluminescence in porous Si[10] (cluster size is between 2-15 nm) and Si ultrafine particles[11, 12, 13] and Si nanoclustures in SiO_2 layers[14] suggest that Si nanoclusters may become a promising material for optical applications.

Electrochemical etching is used to fabricate nanoporous Si[10]. There are several other techniques to prepare Si nanostructures such as plasma deposition from silane[15], crystallization of amorphous silicon[16], gas pyrolysis of Si_2H_6 and O_2[17] and ion implantation[14]. In the ion implantation technique, a given numbers of ions can be placed in a control depth distribution by changing the ion doses and the acceleration energies [18, 19]. Thus, this technique is considered as a potential candidate for manufacturing pure Si nanoclusters.

Photoluminescence studies of Si nanoclusters have been carried out by several other groups[20, 21]. Ion implanted nanocrystals have several photoluminescence bands in the visible[14, 22]. Emission from Si implanted samples has been identified as originating from defects in the SiO_2 matrix, generated during the implantation[14, 22].

Quantum (volume) confined and surface states play an important role on the characterization of the optical properties of semiconductor nanostructures. The next section presents a short description of these states in semiconductor nanostructures.

The nonlinear optical properties of Si nanoclusters into SiO_2 matrices have been studied by the group of Dr. H. Grebel at New Jersey Institute of Technology, using nanosecond pulses[23]. However, these properties have not been explored yet in the ps-fs

range. We present here the results of investigations of the nonlinear optical response of Si nanoclusters in the fs-ps range.

6.1.2. Quantum confinement and surface states

When a three-dimensional semiconductor is subject to one-, two-, and three-dimensional confinement, the density of states change[24]. Figure 6.1 schematically depicts the density of states. As seen from the figure, when the three-dimensional semiconductor is subject to a three-dimensional confinement, the density of states becomes discrete; consequently, discrete energy levels are formed. These energy levels are called quantum-confined states. The spacing of the quantum confined levels depend on the size of the confined region (L) and can be modified by an appropriate choice of L. The quantum confinement also causes the effective bandgap of semiconductor to increase relative to the bandgap of the bulk material. At the same time, the selection rules of the transitions between these levels introduce fundamentally new features in the optical spectrum.

As a result of the formation of the discrete energy levels, new and sharp resonances are created in the material. The transitions to these energy levels cause the observed enhancement of the third order nonlinear response of semiconductor nanostructures.

On the other hand, in quantum – confined structures a large fraction of

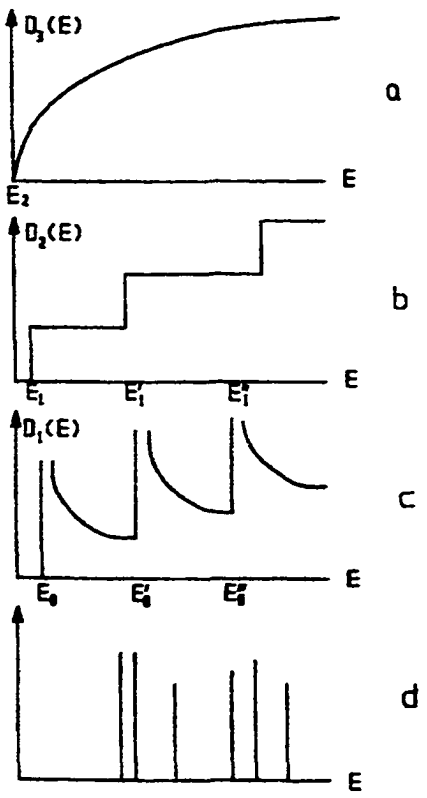

Fig.6.1 Modification of the density of states of an ideal three dimensional semiconductor (a) as it is gradually subject to one-, two-, and three-dimensional confinement (curves b, c, and d respectively), adapted from reference 29.

nanostructures (Si atoms in our case) is on the surface. In principle, there is one surface state for each broken surface chemical bond[25]. Surface states energies depend on local surface bond reconstruction and possible bonding to capping the molecules or solvent. In the case of Si nanocrystals with little reconstruction and surface capping, surface states exist inside the nanocrystal bandgap. In this case, the surface states act as deep traps. The possible transitions to the surface states are expected to enhance the nonlinear response of the nanostrucutes.

6.2. Introduction

Semiconductor nanocrystals have been widely studied in recent years for their potential use in nonlinear optical devices. However, the role of the quantum-confined states and surface states in the nonlinear optical characteristics has not been clarified yet. Such studies are often obscured by the complexity of the nanomaterial itself. Therefore, we have set to investigate a rather simple nanomaterial such as, silicon nanoclusters embedded in fused silica. While several methods of producing Si nanocrystals exist, ion implantation has established itself as a mature technology to produce a relatively narrow distribution of isolated nanocrystals in a large variety of matrices. In addition, large optical nonlinear coefficients at nanosecond pulses at λ=532 nm raised the question on the role of surface and quantum confined energy levels. For example, it was found, $Re\{\chi^{(3)}\}=10^{-7}$ esu for 3-4 nm Si crystals at λ=355 nm and $Re\{\chi^{(3)}\}=10^{-6}$ esu for 5-6 nm Si clusters at λ =532 nm[23]. Based on transient absorption measurements it was suggested [26] that deactivation of surface states was more efficient than quantum confinement effects in the PL of Si nanocrystals. In this study, we investigated the role of quantum states and surface states on the optical nonlinearities by performing nonlinear studies at pico- and femto-second pulse durations. We present a complete report on the nonlinear optical properties of two different samples: (i) Sample S1, 3-4 nm Si crystals in SiO_2 matrix, and (ii) Sample S2, 5-6 nm Si crystals in SiO_2 matrix.

6.3. Material preparation

Silicon nanocrystals were formed by Si (400 keV) implantation into fused silica glass matrices (1 mm thick Corning 7940) followed by 1hour of annealing at 1100 ^{0}C in flowing Ar + 4% H_2. The process has been described elsewhere[23]. At this energy, the projected range of excess Si is ~ 600 nm and the profile has a full width at half maximum of ~ 300nm. Two examples of such samples are described here: S1 sample was implanted to a dose of $1.5x10^{17}$ cm^{-2} with a peak excess Si concentration of $5x10^{21}$ cm^{-3} and S2 sample was implanted to a dose of $6x10^{17}$ cm^{-2} and a peak excess Si concentration of $2x10^{22}$ cm^{-3}. Sample S1 contained Si nanocrystals with diameters 3-4 nm and sample S2 contained crystals of 5-6 nm in diameter on the average. These sizes were estimated by use of a Transmission Electron Microscope (TEM) at New Jersey Institute of Technology. The clusters in both samples were spherical and crystalline. Linear absorption spectra of these samples were presented elsewhere[23].

6.4. Experimental apparatus

The optical nonlinear properties were measured by the Z-scan method with a frequency-doubled or, tripled Nd:YAG at $\tau \approx 70$ ps. Ultra short pulses from a diode pumped Ti-sapphire laser, with further amplification, was used for short pulse experiments. An Optical Parametric Amplifier (OPA) was used for wavelength variation.

6.5. Experimental results

As mentioned earlier, optical nonlinearity was measured using z-scan method. Intensity dependent absorption is defined as $\alpha(I) = \alpha_0+\Delta\alpha(I) = \alpha_0+\beta I+\ldots$. Here, β is the nonlinear absorption coefficient measured in cm/W, I is the peak intensity in W/cm^2 and $\Delta\alpha(I)$ is the overall nonlinear absorption change. Similarly, the nonlinear refractive index can be written as $n(I) = n_0+\Delta n(I) = n_0+\gamma I+\ldots$, where, γ is the nonlinear refraction coefficient (in cm^2/W) and $\Delta n(I)$ is the overall nonlinear refractive index change. For picosecond (ps) laser beam, it was verified experimentally that $\Delta\alpha(I)$ and $\Delta n(I)$ of *non-implanted* substrates silica are negligibly small compared to the implanted samples. Thus, we were able to directly attribute the nonlinearity to the existence of Si nanocrystals in the sample. However, the contribution of the substrate silica in femtosecond (fs) experiments is significant. To correct for the substrate contribution, the sample and the non-implanted substrate were measured separately and the nonlinear refractive index was calculated as described in chapter 2.

6.5.1. Z-scan experiments on 3 nm Si in SiO_2 matrix (Sample S1)

Measurements with picosecond pulses:

At λ=355 nm and τ=70 ps pulse duration, the sample exhibited a positive nonlinear absorption change, $\Delta\alpha$=1.5 x 10^5 cm^{-1} and a negative nonlinear refraction change, Δn=-0.29 at I=3.4 x 10^9 W/cm^2. When measured at 532 nm, this sample exhibited only nonlinear absorption and no nonlinear refraction.

Measurements with femtosecond pulses:

The experiments were performed at wavelengths λ=400, 590, 645, 710 and 800 nm. The absorption change, $\Delta\alpha(I)$, was independent of the incident intensity, I, when measured at λ=800 nm and pulse duration, τ=150 fs. This may be attributed to a saturation behavior or, to simply a small absorption value at that wavelength. The nonlinear refractive index change, $\Delta n(I)$ exhibited a behavior shown in figure 6.2 at λ=800 nm at various pulse durations keeping the pulse energy constant. As can be seen from the curve, $\Delta n(I)$ changes significantly around I=0.25 TW/cm^2. In figure 6.3, we show the variation of Δn around that point. Here we varied the intensity by varying the pulse energy keeping the pulse duration at τ=1.1 ps. The wavelength dependence of $\Delta n(\lambda)$ at τ=150 fs is shown in Figure 3. In general, figure 6.4 shows three distinct bands around λ=400, λ=600 nm and λ=700 nm.

6.5.2. Z-scan experiments on 5 nm Si in SiO_2 matrix (Sample S2)

Measurements with picosecond pulses:

Z-scan measurements were performed at λ = 532 nm and τ = 70 ps at various intensities. The peak intensity was varied between 0.7 to 11.4 GW/cm^2 and the absorption change, $\Delta\alpha(I)$ was independent of intensity; $\Delta\alpha(I) \approx 2\times10^5$ cm^{-1}. The nonlinear refraction was also independent of the peak intensity, $\Delta n(I) \approx -1$. $\Delta\alpha$ was positive indicating nonlinear absorption and Δn was negative. We note that the sign of Δn is opposite to the corresponding sign at nanosecond pulses.

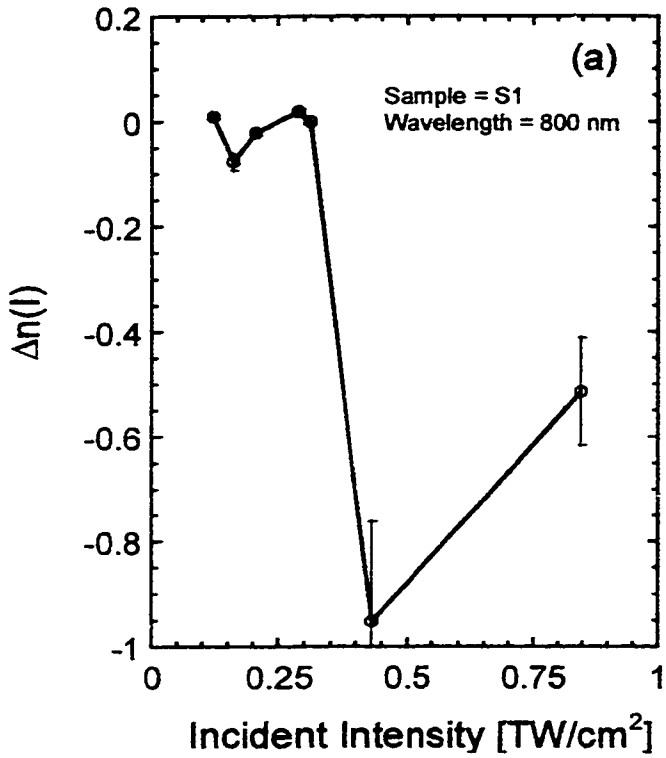

Fig.6.2 Intensity dependence of Δn(I) for sample 1 achieved by varying the pulse duration between 150 fs - 1 ps and keeping the pulse energy constant at 800 nm

Measurements with femtosecond pulses:

Experiments with femtosecond pulses at λ=400, 590, and 800 nm revealed that the nonlinear refraction was heavily shadowed by nonlinear absorption. The sample showed positive absorption at all wavelengths. The net change of the nonlinear refraction, Δn, were very small at λ=800 nm and at relatively low laser intensities (I=2.0 x 10^{11} W/cm^2).

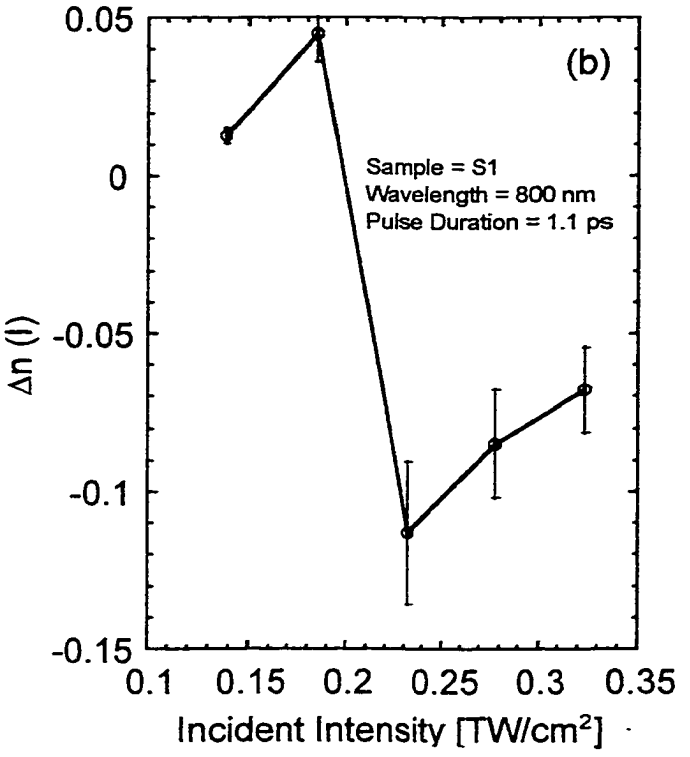

Fig.6.3 Intensity dependence of Δn(I) for sample 1 achieved by varying the pulse energy and keeping the pulse duration constant at 1.1 ps

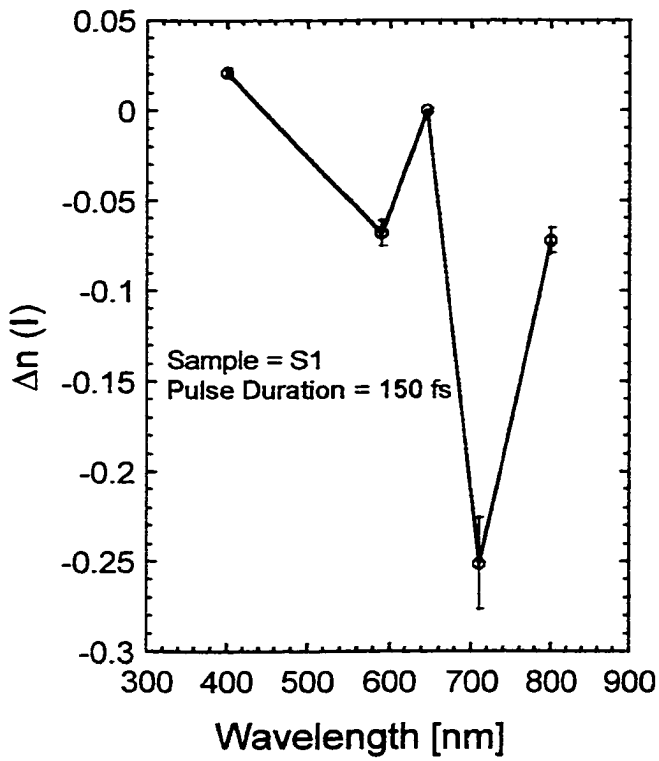

Fig.6.4 Wavelength dependence of the nonlinear refraction change, Δn, at a pulse duration of τ = 150 fs for sample S1 (3-4 nm crystals)

6.6. Discussion

White light[23] and photoluminescence[27] measurements exhibited three spectral bands in the spectral region between λ=350 nm to λ=800 nm: One absorption band is around λ=400 nm. The second absorption band is around λ=590 nm. A third band, around λ=750 nm is quite broad and is associated with photoluminescence. The peak absorption of the first band is cluster size dependent; it is blue-shifted for the small crystals (3-4 nm) in sample S1 when compared to the larger nano silicon crystals in sample S2 (5-6 nm). The white-light measurements indicate that the absorption of the second band, around λ=590 nm, is *independent* of cluster size. The photoluminescence peak wavelength is cluster size *dependent*[28] and led many researchers to believe it into a quantum-confined transition. Transient absorption measurements[26] with a pump pulse at λ=400 nm and a probe pulse at λ=590 nm indicate difference in the initial carriers dynamic of the small and large silicon nanocrystals in silica. Also, a spectral shift of 30 nm in the peak transient absorption around λ=590 nm between the two samples was found. This shift is too small to account for only quantum-confined states and could be attributed to size dependent surface states[29]. One can fit the effective band-gap as a function of cluster size, $E_g=E_{gb}+Ad^n$, where E_g is the effective band-gap of the nanocluster, E_{gb} is the bandgap of the bulk material, A being a constant and d is the nanocluster size. Theoretical models[30, 31] predict a value of n~1.4 for silicon nanoclusters. An absorption peak-wavelength difference of at least 70 nm is expected between the S1 and S2 samples. Thus, we conclude that the first band around λ=400 nm is a quantum-confined band and the other two bands are related to surface states. Based on this we can interpret the nonlinear data.

Z-scan experiments were performed on the same samples at New Jersey Institute of Technology at pulse duration τ=8 ns[32]. The third order susceptibilities at 8 ns pulse duration was about four order magnitude larger than that of measured at fs and ps pulse durations. According to their experiments with nano-second pulses on the 3-4 nm crystals did not reveal any nonlinear behavior other than in the UV. The 5-6 nm crystals exhibited two distinct nonlinear loss behaviors. One group showed an increase in nonlinear loss followed by saturation. To this group belong the spectra at λ=532 nm and λ=610 nm. The other group showed a decrease in the nonlinear loss followed by saturation. To this group belong the spectra in the range between 570, 590 nm and at λ=645 nm. A two-photon absorption process in the 570 to 645 nm spectral region is ruled out due to the relatively low intensity of the laser beam. A single-photon transition is unlikely as well. The reason is that a single-photon transition is usually accompanied by a refraction sign change across resonance in contrast to the present data. Thus, the transitions at nanosecond pulse durations at λ=532 nm and around λ=590 nm are governed by the transitions from the first excited state.

The Raman spectral width for sample S2 (5-6 nm crystals) is quite narrow[23], indicating a well-defined phonon. This means that momentum conservation laws are quite strict. On the other hand, the sample S1, which contains 3-4 nm silicon crystals *did not* exhibit any nonlinearity in the spectral range between λ=570 to λ=645 nm despite the existence of an absorption band at λ~590 nm. The Raman spectra for 5-6 nm crystals are shifted by 516 cm^{-1} or, by approximately 10 nm with respect to the laser line. The Raman spectra for 3-4 nm Si crystals look like that of an amorphous material. Thus, it is

our conclusion that the transitions around λ=590 nm are phonon assisted. In particular, the transition at λ=610 nm is resonantly enhanced by an anti-Stoke process.

From the absorption cross section[32], $\sigma=\sigma_{NL}\sim10^{-17}$ cm^2 at λ=532 nm and $\sigma=2\times10^{-18}$ cm^2 at λ=590 nm, the photon energy, $\hbar\nu$, and saturation intensity, $I_0\sim100$ MW/cm^2, we can estimate the lifetime of the nonlinear process through $\tau=\hbar\nu/\sigma I$. We estimate: τ=0.34 ns at λ=532 nm and τ=6.8 ns at λ=590 nm. This is in further support to the distinction between transitions at λ=532 nm and λ=590.

Picosecond pulse experiments for sample S2 at λ=532 nm exhibited a large negative nonlinear refraction effect which is in contrast to the positive value at nanosecond pulse duration. This could be explained using the arguments given in the previous section: The 70 ps pulse is much shorter than the time constant required for complete three-level transitions. The related nonlinear time constant for the picosecond pulse at λ=532 nm with $\sigma\sim2\cdot10^{-17}$ cm^2 is estimated as, $\tau\sim20$ ps, shorter than the pulse duration itself. Unlike the transition at nanosecond pulses there are fewer photo-excited carriers involved. For example approximately 30 e-h pairs were generated per single, 10 nanosecond pulse, per cm^2. The corresponding value for the picosecond pulse is only 3 e-h pairs/(1 ps pulse)/cm^2. Therefore, the transition at picosecond pulses was governed by the electric field intensity rather than by the pulse energy. The sign for the nonlinear index change is negative due to a single-photon transition below the resonance at $\lambda\sim400$ nm.

Femtosecond pulse experiments for the 5-6 nm crystals of sample S1 were masked by large nonlinear absorptions, meaning that there are resonances overlap in that spectral range. The 3-4-nm crystals of sample S1 produced a clear Z-scan response

probably because the resonance lines were further separated. The negative nonlinear refraction behavior at λ=800 nm and the positive value at λ=400 nm are indicative of a two-photon absorption at λ=800 nm. The nonlinear refraction is maximized around λ=700 nm, a transition, which, is also correlated with the peak photoluminescence. The nonlinear refraction is minimized at λ=640 nm; the nonlinearity in that spectral region is governed by the resonances from the first excited states. The ultra short pulse is too fast for the non-radiative transitions to be completed hence the low efficiency. The nonlinear refraction is maximized again around λ=590-nm as a result of a resonance-enhanced, two-photon absorption process. The large nonlinear refractive index change occurs when the pulse duration is on the order of τ~1 ps (with a corresponding peak intensity value of I_0~0.25 TW/cm^2). This also correlates with initial lifetime constants, which are on the order of a few picoseconds[26]. The fact that we can get this change through a change in the pulse duration (Figure 6.2) or, by a change in the pulse energy (Figure 6.3) means that the nonlinear processes are governed by intensities and not energies at this pulse durations.

6.7. Conclusions

In summary, we have studied the nonlinear properties of nano silicon crystals within the silica matrix. The system exhibited a rich spectrum of nonlinear transitions at various wavelengths and pulse durations. There are resonances from the first excited state to upper states at 532 nm and 590 nm wavelength regions. As it was discussed in chapter 3, longer pulse duration is more likely to stimulate the excited state transitions. Therefore, experiments with 8 ns pulse duration[32] showed three order of magnitude larger nonlinearity than the experiments with ps and fs pulse durations. The other wavelength region is around 700 nm. The nonlinearity is enhanced at this wavelength due to surface state resonance enhancement.

We can conclude that in Si nanoclusters in silica matrix the surface states and the discrete energy levels formed by the quantum confinement enhanced the nonlinearity through the nonlinear transitions to these states.

References:

[1] Al. L. Efros, and A. L. Efros, Sov. Phys. Semicond. 16, 772 (1982).

[2] L. E. Brus, J. Chem. Phys, 80, 4403 (1984).

[3] L. Brus, IEEE J. Quantum Electron, QE-22, 1909 (1986).

[4] S. Schmitt-Rink, D. A. B. Miller, and D. S. Chemla, Phys. Rev. B35, 8113 (1987).

[5] W. L. Wilson, P. F. Swajowski, aand L. E. Brus, Science, 262, 1242 (1993).

[6] Y. Kanemitsu, Phys. Rev. B, 49, 16845 (1994).

[7] M. Ehbrecht, H. Ferkel, F. Huisken, L. Holz, Y. N. Polivanov, V. V. Smirnov, O. M. Stelmakh, and R. Schmidt, J. Appl. Phys. 78, 5302 (1995).

[8] P. Roussigonal, D. Richard, and C. Flytzanis, Appl. Phys. A, 44, 285 (1987).

[9] N, Hill, K. Whaley, J. Electron Mater, 25, 269 (1996).

[10] L. T. Canham, Appl. Phys. Lett. 57, 1046 (1990).

[11] S. Frukawa, T. Miyasato, Phys. Rev. B, 38, 5726 (1988).

[12] H. Takagi, H. Ogawa, Y. Yamazaki, A. Ishizaki, and T. Nakagri, Appl. Phys. Lett., 56, 379 (1990).

[13] H. Morisaki, H. Hashimoto, F. W. Pimg, H. Nozawa, and H. Ono, Appl. Phys. Lett.74, 2977 (1993).

[14] T. Shimizu-Iwayama, M. Ohshima, T. Niimi, S. Nakao, K. Saitoh, T. Fujita, and N. Itoh, J. Phys.:Condens. Matter, 5, L375 (1993).

[15] D. Zhang, R. Kolbas, P. Milewski, D. Lichtenwalner, A. Kingon, and J. Zavada, Appl. Physics Lett., 65, 2684 (1994).

[16] X. Zhao, O. Schoenfeld, J. Kusano, Y. Aoyagi, and T. Sugano, Jpn. J. Appl. Phys., part 2, 33, L649 (1994).

[17] L. Brus, P. Szajowski, W. Wilson, T. Harris, S. Schuppler, and P. Citrin, J. Am. Chem. Soc. 117, 2915 (1995).

[18] J. F. Ziegler, in "Ion Implantation Technology", edited by J. F. Ziegler, North Holland, Amsterdam, p1 (1992).

[19] P. D. Townsend, P. J. Chandler, and L. Zhang, Optical Effects of Ion Implantations, ambridge University Press, Cambridge (1994).

[20] T. Komoda, J. P. Kelly, A. Nejim, K. P. Homewood, P. L. F. Hemment, and B. J. Sealy, Mater. Res. Soc. Symp. Proc., 358, 175 (1995).

[21] S. Guha, M. D. Pace, D. N. Dunn, and I. L. Singer, Appl. Phys. Lett., 70, 1207 (1997).

[22] H. Song, X. Bao, Phys. Rev. B, 55, 6988 (1997).

[23] S. Vijayalakshmi, H. Grebel, Z. Iqbal and C. W. White, J. App. Phys. 84, 6502(1998).

[24] C. Flytzanis and J. Hutter, in "Contemporary nonlinear optics", edited by G. P. Agrawal and R. W. Boyd, Academic Press, p305 (1992).

[25] L. Brus, in "Nanotechnology", edited by G. Timp, Springer Verlag, p266 (1999).

[26] V. I. Klimov, Ch. J. Schwar, D. W. McBranch and C. W. White, Appl. Phys. Lett., 73, 2603 (1998).

[27] Y. Zhang, S. Vijayalakshmi, M. Ajgaonkar, H. Grebel and C. W. White, accepted by *JOSA B*, 1999.

[28] C. W. White, J. D. Budai, S. P. Withrow, J. G. Zhu, S. J. Pennycook, R. A Zuhr, D. M. Hembree, D.O. Henderson, R. H. Magruder, M. J. Yacaman, G. Mondragon and S. Prawer, Nuc. Instrum. And Methods in Physics Res. B, 127/128, 545, (1997).

[29] X. L. Wu, T. Gao, G. G. Siu, S. Tong and X. M. Bao, Appl, Phys. Letts., 74, 2420 (1999).

[30] S. Y. Ren and J. D. Dow, Phys. Rev. B, 45, 6492 (1992).

[31] S. Ogut, J. R. Chelikowsky and S. G. Louie, Phys. Rev. Letts., 79, 1770 (1997).

[32] S. Vijayalakshmi, H. Grebel, G. Yaglioglu, R. Pino, R. Dorsinville, and C. W. White, J. of Appl. Phys., 22, 1 (2000).

CHAPTER 7

REMARKS AND FUTURE EXPERIMENTS

7.1. Remarks

We have studied the nonlinearity of various nanostructured materials. The main results of this thesis can be summarized as follows:

We have investigated the third order nonlinear optical properties of nanostructured Gd_2 doped C_{80} metallofullerene for the first time. We have performed Z-scan experiments at different wavelengths and different pulse durations to be able to investigate the mechanism contributing to the nonlinearity in this sample. The nonlinear response increased when the pump wavelength was tuned toward the single photon absorption peak of the material. This is a well-known result and this increase is attributed to single photon resonance enhancement. On the other hand, we have shown that the nonlinearity of $Gd_2@C_{80}$ strongly depends on the pulse duration. The effect of the pulse duration on the nonlinearity has not been studied before. We studied the excited state dynamics of $Gd_2@C_{80}$ by the pump-probe spectroscopy technique. We have showed that the third order nonlinearity of $Gd_2@C_{80}$ is enhanced by two photon absorption followed by an excited state absorption mechanism. The excited state transitions are more likely to happen with longer pulse durations, consequently longer pulse duration yielded higher nonlinearity. An important accomplishment of this thesis is to have shown that the transitions from the first excited state to the upper states enhance the nonlinear response.

For example, in the case of nanostructures, since new energy states can be generated through quantum confinement, one can get a variety of new transitions between induced states, and consequently, the third order nonlinear optical properties of the nanostructures can be substantially enhanced.

We have also investigated the time resolved dynamics of TDBC cyanine dye aggregates on silver nanosize colloids. We have performed femtosecond pump and white light continuum probe experiments on these samples. For the first time, we have shown stimulated emission from these nanostructured systems. The transition from the two-exciton state stimulates the emission from the one-exciton state to the ground state. Since J-aggregate of the TDBC dye in water does not show this property, this effect can be attributed to the confinement effects. As discussed in the following section more investigations are needed to understand the effect of the confinement clearly.

We have investigated the Langmuir-Blodgett films of some aromatic polydiacetylenes. We have shown that incorporation of aromatic group into the polydiatetylene increased the conjugation length; consequently, the third order nonlinear optical susceptibility was enhanced.

Finally, we have carried out investigations of the nonlinear optical properties of Si nanocrystals embedded in silica matrices. We have performed Z-scan experiments on these samples at various wavelengths and pulse durations in the fs-ps regime. We have shown that quantum confined and surface states created through quantum confinement play an important role on the size of the nonlinearity. Transitions from the first excited state to surface states enhance the nonlinearity. The required pulse duration for these transitions to be completed was calculated to be several ps. Thus, fs and <2 ps pulse

duration experiments yielded less nonlinearity, compared to ns pulse duration experiments conducted by Dr. Grebel's group at NJIT.

7.2. Future experiments

The nonresonant third order nonlinear optical effect required for device applications is in the order of 10^{-8} esu. The largest value that we have measured is 10^{-10} esu, for $Gd_2@C_{80}$ metallofullerene. Improvements are needed for device applications utilizing third order processes. The following areas offer opportunities for future research:

1) In the case of metallofullerene nanostructures, the effect of the fullerene cage size and the trapped metal atom should be studied. While changing one parameter at a time under the same experimental conditions (wavelength, pulse duration, pump power etc.) should be performed. This programmed study will help to find the best conditions for the use of metallofullerenes in devices.

2) Based on their emission properties J-aggregates are very good candidates for mirrorless laser applications. Future experiments should investigate the properties of aggregates on various nanostructure surfaces with different size and structures. This research will help to understand the effect of quantum confinement on the superradiant lasing.

3) Langmuir-Blodgett films of aromatic polydiacetylenes showed the contribution of the delocalization length to the nonlinearity. Synthesizing new organic polymers with

longer delocalization length such as co-polymers will help to improve the third order nonlinear susceptibilities of these materials.

4) Semiconductor nanostructures are the other promising materials and this research has not been explored yet. Studying various semiconductors embedded into various matrices would help to optimize the nonlinearity of these materials. Nonlinearity can be enhanced by controlling the size of the clusters i.e. by controlling the energy states created by the quantum confinement.

Silicon nanocrystals embedded into three-dimensional structures such as photonic crystals have the potential of manipulating ultrashort pulses. The frequency chirp created by the nonlinear medium, such as the silicon nanocrystals can be compensated by the dispersion created by the photonic crystal, resulting with pulse compression in a single element. Therefore, the study of the nonlinear dispersion properties of such systems could lead to a compact pulse compression device.

BIBLIOGRAPHY

Chapter 1

H.M. Gibbs, Optical Bistability: Controlling Light with Light, Academic Press, Orlando, Florida (1985)

D. H. Auston, et al., Appl. Opt., 26, 211 (1987).

E. Kopan, M. C. Tamargo, D. M. Huan, Appl. Phys. Lett, 50, 347 (1987).

P. M. Petroff, A. C. Gossard, and W. Wiegman, Appl. Phys. Lett. 45, 620 (1984).

H. M. Cox, P. S. Lin, A. Yi Yan, K. Kash, M. Seto, and P. Bastos, Appl. Phys. Lett., 55, 472 (1989).

Z. L. Zang, and N. C. MacDonald, J. Vac. Sci. Technol. B, 4, 2538 (1993).

J. Yao, S. Arney, and N. C. MacDonald, J. of Microelectromechanical systems 1, 14 (1992).

J. Yao, and N. C. MacDonald, J. Microtech. Microeng.,5, 257 (1995).

J. H. Hong, and D. Psaltis, in "Contemporary Nonlinear Optics", edited by G. P. Agrawal, R. W. Boys, Academic Press, p246 (1992).

P. N. Prasad, D. J. Williams, Introduction to nonlinear optical effects in molecules and polymers, John Willey and Sons, New York (1991).

J. Messier, F. Kajzar, P. N. Prasad, and D. Ulrich, in "Nonlinear Optical Effects in Organic Polymers", Kluwer Academic, Dordrecht (1989).

J. L. Bredas, and R. R. Chance, Conjugated Polymeric Materials: Opprotunities in Electronics, Optoelectronics, and Molecular Electronics, Kluver academic, Dordrecht (1990).

L. Y. Chiang, P. M. Chaikin, and D. O. Cowan, Advanced Organic Solid State Materials, MRS, Pittsburgh (1990).

J. Messier, F. Kajzar, and P. Prasad, Organic Molecules for Nonlinear Optics and Photonics, Kluver Academic, Dordrecht (1991).

L. Yang, Q. Z. Wang, P. P. Hho, R. Dorsinville, R. R. Alfano, W. K. Zou, N. L. Yang, Appl. Phys. Lett., 53, 1245 (1988).

M. J. S. Dewar, J. Am. Chem. Soc., 106, 669 (1984).

Z. H. Kafafi, et al., Chem. Phys. Lett., 188, 492 (1992).

S. R. Flom, et al., Phys. Review B, 46, 15598 (1992).

H.W. Kroto, J. R. Heath, S. C. O'Brien, R. F. Curl, and R. E. Smalley, Nature 318, 162 (1985).

W. Kradschemer, L. D. Lamb, K. Fostiropoulos, and D. R. Huffman, Nature 374, 354 (1990).

Y. Chai, T. Guo, C. Jin, R. E. Haufler, L. P. F. Chibante, J. Fure, L. Wang, J. M. Alford, and R. E. Smalley, J. Phys. Chem., 95, 7564 (1991).

M. J. Rosker, H. O. Marcy, Y. C. Tallis, J. T. Kooury, K. Hansen, R. L. Whetten, Chem. Phys. Lett., 196, 427 (1992).

J. R. Lindle, R. G. S. Pong, F. J. Bartoli, Z. H. Kafafi, Physical Review B, 48, 9447 (1993).

F. Kajzar, C. Taliani, R. Danieli, S. RRRossini, R. Zamboni, Phys. Rev. Lett., 73, 1617 (1994).

L. Yang, E. Royer, A. D. Walser, R. Dorsinvile, Chem. Phys. Lett., 239, 399 (1995).

H. Huang, G. Gu, S. Yang, J. Fu, P. Yu, G. K. L. Wong, Y. Du, J. Phys. Chem. B, 102, 61 (1998).

G. M. Carter, Y. J. Chen, S. K. Tripathy, Appl. Phsy. Lett. 43, 891 (1983).

D.A.D.Miller, D. S. Chemla, D. J. Eilenberger, P. W. Smith, A. C. Gossard, and W. T. Tsang, Appl. Phys. Lett., 41, 679 (1982); 42, 925 (1983).

R. K. Jain, R. C. Lind, J. Opt. Soc. Am. 73, 647 (1983).

J. Drag, G. Hernandez, S. Mukamel, Phys. Rev. A, 37, 3835 (1988).

F. C. Spano, and S. Mukamel, J. Chem. Phys. 91, 683 (1989).

W. L. Wilson, P. F. Swajowski, and L. E. Brus, Science, 262, 1242 (1993).

M. Ehbrecht, H. Ferkel, F. Huisken, L. Holz, Y. N. Polivanov, V. V. Smirnov, O. M. Stelmakh, and R. Schmid, J. Appl. Phys., 78, 5302 (1995).

C. Flytzanis, and J. Hutter, in "Contemporary nonlinear optics", Academic Press Inc., New York, p 299 (1992).

G. Timp, Nanotechnology, Springer Verlag, New York, p 330 (1999).

J. S. Lindsey, NewJ. Chem., 15, 153 (1991).

P. N. Prasad, D. J. Williams, Introduction to nonlinear optical effects in molecules and polymers, John Willey and Sons Inc., p .161 (1991).

L. Canham, Appl. Phys. Lett., 57, 1046 (1990).

Chapter 2

A. D. Walser, G. Coskun, R. Dorsinville, in "Electrical and optical polymer systems fundamentals, methods, and applications" edited by L. W. Donald, E. W. Gary, J. T. Debra, M. C. Thomas, D. G. Joseph, Marcel Dekker, New York, pp 423-452.

M Sheik, A. A. Said and E. W. Van Stryland, Opt. Lett. 14, 955 (1989).

M . Sheik, A. A. Said, T. H. Wei, D. J. Hagan and E. W. Stryland, IEEE J. Quantum Electron. QE-26, 760 (1990)

H. Kogelnik, T. Li, Appl. Opt., 5, 1550 (1966).

D. Weaire, B. S. Wherrett, D. A. B. Miller, and S. D. Smith, "Effect of Low Power Nonlinear Refraction on Laser Beam Propagation in LnSb," Optics Lett., vol. 4, pp. 331-333, (1974)

W. Demtroder, Laser Spectroscopy: basic concepts and instrumentation, Second edition, Springer Verlag, Berlin, Germany (1996).

R. Alfano, S. L. Shapiro, Phys. Rev. Lett., 24, 584 (1970).

M. Yang, PhD thesis submitted to Graduate faculty in Electrical Engineering Department, The City University of New York (1993).

R. W. Boyd, "Nonlinear Optics", Academic Press, London, UK, p275 (1992).

Chapter 3

M. S. Dresselhaus, G. Dresselhaus, R. Saito, in 'Nanotechnology' edited by G. Timp, Springeer Verlag, New York (1999).

G. Dresselhaus, M.S. Dresselhaus, P. C. Eklund, Phys. Rev. B, 45, 6923 (1992).

W. Kradschemer, L. D. Lamb, K. Fostiropoulos, and D. R. Huffman, Nature (London) 347, 354 (1990).

J.E. Fischer, P. A. Heiney, A. B. Smith III, Accounts Chem. Res. 25, 112 (1992).

D. E. Manolopoulos, P. W. Fowler, Chem. Phys. Lett., 187, 1 (1991).

Y. Achiba, K. Kikuchi, Y. Aihara, T. Wakabayashi, Y. Miyake, andM. Kainosho, Mat. Res. Soc. Symp. Proc., 359, 3 (1995).

S. Nagase, K. Kobayashi, T. Akasaka, in "Fullerenes", The Electrochemical Society Inc., Pennington New Jersey, 3, 558 (1996).

H.W. Kroto, J.R. Heath, S. C. O'Brein, R. F. Curl, and R. E. Smalley, Nature (London) 318, 162 (1985).

Y. Chai, T. Guo, C. Jin, R. E. Haufler, L. P. F. Chibante, J. Fure, L. Wang, J. M. Alford, and R. E. Smalley, J. Phys. Chem., 95, 7564 (1991).

K. Kobayashi, S. Nagase, and T. Akasaka, Chem. Phys. Lett., 245, 230 (1995).

K. Kobayashi, S. Nagase, Chem. Phys. Lett., 262, 227 (1996).

E. Sohmen, J. Fink, W. Kratschmer, Z. Phys. B, 86, 86 (1992).

F. Kajzar, Y. Okada-Shudo, C. Meritt, Z. Kafafi, Synthetic Metals, 94, 91 (1998).

R. D. Johnson, M. S. de Vries, J. R. Salem, D.S. Bethune, and C. S. Yannoni, Nature, 355, 239 (1992).

D.S. Bethune, R. D. Johnson, J. R. Salem, M. S. de Vries, and C. S. Yannoni, Nature, 366, 123 (1993).

J.R. Heflin, D. Marciu, C. Figura, S. Wang. P. Burbank, S. Stevenson, and H.C. Dorn, Applied Physics Letters, 72, 2788 (1998).

M. J. Rosker, et al., Chem. Phys. Lett., 196, 427 (1992).

J. R. Lindle, R. G. S. Pong, F. J. Bartoli, Z. H. Kafafi, Phys. Review B, 48, 9447 (1993).

F. Kajzar, C. Taliani, R. Danieli, S. Rossini, R. Zamboni, Physical Review Lett, 73, 1617 (1994).

H. Huang, G. Gu, S. Yang, J. Fu, P. Yu, G. K. L. Wong, Y. Du, J. Phys. Chem. B. 102, 61 (1998).

F. J. Aranda, D. V. G. L. N. Rao, J. F. Roach, P. Tayebati, J. Appl. Phys, 73, 7949 (1993).

S. Jouris, E. Koudoumas, A. A. Ruth, S. Leach, J. Phys. B:At. Mol. Opt. Phys. Printed in UK, 28, 4537 (1995)

D. Neher, G. I. Stegeman, F. A. Tinker, N. Peyghambarian, Optics Letter, 17, 1491 (1992).

A. Rosen, and B. Wastberg, J. Am. Chem. Soc., 110, 8701 (1988).

A. Chang, W. C. Ermler, and R. M. Pitser, J. Chem. Phys, 94, 5004 (1991).

J. Feng, M. C. Li, M. C. Li, and M. C. Zerner, Int. J. Quant. Chem., 39, 331 (1991).

S. Saito, and A. Oshiyama, Sollid. St. Commun., 83, 107 (1992).

S. Bandow, et al., J. Phys. Chem., 96, 9609 (1992).

J. Weaver, et al., Chem. Phys. Lett., 190, 460 (1992).

M. Hoinkis, et al., Chem. Phys. Lett, 198, 461 (1992).

H. Huang, G. Gu, S. Yang, J. Fu, P Yu, G. K. L. Wong, Y. Du, Electrochemistry Society Proceedings, 94-14, 401 (1997).

G. Gu, H. Huang, S. Yang, P. Yu, J. Fu, G. K. Wong,, X. Wan, J. Dong, Y. Du, Chem. Phys. Lett. 289, 167 (1998).

S. W. McElvany and M. M. Ross, J. Am. Soc. Mass Spectrum, 3, 268 (1992).

J. R. Heath et al, J. Am. Chem. Soc., 107, 77 (1985).

S. Couris, E. Koudoumas, F. Dong, and S. Leach, J. Phys. B: At. Mol. Opt. Phys., 29 5033 (1996)

R. H. Stolen and C. Lin, Phys. Rev. A17, 1448 (1978)

Minoshina K, Taiji M, and Kobayashi, Opt. Lett., 16, 1683 (1991)

S.Couris, E. Coudoumas, F.Dong, and S. Leach, J. Phys. B.: At. Mol. Opt. Phys., 29, 5033 (1996).

Qihuang Gong, Yuing Sun, Zongju Xia, Y. H. Zou, Zhennan Gu, Xihuang Zhou, and Di Qiang, J. Appl. Phys., 71, 3025 (1992)

S. C. Chapra, R. P. Canale, "Numerical methods for engineers", 3rd ed., McGraw-Hill: Boston, p 701 (1998)).

L.Yang, E. Royer, A.D. Walser, R. Dorsinville, Chem. Phys. Lett. 239, 399 (1995).

M. Zhao, Y. Cui, M. Samoc, P. N. Prasad, M. R. Unroe, B. A. Reinhardt, J. Chem. Phys. 96, 3991 (1991).

E. F. Hilinski, P. A. Lucas, Y. Wang, J. Chem. Phys. 89, 3435 (1988).

H. Kalt, K. Bohnert, D. P. Norwood, T. F. Boggess, A. L. Smirl, I. J. D'Haennes, J. Appl. Phys. **62**, 4187 (1987).

Y. Zhao, C. Wu, P. Shah, M. K. Kim, L. R. Dawson, Appl. Phys. Lett. **63**, 281 (1993).

J. S. Weiner, D. B. Pearson, D. A. B. Miller, D. S. Chemla, D. Sivco, A. Y. Cho, Appl. Phys. Lett. **49**, 531 (1986).

D. S. McCallum, X. R. Huang, M. D. Dawson, T. F. Boggess, A. L. Smirl, T. C. Hasenberg, A. Kost, J. Appl. Phys. **70**, 6891 (1991).

Z. H. Kafafi, J. R. Lindle, R. G. S. Pong, F. J. Bartoli, L. J. Lingg, and J. Milliken, Chem. Phys. Lett. 188, 492 (1992).

J. R. Lindle, R. G. S. Pong, F. J. Bartoli, and Z. H. Kafafi, Phys. Review B **48**, 9447 (1993).

Chapter 4

E. E. Jelley, Nature, 138, 1009(1936).

G. Scheibe, Angeew. Chem. 49, 563(1936).

W. West, P. B. Gilman, Jr. in "The theory of the photographic process", 4th ed., Macmillan: New York,pg 251(1977).

V. Sundstrom and R. van Grondelle, J. Opt. Soc. Am. B7, 1595 (1990).

F. C. Spano, S. Mukamel, Phys. Rev. A, 40, 5783(1989).

S. Ozcelik, D. L. Akins, Appl. Phys. Lett.. 71, 3057 (1997).

M. Van Burgel, D. A. Wiersma, K. Duppen, J. Chem. Phys. 102, 20 (1995).

H. Fidder, et. al., J. Chem. Phys., 98, 6564(1993).

K. Minoshima, et. al., Chem. Phys. Lett, 218, 67(1994).

A. Johnson, et. al., Chem. Phys. Lett., 211, 511(1993).

S. Makio, N. Kanamaru and J. Tanaka, Bull. Chem. Soc. Jpn. 53, 3120 (1980).

M. Lindrum, A. Glismann, J. Moll and S. Daehne, Chem. Phys. 178, 423 (1993).

K. Misawa, K. Minoshima, H. Ono and T. Kobayashi, Chem. Phys. Lett. 220, 251 (1994).

A.S. Davydov, "Theory of Molecular Excitons", Plenum, New York (1971).

D.B. Chesnut and A. Suna, J. Chem. Phys. 39, 146 (1963).

F.C. Spano, Phys. Rev. Lett. 67, 3424 (1991); 68, 2976 (1992).

J. Knoester, Phys. Rev. A 47, 2083 (1993).

F.C. Spano and S. Mukamel, J. Chem. Phys. 91, 683 (1989).

A.H. Herz, Adv. Colloid Interface Sci. 8, 237 (1977).

H. Fidder, J. Knoester and D.A. Wiersma, J. Chem. Phys. 95, 7880 (1991).

F.C. Spano, V. Agranovich and S. Mukamel, J. Chem. Phys. 95, 1400 (1991).

S. Mukamel, "The Principles of Nonlinear Optical Spectroscopy", Oxford University Press, New York, (1995).

M. Kasha, H.R. Rawls and M. Ashraf El-Bayoumi, Pure Appl. Chem. 11, 371 (1965).

J. Moll, S. Daehne, J.R. Durrant and D.A. Wiersma, J. Chem. Phys. 102, 6362 (1995).

A. Herz, "Theory of photographic process, 4th ed.", Macmillan, New York, pp235-250 (1007).

A. H. Herz, R. P. Danner, G. A. Janusonic, "Adsorption from Aqueous Solution", ACS Monograph 79, Rheinhold, New York, pp 173-197 (1968).

D. L. Akins, J. Colloid Interface Sci., 90, 373 (1982).

X. Li, B. Gu, D. L. Akins, Chem. Phys. Lett., 105, 263 (1984).

K. Kemnitz, K. Yoshihara, T. Tani, J. Phys. Chem., 94, 3099 (1990).

E. L. Quitevis, M. N. Horng., Y. S. Chen, J. Phys. Chem., 92, 256 (1988).

M. L. Horng, E. L. Quitevis, J. Phys. Chem., 93, 6198 (1989).

S. Ozcelik et al, J. Phys.Chem.B, 101, 3021(1997).

J. Franck, et al, J. Chem. Phys. 6, 861 (1938).

J. Durrant, et. al., Chem. Phys. Lett., 222, 450(1994).

A. Chakrabarti, Phys. Rev. B, 57, R4206(1998).

F. Spano, Chem. Phys. Lett., 220, 365(1994).

F. Spano, Chem. Phys. Lett., 234, 29(1995).

M. Furuki, L. S. Pu, F. Sasaki, S. Kobayashi, T. Tani, Appl. Phys. Lett. 72, 2648 (1998).

Chapter 5

G. M. Carter, M. K. Thakur, Y. J. Chen and J. V. Hryniewicz, Appl. Phys. Lett. **47**, 457(1985).

M. Schot, and G. Wegner, in "Nonlinear Optical Properties of Organic Molecules and Crystals", edited by D. S. Chemla and J. Zyss, vol2, Academic Press, New ork.

P. N. Prasad and D. J. Wiliams, "Introduction to nonlinear optical effects in molecules and polymers", John Willey & Sons, New York, (1991).

C. Sauteret, J. P. Hermann, R. Frey, F. Pradere, J. Ducuing, R. H. Baughman, and R. R. Chance, Phsy. Rev. Lett., 36, 956(1976).

T. Kurihara, K. Kubodera, S. Matsumoto, and T. Kaino, Polymer preprints, The Society of Polymer Science, Japan, 36, 1175(1987).

T. Koda, K. Ishikava, T. kanetake, T. nishikawa, Y. yotukara, S. Koshihara, K. Takeda, and K. Kubodera, Third Asia Pacific Physics Confernce, Hong Kong, June (1988).

J. LeMoigne, A. Thierry, P. A. Chollet, F. Kajzar, J. Messier, J. Chem. Phys., 88, 6647(1988).

G. M. Carter, Y. J. Chen, M. F. Rubner, D. J. Sandman, M. K. Thakur, and S. K. Tripathi, in D. S. Chemla and J. Zyss (Eds.), Nonlinear Optical Properties of Organic Molecules and Crystals, Vol. 2, Academic, New York, p. 85 (1987).

S. Tomaru, K. Kubodera, S. Zembutsu, K. Takeda, and M. Hasgawa, Elect. Lett. 23, 585(1982).

D. N. Rao, P. Chopra, S. K. Ghoshal, J. Swiatkiewicz, and P. N. Prasad, J. Chem. Phys. Lett. 84, 7049(1986).

D. N. Rao, J. Swiatkiewicz, P. Chopra, S. K. Ghoshal, and P. N. Prasad, Appl. Phys. Lett. 48, 1187(1986).

J. M. Nunzi, J. L. Ferrier, and R. Chevalier, in J. Messier, F. Kajzar, P. Prasad, and D. Ulrich (Eds.), Nonlinear Optical Effects in Organic Polymers, NATO ASI Series, Vol. 12, Kluwer Academic, Dordrecht, p. 365(1989).

P. P. Ho, R. Dorsinville, N. L. Yang, G. Odian, G. Eichmann, T. Jimbo, Q. Z. Wang, G. C. Tang, N. D. Chen, W. K. Zou, Y. Li, R. R. Alfano, SPIE Proc. 682, 36(1986).

P. P. Ho, N. L. Yang, T. Jimbo, Q. Z. Wang, and R. R. Alfano, J. Opt. Soc. Am. B, 4, 1025(1987).

G. Berkovic, Y. R. Shen, and P. N. Prasad, J. Chem. Phys. 87, 1897(1987).

L. Wang, T. Wada, T. Yuba, M. Kakimoto, Y. Imai, H. Sasabe, J. Appl. Phys. 79, 12 (1996).

R. F. Shi, A. F. Garito, in "Characterization technique and tabulations for organic nonlinear optical materials", edited by M. G. Kuzyk, C. W. Dirk, Marcel Dekker Inc., New York (1998).

P. N. Parasad, D. J. Williams, Introduction to nonlinear optical effects in molecules and polymers, John Willey and Sons Inc., New York, p 54 (1991).

K. C. Rustagi, and J. Ducuing, Opt. Commun., 10, 258 (1974).

G. Wegner, Z. Naturforsch, 2B, 8248(1969).

B. Tieke, G. Lieser, and G. Wegner, J. Polym.Sci., Poly. Chem. Ed., 17, 1631(1979).

B. Tieke and G.Lieser, J. Colloid Interface Sci., 88, 471(1982).

G. Lieser, B. Tieke, and G. Wegner, Thin Solid Films, 68, 77(1980).

B. Tieke and G. Lieser, Macromolecules, 18, 327(1985).

D. Harris et al., Synthetic Metals, 101, 204 (1999).

M.P. Carreon, G. Burillo, V.Agabekov, and T.Ogawa, Polym.J., 29, 103(1997).

M.P. Carreon, G. Burillo, L.Fomina, and T.Ogawa, Poly. J., 30, 95(1998).

S. Yamada, Y. Shimoyama, Jpn. J. Appl. Phys. 36, 5242 (1997).

F. Kajzar and J.Messier, Polym. J., 19, 275(1987).

F. Kajzar and J. Messier, Thin Solid Films, 132, 11(1985).

Chapter 6

Al. L. Efros, and A. L. Efros, Sov. Phys. Semicond. 16, 772 (1982).

L. E. Brus, J. Chem. Phys, 80, 4403 (1984).

L. Brus, IEEE J. Quantum Electron, QE-22, 1909 (1986).

S. Schmitt-Rink, D. A. B. Miller, and D. S. Chemla, Phys. Rev. B35, 8113 (1987).

W. L. Wilson, P. F. Swajowski, aand L. E. Brus, Science, 262, 1242 (1993).

Y. Kanemitsu, Phys. Rev. B, 49, 16845 (1994).

M. Ehbrecht, H. Ferkel, F. Huisken, L. Holz, Y. N. Polivanov, V. V. Smirnov, O. M. Stelmakh, and R. Schmidt, J. Appl. Phys. 78, 5302 (1995).

P. Roussigonal, D. Richard, and C. Flytzanis, Appl. Phys. A, 44, 285 (1987).

N, Hill, K. Whaley, J. Electron Mater, 25, 269 (1996).

L. T. Canham, Appl. Phys. Lett. 57, 1046 (1990).

S. Frukawa, T. Miyasato, Phys. Rev. B, 38, 5726 (1988).

H. Takagi, H. Ogawa, Y. Yamazaki, A. Ishizaki, and T. Nakagri, Appl. Phys. Lett., 56, 379 (1990).

H. Morisaki, H. Hashimoto, F. W. Pimg, H. Nozawa, and H. Ono, Appl. Phys. Lett.74, 2977 (1993).

T. Shimizu-Iwayama, M. Ohshima, T. Niimi, S. Nakao, K. Saitoh, T. Fujita, and N. Itoh, J. Phys.:Condens. Matter, 5, L375 (1993).

D. Zhang, R. Kolbas, P. Milewski, D. Lichtenwalner, A. Kingon, and J. Zavada, Appl. Physics Lett., 65, 2684 (1994).

X. Zhao, O. Schoenfeld, J. Kusano, Y. Aoyagi, and T. Sugano, Jpn. J. Appl. Phys., part 2, 33, L649 (1994).

L. Brus, P. Szajowski, W. Wilson, T. Harris, S. Schuppler, and P. Citrin, J. Am. Chem. Soc. 117, 2915 (1995).

J. F. Ziegler, in "Ion Implantation Technology", edited by J. F. Ziegler, North Holland, Amsterdam, p1 (1992).

P. D. Townsend, P. J. Chandler, and L. Zhang, Optical Effects of Ion Implantations, ambridge University Press, Cambridge (1994).

T. Komoda, J. P. Kelly, A. Nejim, K. P. Homewood, P. L. F. Hemment, and B. J. Sealy, Mater. Res. Soc. Symp. Proc., 358, 175 (1995).

S. Guha, M. D. Pace, D. N. Dunn, and I. L. Singer, Appl. Phys. Lett., 70, 1207 (1997).

H. Song, X. Bao, Phys. Rev. B, 55, 6988 (1997).

S. Vijayalakshmi, H. Grebel, Z. Iqbal and C. W. White, J. App. Phys. 84, 6502(1998).

C. Flytzanis and J. Hutter, in "Contemporary nonlinear optics", edited by G. P. Agrawal and R. W. Boyd, Academic Press, p305 (1992).

L. Brus, in "Nanotechnology", edited by G. Timp, Springer Verlag, p266 (1999).

V. I. Klimov, Ch. J. Schwar, D. W. McBranch and C. W. White, Appl. Phys. Lett., 73, 2603 (1998).

Y. Zhang, S. Vijayalakshmi, M. Ajgaonkar, H. Grebel and C. W. White, accepted by *JOSA B*, 1999.

C. W. White, J. D. Budai, S. P. Withrow, J. G. Zhu, S. J. Pennycook, R. A Zuhr, D. M. Hembree, D.O. Henderson, R. H. Magruder, M. J. Yacaman, G. Mondragon and S. Prawer, Nuc. Instrum. And Methods in Physics Res. B, 127/128, 545, (1997).

X. L. Wu, T. Gao, G. G. Siu, S. Tong and X. M. Bao, Appl, Phys. Letts., 74, 2420 (1999).

S. Y. Ren and J. D. Dow, Phys. Rev. B, 45, 6492 (1992).

S. Ogut, J. R. Chelikowsky and S. G. Louie, Phys. Rev. Letts., 79, 1770 (1997).

S. Vijayalakshmi, H. Grebel, G. Yaglioglu, R. Pino, R. Dorsinville, and C. W. White, J. of Appl. Phys., 22, 1 (2000).